Skoltech
Skolkovo Institute of Science and Technology

Skolkovo Institute of Science and Technology

DETERMINING THERMAL PROPERTIES OF SEDIMENTARY ROCKS
FROM WELL-LOGGING DATA

Doctoral Thesis

by

ANUAR SHAKIROV

DOCTORAL PROGRAM IN PETROLEUM ENGINEERING

Supervisor
Professor Yuri Popov
Co-supervisor
Doctor Evgeny Chekhonin

Moscow - 2021

I hereby declare that the work presented in this thesis was carried out by myself at Skolkovo Institute of Science and Technology, Moscow except where due acknowledgement is made, and has not been submitted for any other degree.

Candidate (Anuar Shakirov)

Supervisor (Prof. Yuri Popov)

Co-supervisor (Dr. Evgeny Chekhonin)

Abstract

Data on the thermal properties of sedimentary rocks are necessary for thermohydrodynamic modelling of physical processes occurring within a reservoir during thermal enhanced oil recovery, for basin and petroleum system modelling, temperature log data interpretation, and heat flow determination. The limitations of the existing techniques for *in situ* rock thermal property measurements and numerous cases with the absence of core samples require the development of methods for rock thermal property determination based on well-logging data. Existing approaches for determining rock thermal properties from well-logging data are appropriate only for isotropic rocks and do not allow reliable determinations of rock volumetric heat capacity. Since many rock types exhibit a considerable degree of heterogeneity and anisotropy, advanced approaches for well log-based determination of rock thermal properties are necessary. The implementation of a new thermal core logging technique, which provides continuous and high-precision measurements of the principal components of the thermal conductivity tensor and volumetric heat capacity from core samples, enabled the development of a new framework for the indirect determination of rock thermal properties. A new technique for the simultaneous determination of rock thermal conductivity and volumetric heat capacity from well-logging data accounting for thermal anisotropy, heterogeneity and *in situ* thermobaric conditions was developed and tested on vast, representative experimental dataset from various hydrocarbon fields, including organic-rich shales and heavy oil field. The novelty of the technique includes integration of thermal core logging and well logging data and the application of theoretical models and regression analysis by means of machine learning techniques. The implementation of the novel well-log based technique for determining rock thermal properties allowed obtaining new data on vertical variations of rock thermal properties and heat flow density that enhanced the quality of the subsequent studies of hydrocarbon fields.

Publications and Patents

Peer-Reviewed Articles in International Scientific Journals

1. **Shakirov**, A., Chekhonin, E., Popov, Y., Popov, E., Spasennykh, M., Zagranovskaya D., Serkin M., 2021. Rock thermal properties from well-logging data accounting for thermal anisotropy. Geothermics 92(6), 102059. https://doi.org/ 10.1016/j.geothermics.2021.102059.

2. Meshalkin, Y., **Shakirov**, A., Popov, E., Koroteev, D., Gurbatova, I., 2020. Robust well-log based determination of rock thermal conductivity through machine learning. Geophysical Journal International 222(2), 978-988. https://doi.org/10.1093/gji/ggaa209.

3. Popov, E., Chekhonin, E., Safonov, S., Savelev, E., Gurbatova, S., Ursegov, S., **Shakirov**, A., 2020. Thermal core profiling as a novel and accurate method for efficient characterization of oil reservoirs. Journal of Petroleum Science and Engineering 193(3), 107384. https://doi.org/ 10.1016/j.petrol.2020.107384.

4. Popov, Y., Spasennykh, M., **Shakirov**, A., Chekhonin, E., Romushkevich, E., Savelev, E., Gabova, A., Zagranovskaya, D., Valiullin, R., Yuarullin, R., Golovanova, I., Salmanova, R., (2021). Advanced determination of heat flow density on an example of a west Russian oil field. Geosciences 11 (8), 346. https://doi.org/10.3390/geosciences11080346.

Patent

Popov Y., Chekhonin, E., **Shakirov**, A., 2019. Approach for determining thermal properties of organic-rich shales. Russian Patent, № RU 2704002 C1.

Extended abstracts in conference proceedings (indexed in Scopus)

1. Popov, Y., Spasennykh, M., **Shakirov**, A., Chekhonin, E., Romushkevich, R., Savelev, E., Zagranovskaya, D., 2021. New Data on Heat flow for Modeling Areas of Hydrocarbon Systems of The Bazhenov and Domanik Formations. EAGE/SPE Workshop on Shale Science. https://doi.org/ 10.3997/2214-4609.202151027.

2. **Shakirov**, A., Meshalkin, Y., Koroteev, D., Popov, Y., 2020. Vertical variations of rock thermal conductivity from well logging data using machine-learning methods. EAGE, Data Science in Oil & Gas. https://doi.org/ 10.1016/j.petrol.2020.107384.

3. **Shakirov**, A., Chekhonin, E., Popov, E., Romushkevich, R., Popov, Y., (2019). Determination of Thermal Conductivity Variations within Oil Shale Reservoirs Using Integration of Thermal Core Logging and Standard Well Logging Data. Sixth EAGE Shale Workshop. https://doi.org/10.3997/2214-4609.201900294.

4. Chekhonin, E., **Shakirov**, A., Popov, E., Romushkevich, R., Popov, Y., Bogdanovich, N., Rudakovskaya S., 2019. The Role of Thermophysical Profiling for Core Sampling for Laboratory Investigations of Source Rocks. EAGE/SPE Workshop on Shale Science. https://doi.org/10.3997/2214-4609.201900478.

5. Popov, Y., Spasennykh, M., Valiullin, R., Ramazanov, A., Zagranovskaya, D., Golovanova, I., Chekhonin, E., Savelev, E., Gabova, A., Popov, E., **Shakirov**, A., 2018. First Experience of Maintenance of Basin Modeling With Up-to-date Complex of Experimental Geothermic Investigations. EAGE Geomodel. https://doi.org/10.3997/2214-4609.201802427.

6. Chekhonin, E., Popov, E., Popov, Y., Romushkevich, R., Savelev, E., and **Shakirov**, A., 2018. Thermal Petrophysics: New Insight into Core Analysis and Characterization of Highly Heterogeneous Tight Oil Formations. 80th EAGE Conference and Exhibition. https://doi.org/10.3997/2214-4609.201800788.

Author contributions to publications and patent: *Conceptualization*: Anuar Shakirov, Yuri Popov, Evgeny Chekhonin, Mikhail Spasennykh, Evgeny Popov; *methodology*, Anuar Shakirov, Yuri Popov, Evgeny Chekhonin, Evgeny Popov, Mikhail Spasennykh; *software*, Inessa Golovanova, Rushana Salmanova; *validation*, Evgeny Chekhonin, Raisa Romushkevich; *formal analysis*, Anuar Shakirov, Yuri Popov, Evgeny Chekhonin, Raisa Romushkevich; *investigation*, Evgeny Popov, Egor Savelev, Alexander Gonsharov, Dmitry Ostrizhniy, Anastasia Gabova, Rim Valiulin, Rashid Yyarullin, Airat Ramasanov; *resources*, Yuri Popov, Dzhulia Zagranovskaya, Mikhail Spasennykh, Irina Gurbatova; *data curation*, Yuri Popov, Raisa Romushkevich, Stanislav Ursegov; *writing* - original draft preparation, Anuar Shakirov, Yuri Popov, Evgeny Chekhonin, Yuri Meshalkin; *writing-review and editing*, Anuar Shakirov, Yuri Popov, Evgeny Chekhonin, Yuri Meshalkin, Dmitry Koroteev; *visualization*, Anuar Shakirov, Yuri Popov, Evgeny Chekhonin; *supervision*, Yuri Popov, Mikhail Spasennykh, Evgeny Chekhonin; *project administration*, Yuri Popov, Mikhail Spasennykh, Dzhulia Zagranovskaya, Maxim Serkin, Svetlana Rudakovskaya.

Acknowledgements

My PhD journey would not have been possible without the support and help of numerous people to whom I am expressing my gratitude and respect.

First, I am sincerely grateful to my scientific supervisor, Professor Yuri Popov, for enrolling me in a world-class scientific journey, constant helping and supporting me whenever needed. Many thanks for giving me the opportunity to obtain practical and theoretical skills, versatile knowledge and sharing with me not only professional but also life experience.

I thank my co-supervisor Dr. Evgeny Chekhonin for his invaluable input to my research and for educating me as a thorough and erudite specialist.

I am very grateful to Raisa Romushkevich for her support and fruitful discussions, comments and advice concerning geological aspects of my research.

I express my gratitude to my lab colleagues – Dr. Evgeny Popov, Egor Savelev, Alexander Goncharov, Dmitry Ostrizhny and Sergey Pohilenko – for their hard laboratory work and conducting experimental measurements.

I thank Professor Mikhail Spasennykh for his valuable recommendations and comments and his constant support during organizing and conducting the research.

Special thanks to all my colleagues and friends from the Skolkovo Institute of Science and Technology for motivating me and being wonderful.

Finally, yet importantly, I am highly indebted to my family for always believing in me and caring about me during my PhD journey. Many thanks.

Table of Contents

10

List of figures

14

List of tables

20

Chapter 1. Existing well-log based approaches for determining rock thermal properties: current state-of-the-art

1.1 Applications of data on rock thermal properties

Diversification of applied tasks at geological and geophysical investigations of hydrocarbon fields during 2000-2020 resulted in the increased necessity of representative and reliable data on rock thermal properties. The data on rock thermal properties are required for prospecting, exploration and development of hydrocarbon fields.

An essential method for assessing hydrocarbon field potential in the prospecting stage is basin and petroleum system modelling (BPSM). The critical aspect of BPSM is a reconstruction of thermal basin history that is to a significant degree determined by rock thermal properties and heat flow density. Twenty per cent uncertainty in data on rock thermal properties or in data on heat flow density in some cases leads up to 100% over- or underestimation of hydrocarbon reserves (Hicks et al., 2012).

In the exploration stage, the modern experimental base of thermal petrophysics (Popov et al., 2016; Popov E. et al., 2020a) provides an effective solution of the following applied tasks:

1. Identification of peculiarities of geological setting via the data on basic physical properties of rocks – thermal conductivity and volumetric heat capacity (Popov E. et al., 2020b).
2. Assessment of rock heterogeneity (Popov E. et al., 2019).
3. Assessment of rock thermal anisotropy that is a distinguishing characteristic for many rock types including organic-rich shales (Popov et al., 2017).

4. Registering detailed profiles of total organic carbon content for organic-rich shales (Popov E. et al., 2020a).

5. Interpretation of temperature logging data (Poulsen & Balling, 2012).

6. Registering and interpreting vertical variations of heat flow density and terrestrial heat flow density (Emmermann et al., 1997; Popov et al., 1999; Kukkonen et al., 2011; etc.).

In the development stage, the data on rock thermal properties are required for thermohydrodynamic modelling of physical properties that occur when thermal enhanced oil recovery (EOR) methods are utilized (Wang et al., 2017). Reliable data on rock thermal properties allow determining optimal parameters for EOR and avoiding significant errors in the assessment of the economic efficiency of the EOR technique.

Moreover, geothermal investigations and high-level radioactive waste disposal in deep underground sites require reliable data on rock thermal properties.

1.2 Traditional approaches for determining thermal properties of sedimentary rock

The existing approaches for determining rock thermal properties can be grouped in the following way:

1. Laboratory measurements on core samples.
2. *In situ* thermal logging.
3. Theoretical modelling.
4. Use of databases.
5. Well-log based approaches.

Numerous steady-state and transient techniques were developed for measuring thermal conductivity and volumetric (or specific) heat capacity of rocks. According

to Blackwell et al. (1989) and Clauser et al. (2006), the most prominent methods for measuring the thermal conductivity of rocks are considered divided-bar, needle-probe, and optical scanning. Today, the most commonly used divided-bar tools in laboratories base on the same working principle as the instrument described by Birch (1950). The most typical and convenient-line source method is a half-space line-source described by Huenges et al. (1990). The optical scanning method developed and suggested by Popov (1983) is currently universally recognized and included in the International Society of Rock Mechanics and Rock Engineering (ISRM) suggested methods for determining rock thermal properties (Popov et al., 2016). Recently, there was also discovered a new opportunity for thermal conductivity evaluation on rock cuttings and nonconsolidated rocks by Popov et al. (2018). Among the various methods for direct measurements of rock volumetric/specific heat capacity, the most widely used methods are heat flux differential scanning (DCS) calorimeters and optical scanning. The data on rock thermal properties obtained with modern laboratory equipment is considered the most reliable to date. The critical problem of this approach for determining rock thermal properties is a limited amount of core material. Thus, data on rock thermal properties are often confined either to a few wells or to view formations.

An ideal solution to the difficulties of sampling and measuring rock thermal properties in the laboratory on core samples could be *in situ* measurement of rock thermal properties. Much effort was made to develop such a particular technique (Beck et al., 1971; Burkhardt et al., 1995; Sanner et al., 2005; Kukkonen et al., 2007; Sauer et al., 2017; etc.). However, the suggested techniques are still not implemented within the geothermal investigations of wells due to the following reasons:

- *Significant measurement errors.* Sauer et al. (2017) recently described a new tool and reported that it provides precision and accuracy of 10% and 7%, respectively, that corresponds to an uncertainty of $>12\%$.

- *Long time required for measurements.* Application of some techniques (e.g., Sanner et al., 2005) requires several days.

- *Unstable conditions of measurements.* Borehole washouts, mud cakes, induced convection of drilling fluid, and other technical reasons essentially affect and usually decrease measurement quality. In most cases, measurement results are unsatisfactory for practical use.

- *Impossibility to assess rock thermal anisotropy and the vertical variation of thermal properties* (like, e.g., in the thermal response test, see Sanner et al., 2005).

Thus, whereas the concept seems sound and some suitable tools are available, these techniques require essential enhancement to be widely used.

Another perspective approach for determining rock thermal properties is an application of theoretical modelling. There are currently more than thirty theoretical models of rock thermal conductivity (see, e.g., Clauser et al., 2009; Abdulagatova et al., 2009; Bayuk et al., 2011; Fuchs et al., 2013). The application of theoretical modelling of thermal conductivity requires data on volumetric fractions of rock components (minerals and fluids), data on its thermal conductivity, and, for some models, data on correction factors. However, there are many cases when the application of theoretical modelling does not provide a satisfactory quality of data on rock thermal properties. For example, the application of the most popular Lichtenecker model (Lichtenecker, 1924) in some cases gives results with uncertainties that amount to 40% (Chekhonin et al., 2019). Moreover, the application of advanced theoretical models, such as the Lichtenecker-Asaad model (Asaad,

1955), requires knowledge on the so-called correction factor that allows accounting for structural and textural peculiarities of rocks. However, reliable determinations of correction factor can be performed via special experimental investigations as described by Popov et al. (2003), and often the data on correction factor is not available. Some theoretical models based on effective medium theory concepts require data on pore geometry, the shape of cracks and mineral grains. It is a promising framework for reliable determination of thermal conductivity as described by Bayuk et al. (2011). However, the application of these models requires data on many additional parameters determined through calibration on experimental data on rock thermal properties, which is not always accessible.

The weighted arithmetic mean model is used to determine rock volumetric heat capacity as it is a scalar property. However, very often, calculating volumetric heat capacity via weighted arithmetic mean model results in large errors. This is reasoned by uncertainties in data on volume fractions of rock components (minerals and fluids) and in data on volumetric heat capacity of rocks and rock components. There is limited available published data on rock volumetric heat capacity due to the lack of applications in the past. Analysis of these data shows that high uncertainties are not rare cases. For example, assessment of volumetric heat capacity via data on rock thermal conductivity and thermal diffusivity presented by Eppelbaum (2014) yields volumetric heat capacity of 4.42 MJ·m^{-3}·K^{-1}, 5.15 MJ·m^{-3}·K^{-1}, 5.21 MJ·m^{-3}·K^{-1} for shale, marlstone and chalkstone, respectively. At the same time, the volumetric heat capacity of water is 4.19 MJ·m^{-3}·K^{-1}. This emphasizes the necessity of accounting for the influence of porosity and pore-filling fluids on rocks' volumetric heat capacity.

Simultaneously, many simulators for BPSM and hydrodynamic modelling use theoretical models (including the Lichtenecker model) for calculating both rock

thermal properties. Results of such modelling in some cases are questionable. Therefore, theoretical modelling is a promising framework for determining the thermal properties of rocks although requiring enhancement.

The application of published experimental data or databases (see, e.g. Bär et al., 2019) on rock thermal properties is not a rare case in today's geothermal investigations. Meanwhile, even small changes in the mineral composition of rocks, its porosity, the geometry of pore-crack space, and pore-filling fluids can essentially change both rock thermal conductivity and volumetric heat capacity. The existing databases on rock thermal properties usually are not satisfying about:

- data on rock volumetric heat capacity;
- data on thermal anisotropy of rocks;
- lithological description of investigated cores;
- data on the influence of different fluid saturation on rock thermal properties;
- data on thermal property dependence on porosity;
- information on the effect of fracturing on rock thermal properties and thermal anisotropy.

Thus, the application of published experimental data or databases can result in significant uncertainties. Despite the availability of extensive previous data on rock thermal properties, laboratory measurements of rock thermal properties on cores are still highly relevant.

Well-log based approaches are one of the most robust and commonly used approaches for determining rock thermal properties. This is because:

1. Well-logging data is available almost for all industrial wells. It is not a rare case when well-logging is conducted from the top to the bottom of the well.
2. Well-logging tools provide registration of rock properties with a relatively high spatial resolution.

3. Well-logging provides data on complex of petrophysical properties (porosity, shaliness, saturation, etc.).

1.3 Possibilities and limitations of traditional approaches for well-log based determining rock thermal properties

Analysis of literature data shows that a significant part of publications in geothermics that refer to well-log based determining rock thermal properties concern thermal conductivity. This is justified by the lack of applications of data on volumetric heat capacity in the past and that the data on rock thermal conductivity are of a key importance for determining conductive heat flow density at geothermal investigations of the Earth crust.

The main part of approaches for determining rock thermal conductivity from well-logging data is based on the analysis of interrelations between thermal and other physical properties of rocks. One of the first research results on interrelations between thermal conductivity and other physical properties were published in the 1950s by Dahnov & Djakonov (1952) and Ziefuss & Vliet (1956).

For the first time, an urgent need for an effective well-log-based approach for determining rock thermal conductivity occurred in Germany for superdeep drilling well KTB (1990-1994). This need was principally conditioned by drilling without coring. Moreover, one of the main objectives of the superdeep drilling project was determining vertical variations of heat flow density, which requires reliable data on rock thermal conductivity along the well. The accompanying increase in relevance of data on rock thermal conductivity for applied geothermics and petroleum engineering stimulated many researchers. It resulted in an increased number of publications concerning well-log based approaches for determining rock thermal properties.

Existing approaches for determining rock thermal properties from well-logging data can be classified into two main categories: (1) regression-based and (2) theoretical model-based.

The regression model-based approach implies determining dependencies between the rock thermal properties and well-logging parameters using standard or advanced regression analysis methods. Numerous authors have demonstrated for different lithological types the interrelation between thermal conductivity and other rock properties (in most cases density or sonic velocity) via statistical analysis (Bullard & Day 1961; Cermak et al., 1967; Anand et al., 1973; Poulsen et al., 1981; Lovell 1985; Beziat et al., 1992; Griffiths et al., 1992; Zamora et al., 1993; Sahlin & Middleton 1997; Kukkonen & Peltoniemi 1998; Sundberg et al., 2009; Popov et al., 2011; Gegenhuber & Schon 2012). Researchers also applied multiple linear and nonlinear regression models to characterize interrelations between thermal conductivity and other rock physical properties inferred from well-logging data (Goss et al., 1975; Goss & Combs 1976; Evans 1977; Balling et al., 1981; Molnar & Hodge 1982; Vacquier et al., 1988; Doveton et al., 1997; Popov et al., 2003; Ozkahraman et al., 2004; Hartmann et al., 2005; Fuchs et al., 2014; Fuchs et al., 2015). Some studies use artificial neural networks for predicting thermal conductivity (Goutorbe et al. 2006; Singh et al. 2007; Khandelwal 2010; Singh et al. 2011; Gasior & Przelaskowska, 2014). For porous rocks, the high contrast between the physical properties of the pore-filling fluids and the rock matrix physical properties is the primary control of the correlations between thermal properties and other physical properties (Popov et al., 2003). Therefore, the application of the regression model-based approach might be challenging in the case of low porosity and low contrast of physical properties in the rock components. Moreover, the established regression equations between rock thermal properties and well-logging

data are related to the deposition environment and can be applied only for the analogous rock with similar well-logging data (Blackwell et al., 1989).

Some of the mentioned disadvantages can be resolved via a theoretical approach. More than thirty theoretical models (or so-called mixing laws) have been developed to determine the effective thermal conductivity of rocks. Some studies are focused on determining appropriate mixing law to compute rock thermal conductivity from knowledge on mineral content (via XRD analysis) and porosity (e.g. Brigaud et al. 1990; Demongodin et al. 1991). Other researchers addressed approaches for determining rock thermal conductivity from either lithology or mineralogy of rocks inferred from well-logging data, data on rock porosity and available data on thermal properties of rock constituents (Merkel et al. 1976; Dove&Williams 1989; Vasseur et al. 1995; Midttømme et al. 1997; Hartmann et al. 2005). The application of mixing laws requires data on the volumetric fractions of the rock-forming components, reliable data on their thermal properties, and, sometimes, a correction factor, which accounts for structural peculiarities of rocks. This approach is not restricted to a specific geological area. It can be applied for well log-based prediction of the thermal properties of low-porosity rocks, with uncertainties of less than 10% (e.g., Fuchs et al., 2018). However, a weak point of this approach is the essential frequent uncertainty of theoretical modelling. Calculating the effective thermal conductivity via different thermal conductivity models using the same rock matrix thermal conductivity and pore-filling fluid values results in considerable variance, sometimes up to 100% (e.g., Hartman et al., 2005).

In literature, there is a lack of studies concerning well-log based predictions of volumetric heat capacity. Fuchs et al. (2015) attempted to develop a universally applicable approach for determining rock specific heat capacity. However, the reported results correspond to artificially created datasets, and its applicability

should be tested on reliable experimental data. A common practice is calculating volumetric/specific heat capacity from the volume fractions of rock constituents or the relation between thermal conductivity, thermal diffusivity, and volumetric heat capacity (see, e.g. Goto & Matsubayashi 2008).

The suggested solutions for well-log based determining rock thermal properties have several disadvantages:

1. Neglecting thermal anisotropy of rocks, which is a distinguishing characteristic for many rock types, especially organic-rich shales and clay-rich rocks (Pribnow and Umsonst, 1993). Recent investigations have revealed that the thermal anisotropy coefficient of organic-rich shales is typically 1.2-2 and can often exceed 2-3 (Popov et al., 2017). One of the few approaches to consider thermal anisotropy was suggested by Deming (1994) and implies analysis of an empirical relationship that relates the thermal conductivity anisotropy and thermal conductivity perpendicular to the bedding (based on measurements on 89 rock samples gleaned from the literature). However, testing the suggested approach with our experimental data showed high and unsatisfactory uncertainties in well log-based predictions of rock thermal conductivity via the Deming correction approach. Another approach presented by Pasquale et al. (2011) implies analysis of the effect of orientation of the clay and mica platelets during burial on the vertical component of thermal conductivity. However, this approach is not universally applicable, e.g. in case of organic-rich shales since thermal anisotropy of these rocks is conditioned not only by orientation of clay and mica platelets but also by the distribution of organic matter.

2. Neglecting influence of *in situ* pressure, temperature and saturation of rock thermal properties in case of thermal anisotropy. Some studies describe an opportunity to account for *in situ* thermobaric conditions and saturation (see, e.g.,

30

Hartamann et al., 2005), but this is applicable only for isotropic rocks. Wang et al. (2018) experimentally showed that in case of thermal anisotropy, distinct effects of temperature on principal components of thermal conductivity exist. Moreover, the effect of imposed fracturing on thermal anisotropy must be assessed in case of thermal anisotropy as described by Popov et al. (2017).

3. Neglecting rock heterogeneity. There are many cases when spatial resolution of instruments used for measuring rock thermal properties differs from the spatial resolution of considered well-logging tools. This was never accounted for during regression analysis or theoretical modelling. For example, the commonly used divided bar technique requires core samples of 10-30 mm thick whereas the typical vertical resolution of standard well-logging tools is about 0.5 m. Obviously, for such cases, the data on rock thermal properties cannot be directly related to well-logging data. Thus, in the case of thin layering or high heterogeneity of rocks, special operations are required to account for the difference in spatial resolution before the regression analysis or theoretical modelling.

4. Lack of implementations of machine learning techniques for problem solution. As previously mentioned, there are only a few publications related to the application of simple fully connected neural networks for determining rock thermal conductivity. However, accounting for modern advances in machine learning algorithms, a comparison study of different machine learning algorithms for predicting thermal conductivity and volumetric heat capacity is required.

5. Lack of studies related to organic-rich shales. In the context of increasing demand on thermohydrodynamic modelling of thermal EOR, the data on lateral variations of thermal properties of organic-rich shales is highly required. Therefore, well-log based approach for determining rock thermal properties is an effective way

31

for the problem solution. However, typical thermal anisotropy and thermal heterogeneity of organic-rich shales, as described by Popov et al. (2017), require the development of advanced algorithms to be accounted for.

6. Poor metrological testing of the suggested approaches. A common practice of existing publications is yielding mean average error (MAE) or root mean squared error (RMSE). Only in some rare cases, authors also provide standard deviation of MAE or RMSE. However, these data do not allow characterizing uncertainty of prediction results. Moreover, when characterizing the uncertainty of prediction results, the confidential probability level must be reported. Another reason for poor metrological testing of the suggested approaches is again related to heterogeneity (see point 3) and differences in spatial resolution of instruments used to measure rock thermal properties and well-logging tools.

7. Lack of sensitivity studies of the influence of uncertainties in well-logging data on results of well-log based determination of rock thermal properties. Sensitivity studies of either regression or theoretical models determine the necessary input data quality for predicting rock thermal properties with specified uncertainty. Moreover, the sensitivity study of the regression model provides information on each well-logs' importance and subsequently allows optimizing the number of well-logs.

8. Lack of well-defined, reproducible workflows for determining rock thermal properties accounting for thermal anisotropy and *in situ* pressure, temperature and saturation. To ensure practical implementation of well-log based approaches for determining rock thermal properties, well-defined reproducible workflows are required. Literature shows that there are only a few publications describing all the necessary operations properly for predicting thermal properties of isotropic rocks (see, e.g. Hartmann et al., 2005). However, advanced workflows are

required for determining rock thermal conductivity and volumetric heat capacity accounting for *in situ* pressure, temperature, saturation, rock heterogeneity and thermal anisotropy.

In summary, the above disadvantages do not allow the exhaustive implementation of well-log based approaches for rock thermal properties prediction at geothermal investigations of geological profiles.

1.4 Importance of accounting for rock anisotropy and heterogeneity

Since many rock types are more or less anisotropic (Pribnow and Umsonst, 1993; Popov et al., 2017; etc.), neglecting thermal anisotropy (that very often amounts to 2 and 3) can negatively affect the results of modelling. Popov et al. (2013) performed a comprehensive sensitivity analysis of the effect of uncertainty in reservoir thermal property data on heavy oil recovery performance. Four technologies (steam flooding, steam-assisted gravity drainage, toe-to-heel air injection, and hot water flooding) of thermal enhanced oil recovery were considered during sensitivity analysis. The sensitivity study revealed that uncertainties in rock thermal properties result in errors in cumulative oil production of about 20-70 %. Therefore, reliable data on rock thermal conductivity accounting for thermal anisotropy determine the economic efficiency of thermal enhanced oil recovery technologies. Moreover, without reliable data on rock thermal properties, largely different scenarios for organic matter maturation may result from basin and petroleum system modelling affecting results of assessment of hydrocarbon potential for a given region (Chekhonin et al., 2019).

Because of the limitations of traditional instruments for measuring rock thermal properties, a very common practice in the previous studies is a joint analysis of well-logging data and incomparable in terms of spatial resolution data on rock thermal

properties (Goss et al., 1975; Vacquier et al., 1988; Fuchs et al., 2014; etc.). Neglecting differences in the vertical resolution of analyzing data in case of heterogeneous rocks obviously leads to unreliable results. Hence, accounting for rock heterogeneity before the regression analysis or theoretical modelling is crucial for obtaining reliable models that can be used to predict thermal properties for similar rocks.

The following example demonstrates the problem. Data on rock thermal conductivity inferred from continuous thermal core logging (with a spatial resolution of 1 mm) were used to assess different scale rock heterogeneity. The data of two organic-rich shales and carbonate rocks of heavy oil field were used in this example. The coefficient of variation (ratio of the standard deviation to mean value; CV) of thermal conductivity is calculated to assess rock heterogeneity. As the average vertical resolution of well logging tools is about 0.5 m and assuming an average length of full-sized core samples of 0.1 m, the coefficient of variation of thermal conductivity was calculated within moving windows of 0.5 m and 0.1 m.

Figure 1 plots the calculated coefficients of variation of thermal conductivity for two organic-rich formations and carbonate rocks of the heavy oil field. There is an essential difference between CV calculated on a well-logging scale and CV calculated on the scale of laboratory investigations. The difference, in some cases, amounts to 100%.

One can conclude, the data inferred from well-logging cannot be directly processed and analysed with data inferred from laboratory investigations of core samples. However, due to limitations of traditional instruments for measurements of rock thermal properties (special requirements to core sample geometry, a limited amount of core samples, etc.), in most cases, there is no possibility to consider and to account for rock heterogeneity of rocks before the regression analysis or

34

theoretical modelling. Thus, the application of published regression equations or parameters of theoretical models for determining rock thermal properties from well-logging data should be carefully used.
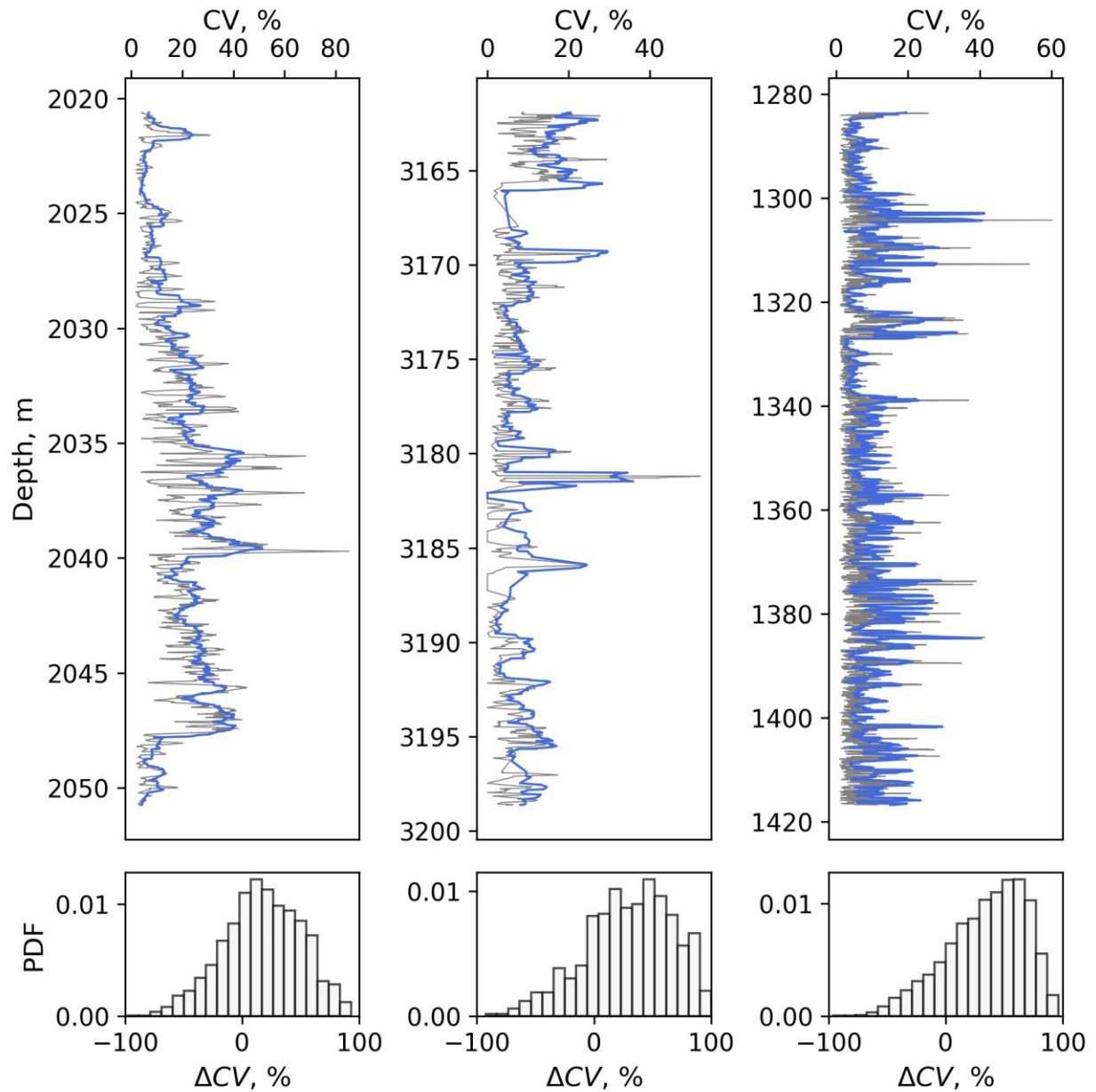
Figure 1. CV for two organic-rich shales (left and central panel) and carbonate rocks of heavy oil field (right panel) within moving windows of 0.1 m (grey colored line) and 0.5 m (blue) colored line. Histograms plot relative difference between CV calculated within 0.5 m and CV calculated within 0.1 m.

1.5 Integration of thermal core logging data with well-logging data – a new framework for the improvement of reliability of data on rock thermal properties inferred from well-logging data

Many of traditional instruments for measuring thermal conductivity and volumetric heat capacity were firstly developed for measurements on industrial materials. Compared to sedimentary rocks, these materials are:

- mainly isotropic and homogeneous,
- mechanically well treated when samples are prepared for measurements,
- stable according to their physical properties,
- sustainable to high pressure that occurs when measuring surface is put on samples.

Moreover, there is no need for a high rate when measuring thermal properties of industrial materials.

The structure of industrial materials is thus so different from sedimentary rocks, especially from highly porous, fractured, anisotropic, heterogeneous samples. As described by Popov et al. (2020a), the principal reasons for discordance between the required level of a measurement instrument for petroleum engineering and the abilities of the traditional instruments are:

1. Traditional instruments cannot provide measurements on full-sized core samples without special mechanical preparation of core samples. This aspect excludes the possibility of massive measurements and registering different-scale spatial variations of rock thermal properties.

2. Poor metrological quality of measurement results for highly porous and fractured core samples due to the significant influence of interfacial thermal resistance.

3. The traditional instruments are not appropriate for standard core plugs that are the basis for petrophysical laboratory investigations.

4. Highly porous and fractured core samples are fragile and, in many cases, are easily crushed under high pressure that occurs when measuring surface is put on samples. Consequently, it excludes the possibility of repeated measurements of rock thermal properties at different fluid saturation.

5. Impossibility of conducting simultaneous measurements of rock thermal conductivity and volumetric heat capacity on the same core samples. Moreover, the modern differential scanning calorimeters measure specific heat capacity on small rock samples, typically less than 1 cm^3. Thus, the data on rock density is required to calculate volumetric heat capacity, and this small volume usually does not reflect rock heterogeneity.

6. Absence of possibility for registering detailed vertical variations of thermal anisotropy coefficient.

7. Absence of possibility for assessing thermal heterogeneity of rocks.

8. Necessity in scrupulous mechanical treatment of flat surface to exclude the influence of interfacial thermal resistance on measurement results.

Concurrently, the optical scanning method was designed especially for measurements of rock thermal properties by Popov (1983) and provided an opportunity for registering data on rock thermal properties on a qualitatively new level. After enhancing the practical and theoretical basis of the suggested method (see, e.g. Popov 1984, 1997; Popov et al. 1985) as described by Popov et al. (2016) and Popov et al. (2019), the modern thermal core logging technique has the following inaccessible previously features:

1. Simultaneous determination of thermal conductivity and volumetric heat capacity during one experiment for the same core sample.

2. Measurements are conducted on full-sized, split, broken core samples, core plugs, and core cuttings without additional mechanical treatment.

3. Absence of contact between the instrument sensors and the rock sample. Thus, measurements are non-destructive.

4. Determining both thermal conductivity and thermal diffusivity tensor components for every rock sample.

5. High productivity of measurements due to high measurements speed and wide range of permissible lengths of core samples.

6. The modern optical scanning technique provides measurements accuracy and precision for the thermal conductivity of $\pm 1.5\%$ and $\pm 1.5\%$ (confidence level 0.95), respectively, within the range of 0.2-45 $W \cdot m^{-1} \cdot K^{-1}$.

7. The modern optical scanning technique provides measurements accuracy and precision for the volumetric heat capacity of $\pm 2.0\%$ and $\pm 2.0\%$ (confidence level 0.95), respectively, within the range of 0.8-4 $MJ \cdot m^{-3} \cdot K^{-1}$.

8. The spatial resolution of thermal property profiling varies according to measuring regime parameters. Today, the minimal spatial resolution that can be provided with laser optical scanning instrument is 0.2 mm, although the typical spatial resolution is 1 mm.

The effective and vast implementation of the developed experimental basis within joint industrial projects of Skoltech and leading Russian oil and gas companies during 2015-2021 allowed us to collect extensive experimental database on rock thermal properties and well-logging data. It enabled a qualitatively new framework for developing an advanced technique for well-log based determining rock thermal properties.

Optical scanning instruments' unique metrological characteristics allowed us to obtain reliable experimental data on rocks' thermal properties, including organic-rich shales and heavy oil reservoirs. Since the optical scanning instrument has a high spatial resolution, the possibilities for considering rock heterogeneity and

accounting for spatial resolution of other logging tools were also enabled. Moreover, thanks to the possibility of registering coefficient of thermal anisotropy for every core sample, the thermal anisotropy of rocks became accessible for thorough analysis. The extensive database on rock thermal properties and well-logging data is an equally important result of the vast implementation. Thus, qualitatively new possibilities opened up to develop the technique for well-log based determining rock thermal properties accounting for thermal anisotropy, heterogeneity, and *in situ* pressure, temperature and saturation via integrating thermal core logging technique with well-logging data.

1.6   Conclusions

1. Enhancement of BPSM, EOR modelling, techniques of terrestrial heat flow density determination and geothermal prospecting requires advancement in well-log based approaches for determining rock thermal properties via integrating thermal core logging data and well-logging data.

2. To satisfy the present-day needs of petroleum engineering and geothermal investigations, the advanced technique for well-log based determining rock thermal properties should provide reliable data on rocks' thermal conductivity and volumetric heat capacity.

3. The advanced well-log based technique for determining rock thermal properties accounting for thermal anisotropy, rock heterogeneity, *in situ* pressure, temperature and saturation is highly required.

4. A well-defined and reproducible workflow of application of an advanced technique for well-log based determining rock thermal properties accounting for thermal anisotropy, heterogeneity and *in situ* pressure, temperature and saturation is required.

5. Extensive testing and implementation of the advanced technique for determining rock thermal properties is a primary concern for enhancing the quality of data on rock thermal properties and terrestrial heat flow density for improvement of basin and petroleum system modelling and thermal EOR modelling in oil & gas science and industry.

Chapter 2. Determining thermal conductivity and volumetric heat capacity of anisotropic rocks based on regression analysis

Literature review (presented in Chapter 1) showed that many studies were performed concerning interrelations between thermal properties and other physical properties. However, the gained results showed that there are no unique correlation trends for sedimentary rocks or other rock types. Therefore, an important conclusion that can be inferred is that many factors can control both rock thermal conductivity and volumetric heat capacity. These factors are mineral composition, porosity, the geometry of pore-crack space, type of saturating fluid, degree of compaction, and characteristics of intergranular contacts. Hence, there are no universally applicable correlations that can be used for predicting rock thermal properties.

Considering the complex nature of interrelations between rock thermal and other physical properties, the studies related to correlation analysis are still highly relevant. Moreover, in the light of the modern experimental basis of thermal petrophysics, these studies should be performed accounting for thermal anisotropy and heterogeneity.

2.1 Determining thermal properties accounting for thermal anisotropy via sonic log data

For most porous rocks, the relation between thermal conductivity and other physical properties (that can be inferred from well-logging data) is principally conditioned by the essential contrast of thermal conductivity of rock matrix and pore-filling fluid. This contrast is often more than ten times, as it may be seen from Figure 2 (upper panel). For low-porous organic-rich shales, the correlations are principally conditioned by low thermal conductivity and high organic matter content, as Popov et al. (2017) described. If the contrast of thermal conductivity of rock matrix and pore-filling fluid is large, a large contrast between volumetric heat

capacity of the rock matrix and pore-filling fluid / organic matter also occurs (Figure 2, bottom panel).
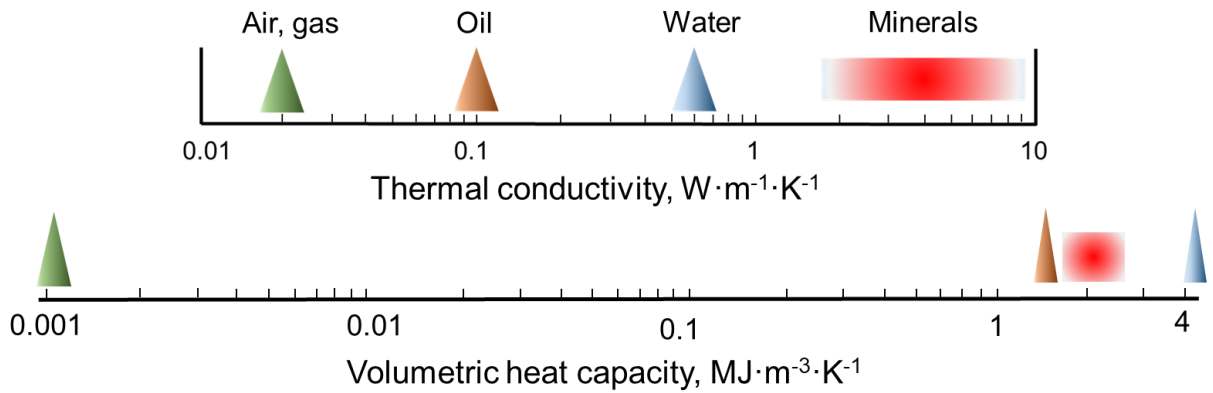
Figure 2. Thermal conductivity and volumetric heat capacity for rock-forming minerals and pore fluids.

The anisotropy of sedimentary rocks can be conditioned by directional alignment of clay particles, microcracks, kerogen inclusions, low-aspect ratio pores and layering as reported by Sayers (2013). Chekhonin et al. (2018) showed a statistically significant correlation between thermal anisotropy coefficient and Young's modulus anisotropy for organic-rich shales that is due to the high content of organic matter and the contrast between properties of the rock matrix and organic matter. Moreover, Kim et al. (2012) performed a set of laboratory experiments and showed for three types of anisotropic rocks (gneiss, shale, and schist) that principal axes of thermal conductivity, elastic moduli, and p-wave velocity coincide and have the same directions. Thus, assuming a structural nature of thermal anisotropy we can conclude that it is in principle possible determining rock thermal conductivity accounting for thermal anisotropy from well-logging data.

2.1.1 Workflow

In this Section, we suggest a novel well-log-based approach for determining rock thermal conductivity and volumetric heat capacity of sedimentary rocks accounting for thermal anisotropy, heterogeneity, in situ pressure, temperature, and saturation. The developed approach consists of several principal steps.

In the first step, lithological differentiation is performed using well-logging data via constructing a rock volumetric mineralogical model. A rock volumetric mineralogical model can be obtained via inversion of standard logs or via pulsed neutron gamma-ray logging (Serra, 1986). Geological differentiation of intervals where core samples are available can be performed by a geologist or based on petrophysical laboratory investigations.

In the second step, for each lithological type, the directions of principal axes of thermal conductivity are determined. This step is of a special significance since directions of principal axes do not always coincide with directions parallel and perpendicular directions to the bedding plane that can be determined via visual analysis of core samples. The directions of principal axes of thermal conductivity can be inferred from results of thermal core logging along several distinct scanning lines as described by Popov et al. (2016). Moreover, these directions can be determined through a set of geomechanical tests of standard core plugs as it was reported by Kim et al. (2012) or through a multilevel ultrasonic sounding as described by Tikhotsky et al. (2018).

In the third step, measurements of rock thermal conductivity along directions of principal axes for each lithological type are performed with optical scanning technique at atmospheric pressure and temperature. Simultaneously, measurements of rock volumetric heat capacity are conducted. Additionally, sonic velocities along

43

these directions are determined from sonic log data. Sonic velocities can be determined on core samples also.

In the fourth step, the dependencies of rock thermal conductivity and volumetric heat capacity from porosity, saturation, pressure and temperature are determined. This can be performed through laboratory investigations, or some of these dependencies can be inferred from literature data.

Additionally, the regression analysis of "rock thermal conductivity – sonic velocity" and "volumetric heat capacity – sonic velocity" is performed for corresponding directions of principal axes of the thermal conductivity tensor and accounting for rock heterogeneity (in other words, accounting for the difference in spatial resolution of optical scanning instrument and, e.g. sonic log tool). For some rocks, there are no statistically significant dependencies between volumetric heat capacity and sonic velocity. For such cases, another well log data can be involved within the workflow for predicting rock volumetric heat capacity. After that, for each lithological type, rock thermal properties are determined within non-coring intervals from sonic log data at atmospheric pressure and temperature using the established regression equations.

In the fifth step, the predicted thermal property data are corrected for *in situ* temperature, pressure and saturation using the established in the fourth step dependencies. The data on *in situ* temperature can be inferred from temperature logging and data on in *situ* pressure can be inferred from results of the formation test. Wang et al. (2018) showed experimentally that there are different dependencies of thermal conductivity components from temperature and pressure for parallel and perpendicular directions. Thus, these corrections should be included for each principal axes of thermal conductivity.

2.1.2 Case study: thermal properties of organic-rich shales

The suggested approach for the sonic log-based determination of rock thermal properties was tested on data from three wells (A, B, C) drilled through the Bazhenov Formation (West Siberia Basin, Asian part of Russia).

2.1.2.1 Analysis and processing of the available input data

The mineral and petrophysical characteristics of the rocks in the case study are given in Table 1. The Bazhenov Formation was formed under coastal-marine conditions. More detailed information about the geological peculiarities of the Bazhenov Formation was provided by Balushkina et al. (2014). The lithological profiles of the Bazhenov Formation were inferred from high-definition spectroscopy.

Table 1. Lithological and petrophysical characteristics of the rocks in the case study based on XRD analysis results.

Wells	Dominant mineral composition		Organic matter		Reservoir properties	
	Mineral	Mean mass content, % (SD)	Kerogen type	Mean TOC, % (SD)	Porosity, % (SD)	ln(Permeability), mD (SD)
A, B, C (Bazhenov Formation)	Silicate minerals (SiO_2)	55.1 (22.3)	II	16.5 (7.0)	1.1 (0.6)	-2.8 (2.3)
	Pyrite	4.3 (4.0)				
	Albite	7.2 (3.4)				
	Illite	9.4 (7.2)				
	Calcite	10.1 (15.6)				
	Carbonate minerals	78.1 (25.8)				
	Clay minerals	1.4 (2.7)				

*SD stands for standard deviation, TOC stands for total organic carbon. Kerogen typing was performed according to Tissot and Welte (1984). ln stands for natural logarithm. For specific depth points, the sum of mineral content, organic matter and porosity yields 100%.

According to Chekhonin et al. (2018), the Bazhenov Formation in the investigating region is characterized by negligible 3D thermal anisotropy (that was assessed on flat ends of full-size core samples) and can, therefore, be treated as a transversely isotropic medium (2D anisotropy) with the vertical axis of symmetry.

2.1.2.2 Thermal core logging results for highly anisotropic rocks of the Bazhenov Formation

Continuous thermal core logging was conducted on 1062 full-sized core samples from three wells (42 m in total). Figure 3 plots typical full-sized core samples of the Bazhenov Formation.

Figure 3. Photograph of typical unsawed full-sized core samples of the Bazhenov Formation.

Since the principal axes of the thermal conductivity tensor are parallel and perpendicular to the bedding plane, scanning lines were chosen parallel and perpendicular to the bedding plane on the flat surfaces of the sawed core samples.

Continuous profiles of the thermal conductivity components parallel and perpendicular to the bedding plane directions and the volumetric heat capacity for full-diameter core samples of the Bazhenov Formation recovered from three wells are plotted in Figure 4. Statistical assessments of the variations in rock thermal conductivity parallel and perpendicular to the bedding plane, coefficient of thermal anisotropy ($K_T = \lambda_{\parallel} \cdot \lambda_{\perp}^{-1}$), and coefficient of thermal heterogeneity ($\beta = (\lambda_{max} - \lambda_{min}) \cdot \lambda_{avr}^{-1}$) are summarized in Table 2.

Table 2. Results of thermal property measurements of the studied core samples.

Formation	Well	$\lambda_{\parallel}$, W·m^{-1}·K^{-1} Mean (SD) (min – max)	$\lambda_{\perp}$, W·m^{-1}·K^{-1} Mean (SD) (min – max)	K_T Mean (SD) (min – max)	β Mean (SD) (min – max)	C, MJ·m^{-3}·K^{-1} Mean (SD) (min – max)	Number of core samples	The total length of core samples under study (m)
Bazhenov Formation	A	1.80 (0.44) (0.75-4.80)	1.28 (0.47) (0.20-4.78)	1.50 (0.36) (1.00-3.12)	0.18 (0.20) (0.03-2.61)	2.00 (0.16) (1.75-2.70)	549	19
	B	1.85 (0.39) (0.82-4.46)	1.36 (0.49) (0.37-2.94)	1.49 (0.36) (1.00-3.01)	0.20 (0.15) (0.04-2.28)	1.90 (0.11) (1.65-2.31)	374	17
	C	1.98 (0.43) (1.28-3.26)	1.55 (0.68) (0.71-3.12)	1.39 (0.28) (1.00-2.78)	0.17 (0.13) (0.03-0.78)	1.95 (0.08) (1.77-2.22)	139	6

Systematic thermal anisotropy of the Bazhenov Formation rocks is principally conditioned by a specific distribution of organic matter (Balushkina et al., 2014). The distribution of kerogen is uniform, and areas with accumulations of kerogen within rock samples have elliptical, spotted, and layered-plane horizontal-lenticular fibre forms.
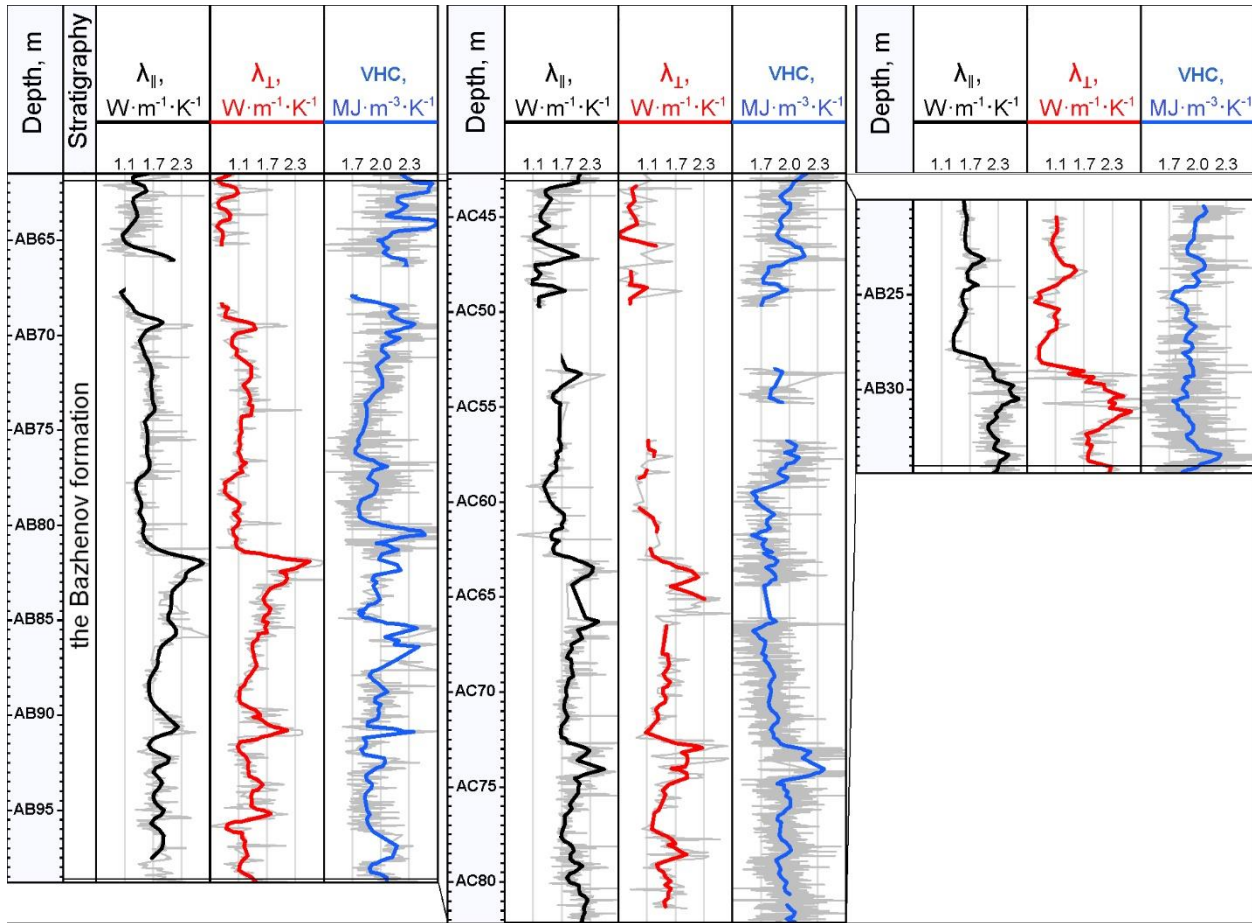
Figure 4. Results of rock thermal property measurements for wells A (left), B (middle), and C (right). λ stands for rock thermal conductivity; subscripts ‖ and ⊥ stand for the thermal conductivity components in the directions parallel and perpendicular to the bedding plane, respectively; VHC stands for volumetric heat capacity; grey lines represent the original profiles of the rock thermal properties. Black, red and blue lines represent averaged thermal property profiles in a moving 0.6 window. The first two digits for the depths are hidden for confidentiality here and elsewhere in the text.

2.1.2.3   *Regression analysis results and prediction of rock thermal properties*

For the investigating wells, the results of cross-dipole sonic logging were available. From these results, sonic velocities for parallel and perpendicular to the bedding plane directions were inferred assuming that elastic constants C_{12} and C_{13} are equal and the Thomsen parameters delta is close to zero (see Schoenberg et al., 1996). The vertical resolution of the sonic scanner was 0.6 m. Thus, before the regression analysis, the results of thermal core logging were upscaled (averaged within 0.6 m moving window) to account for rock heterogeneity.

Regression analysis of the data revealed that the dependency between rock thermal conductivity and sonic velocity is the same for all lithological types of the Bazhenov Formation. It may be reasoned by the relatively stable elastic properties of the rock matrix. Therefore, the considering data was not subdivided into smaller datasets according to the results of lithological differentiation. During correlation analysis, a simple linear regression model was used. The available data were subdivided into two random datasets: (1) a training dataset (67% of all the data) and (2) a test dataset (comprising 33% of all the data). The training dataset was used to fit the regression model to experimental data, while the test dataset was used to provide and unbiased evaluation of the regression model fit on the training dataset (terms train and test dataset in a more detailed way are described, e.g, by Goodfellow et al., 2016). The regression analysis of data on rock volumetric heat capacity and sonic velocity revealed no statistically significant dependencies for the considering rocks. Nevertheless, a statistically significant dependence was observed between the rock volumetric heat capacity and the photoelectric factor (PEF). Therefore, subsequent predictions of rock volumetric heat capacity were performed via the data on rock photoelectric factor. The results of correlation analysis of rock thermal conductivity and sonic velocity accounting for thermal anisotropy and rock

48

volumetric heat capacity and photoelectric factor of rocks for training data are plotted in Figure 5.
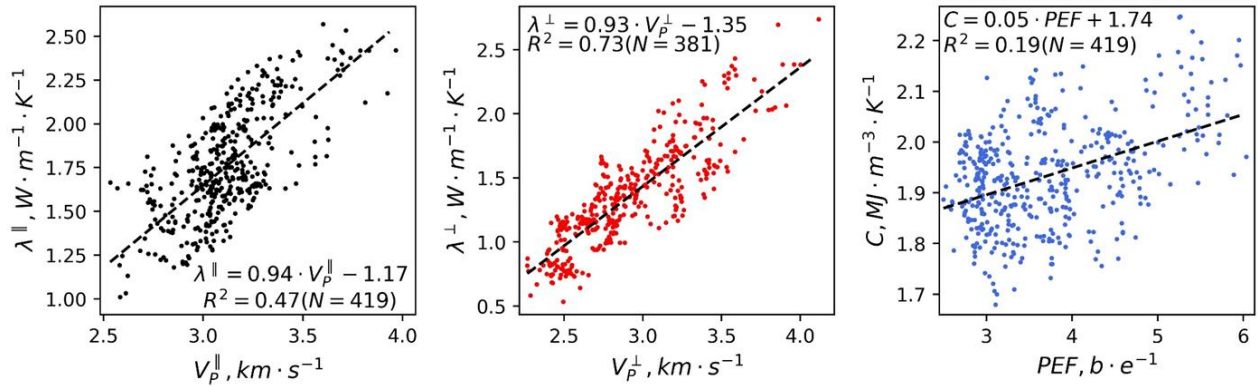
Figure 5. Results of correlation analysis between thermal conductivity and sonic velocity of rocks for parallel (left panel) and perpendicular (central panel) direction to the bedding plane and rock volumetric heat capacity and photoelectric factor (right panel). Dashed line represents the regression trend.

The presented correlations coefficients (square root from the determination coefficient in case of linear regression model) in Figure 5 are statistically significant for a 0.95 confidence level.

The established regression equations were used to predict thermal properties on a train dataset. There are different ways of evaluating the quality of the performance of the proposed approach. To provide a comprehensive evaluation, the following set of statistical parameters were used:

$$RMSE = \sqrt{\frac{\Sigma_{i=1}^{N}\left(X_{meas}^{i} - X_{pred}^{i}\right)^2}{N}} \qquad (1)$$

$$P = \sigma[\Delta] = \sqrt{\frac{\Sigma_{i=1}^{N}(\Delta_i - \overline{\Delta})^2}{N-1}} \qquad (2)$$

$$A = \frac{1}{N}\Sigma_{i=1}^{N}(X_{meas}^{i} - X_{pred}^{i}) \qquad (3)$$

where RMSE is the root mean squared error; P represents the precision; A represents the accuracy; X_{meas} is a measured value, X_{pred} is a predicted value; N is the number

of points; Δ is the relative divergence between the measured and predicted values; and $\bar{\Delta}$ is the mean relative divergence between the measured and predicted values; σ is the standard deviation. In addition, the coefficient of determination (R^2) between predicted and measured values was calculated. The results of prediction of thermal conductivity and volumetric heat capacity on a test dataset are plotted in Figure 6.
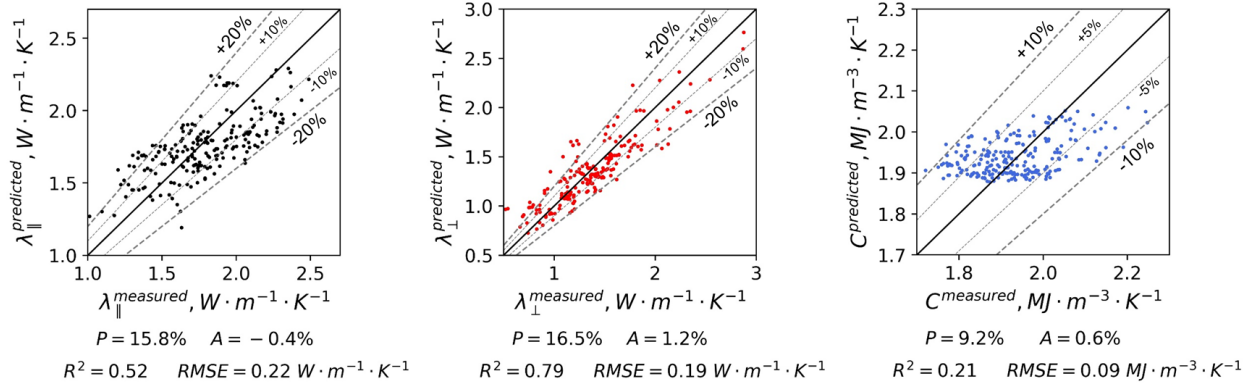
Figure 6. Results of prediction of thermal conductivity for parallel (left panel) and perpendicular (central panel) direction to the bedding plane from sonic velocity and rock volumetric heat capacity from photoelectric factor (right panel). Solid line presents a perfect prediction of rock thermal properties (x=y), grey dashed lines present the prediction uncertainty intervals.

2.1.2.4   Corrections for in situ temperature and pressure

Based on the hydrodynamic well tests results for well A, the approximate average formation pressure and temperature for the Bazhenov Formation are 36 MPa and 100 °C, respectively. Accurate assessment of in situ saturation for the investigated formation is complicated because it exhibits low permeability and porosity (Table 1). Moreover, the formation exhibits a high degree of anisotropy. Hence, we considered that investigated rocks are saturated only by oil.

Following the foregoing workflow, the predicted rock thermal properties require correction for in situ temperature and pressure. As we did not measure rock

thermal properties at high temperature and pressure for the studied core samples, we use data available in the literature to account for in situ conditions.

Recent investigations of rock samples from the Bazhenov Formation performed by Gabova et al. (2020) have revealed that the average decrease in thermal conductivity (λ_l) s at 100 °C is ~2%. However, there are still no reliable experimental data in the literature on the dependencies of thermal conductivity on temperature accounting for the thermal anisotropy of the rocks of the Bazhenov Formation. Thus, we consider that parallel and perpendicular directions, the necessary temperature corrections for the thermal conductivity of core samples from the Bazhenov amounts to 2%.

There is a lack of reliable experimental data on the dependencies of thermal conductivity of organic-rich shales on pressure. For oil shale samples from the Green River formation, an increase of 2% in thermal conductivity was observed at 12 MPa (Prats and O'Brien, 1975). However, for the Bazhenov Formation, the approximate *in situ* pressure exceeds 30 MPa. Research results reported by DuBow et al. (1976) show that the pressure effect on the thermal conductivity of oil shales becomes significant only at high temperatures (400-600 °C). Thus, we can assume that the necessary pressure correction for thermal conductivity is less than 5%.

Waples D. & Waples S. (2004) noted that pressure effects on volumetric heat capacity are negligible because the changes in the specific heat capacity and density of rocks are minor (for the *in situ* pressure of the Bazhenov Formation, the increase in pressure is less than approximately 1%). Thus, the effects of pressure on volumetric heat capacity are not considered in our research. The temperature correction for rock volumetric heat capacity can be inferred from the research results presented by Savest & Oja (2013). According to the given experimental data, the

increase in volumetric heat capacity for oil-bearing shales at temperature 104 °C is approximately 10%.

2.1.3 Conclusions

An approach for determining the thermal properties of rocks accounting for thermal anisotropy from sonic log data was suggested and tested. The approach enables simultaneous determination of the rock thermal conductivity and volumetric heat capacity. Moreover, this approach accounts for the influence of *in situ* thermobaric conditions on thermal properties with differentiation of the effect on distinct thermal conductivity tensor components. It was shown that the approach could be successfully applied based on thermal core logging.

The experimental dataset of rock thermal properties inferred from continuous thermal core logging and reliable sonic-logging data from three wells drilled through anisotropic organic-rich shales were used to develop this approach. The results show that rock thermal conductivity components can be predicted from well-logging data with uncertainties of less than ±16 % for thermal conductivity parallel to the bedding plane and less than ±17 % for thermal conductivity perpendicular to the bedding plane (for a 0.95 confidence level). Volumetric heat capacity can be predicted from well-logging data with an uncertainty of less than ±10 % (for a 0.95 confidence level).

The effectiveness of the new approach is supported by:

- determination of principal axes of thermal conductivity,
- determination of key components of thermal conductivity along its principal axes,
- accounting for rock heterogeneity,
- regression analysis applied to the components of the thermal conductivity.

2.2 Machine learning for determining rock thermal properties from well-logging data

Many studies related to well-log based predictions of rock thermal properties were focused on multiple regression analysis and establishing regression equations that will provide the most precise predictions of rock thermal properties. Some of them used linear regression models (Goss et al., 1975; Goss and Combs, 1976; Hartmann et al., 2005; etc.) when others concentrated on non-linear dependencies (Evans, 1977; Vacquier et al., 1988; etc.).

However, considering traditional theoretical models of rock thermal conductivity (see, e.g. Clauser 2009), I can conclude that there are non-linear and implicit dependencies between rock thermal properties and other physical properties in high-dimensional space. Considering the recent advances in machine-learning methods, the application of such techniques is a promising framework for well-log based determination of rock thermal properties.

As it was mentioned in Section 1.3, there were only several attempts to apply neural network algorithms for predicting rock thermal conductivity (Goutorbe et al. 2006; Gasior and Przelaskowska 2014). Therefore, the applicability of diverse machine learning methods for well-log based determination of rock thermal conductivity should be assessed.

Extending the approach described in Section 2.1 for predicting rock thermal properties from sonic log data, we involve additional logs and multiple regression analysis for predictions. The assessment of the effectiveness of diverse machine learning methods for determining rock thermal properties was performed. The objects of investigations are (1) a conventional reservoir of a heavy oil field that mainly consists of carbonate rocks and (2) an unconventional hydrocarbon reservoir consisting of organic-rich shales, described in Section 2.1.2.

2.2.1 Effectiveness of distinct machine learning algorithms for predicting rock thermal properties: case studies from conventional and unconventional hydrocarbon reservoirs

For the task at hand, supervised machine learning algorithms were considered to reconstruct thermal properties from well-logging data. Well-logging data were used as input data, while experimental data on rock thermal properties were used as an output. The following set of algorithms conceptually distinct from each other were tested for the indirect determination of rock thermal properties: k-Nearest Neighbours (Larose 2014), Neural Network (Hinton 1989), Gaussian Process (Rasmussen & Williams 2006), Random Forest (Breiman 2001), AdaBoost (Freund & Schapire 1997), Gradient Boosting (Friedman 1999), Extra Trees (Pierre et al. 2006) and support vector regression (Platt 1999).

2.2.1.1 Geological settings and field data

The first case study is the heavy oil field located in the Timan- Pechora Basin (the northeastern part of the East European Craton). Target intervals are mainly composed of limestones of the Carboniferous-Lower Permian age. According to petrophysical data, rock porosity within the target interval varies from 0.7 to 26.5 per cent; mean rock porosity is 10.1 per cent (the standard deviation is 7.6 per cent), rock permeability varies from 0.01 up to 1151.18 mD, mean rock permeability is 33.7 mD (standard deviation is 127.96 mD). Pore space is composed of fractures and intergranular space. Reservoir oil is highly viscous (mean value of oil viscosity is 710 mPa·s). Experimental data from the two wells (D and E) were involved in our research. The total length of the investigated interval is 307 and 134 m for wells D and E, respectively.

The thermal properties of rocks were measured using the thermal core logging technique. The total measurement uncertainty was not more than ±2.5 per cent (for

0.95 confidence level). The results of thermal core logging for considering wells D and E are plotted in Figure 7.

According to the results of thermal core logging, we can conclude that the investigated carbonate rocks are characterized by negligible thermal anisotropy and, therefore, can be treated as isotropic rocks.

The second case study is the same described in Section 2.1.2 (see Tables 1 and 2). The results of thermal core logging are presented in Figure 4. Wells A, B and C are also considered in this Section.

The following set of well-logging methods for wells D and E was available: spectral gamma-ray log, density log, sonic log, induction log, calliper and compensated neutron porosity log. Well logging data available for wells A, B and C include the same set of logs and, additionally, cross-dipole sonic log and nuclear magnetic resonance log data. The vertical resolution and depth of investigation depend on the measurement method (see, e.g., Flaum and Theys, 1991), tool specifications, logging speed, etc. Nevertheless, in Table 3, some specifications of the logging tools are summarized to underline (1) the difference in the vertical resolution of thermal core-logging and well-logging data (and the necessity of thermal property upscaling before a joint analysis of the input data in reference intervals) and (2) the vertical resolution of the results obtained via the suggested approach for determining the rock thermal properties from the well-logging data. Well logging data for wells A and E are presented in Figure 8.
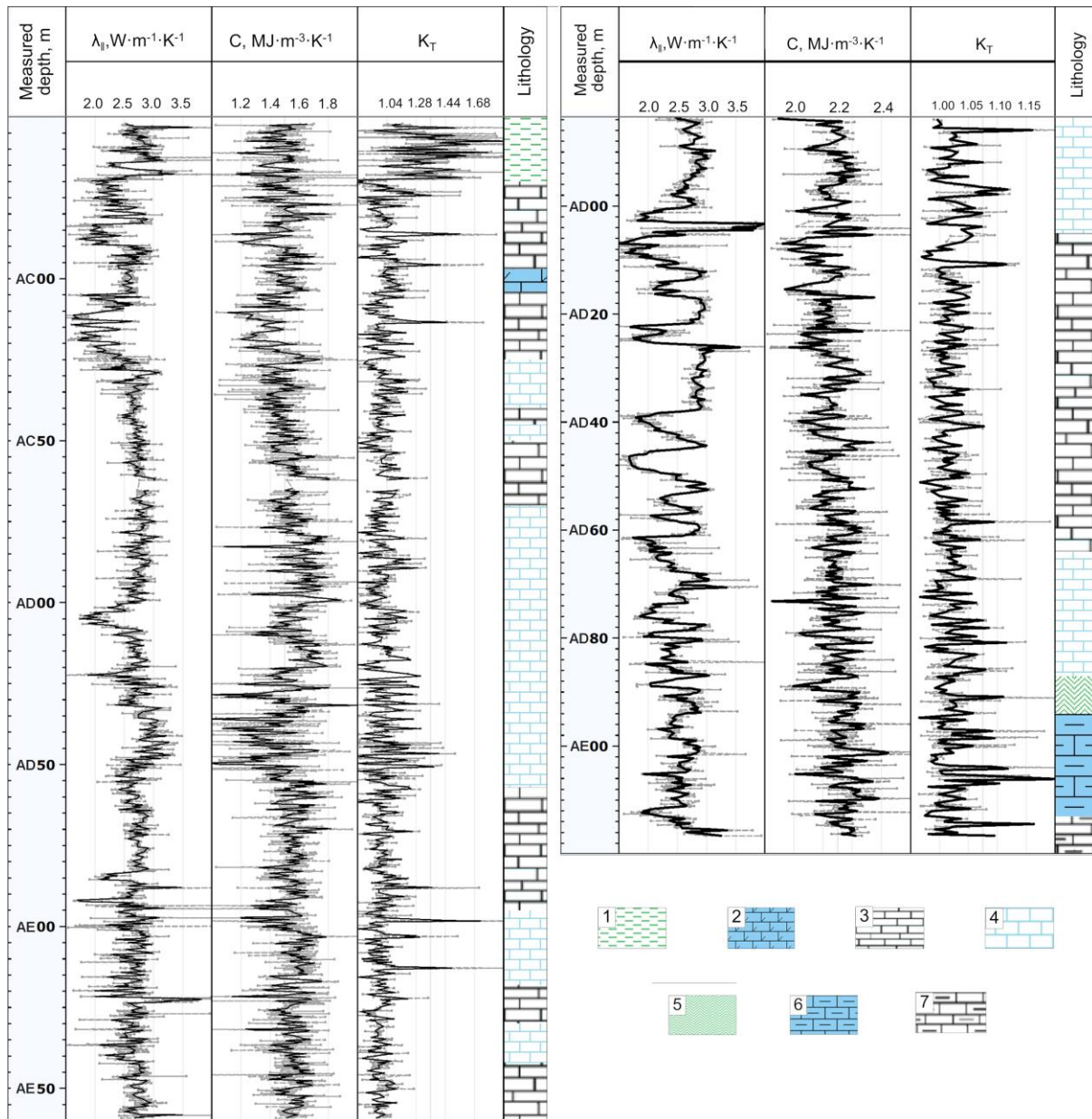
Figure 7. Results of thermal core logging for wells D and E. λ stands for thermal conductivity, C stands for volumetric heat capacity and K_T stands for coefficient of thermal anisotropy. 1 - pelitomorphic with irregular silicification and pyritized, weakly clayey limestones, 2 - argillaceous-terrigenous, pyritized, fissured formations, 3 - organogenic-detrital limestones, 4 – siliceous organogenic-detrital limestones, 5 - interbedding of organogenous-detrital, with silicification, clayey limestone and highly clayey dolomite, 6 - organogenous-detrital, irregularly dolomitized, highly clayey limestones, 7 - organogenous detrital, with silicification, clayey limestones.. Measurement results for each core sample are shown in grey; corresponding results modified to the logging scale are shown in black.
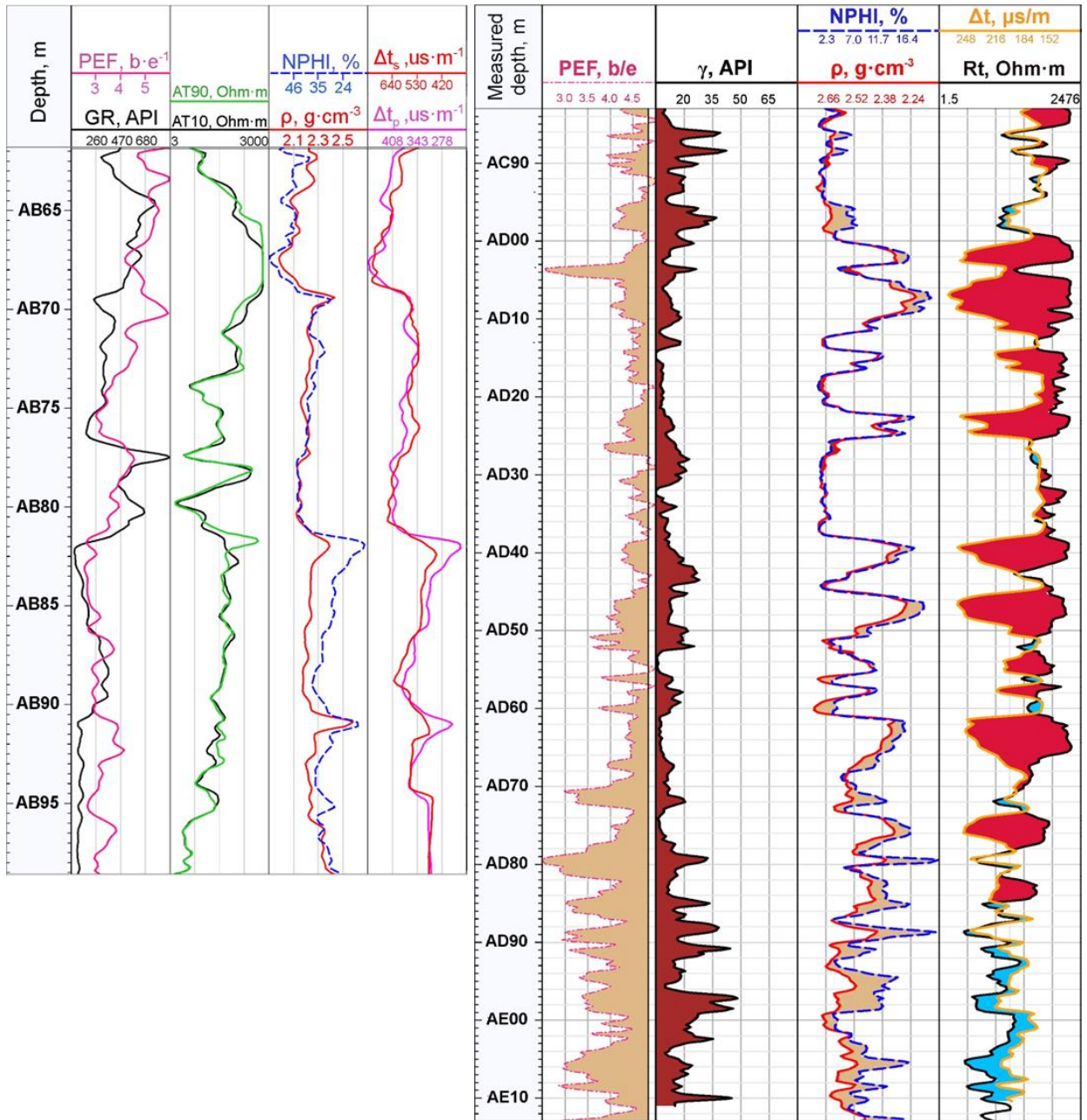
Figure 8. Results well logging for wells A (left panel) and E (right panel).

Table 3. Key specifications of the well-logging tools used.

Parameters	Well-logging tool	Vertical resolution, cm	Depth of investigation, cm	Precision*
Natural radioactivity (γ)	Gamma-ray spectrometry (NGS)	30	25	±2%
Neutron porosity (NPHI)	Compensated neutron logging (CNL) tool	30	23	±6%
Bulk density (ρ) Photoelectric factor (PEF)	Three-Detector Lithology Density (TLD) tool	45	12	±0.01 g·cm^{-3} ±0.8 b/e
Sonic velocity** (V_P and V_S)	Sonic scanner	60	7 borehole radii	±2%
Elemental fractions	LithoScanner	45	20	Depends on logging speed (usually ±2%)
Total porosity, volume of bound water	MR Scanner	45	3-10	Total porosity: ±1%; free fluid porosity: ±0.5%.
Electrical resistivity	Array induction tool (AT10, AT90)	0.3-1.22	25-228	±2%

*Precision of the used tools are given according to the tool documentation and can vary depending on logging speed, absolute values of the physical properties, borehole size, etc.

**For estimation of the Thomsen's anisotropy parameters, the data from a full set of receivers are usually used, so the vertical resolution becomes worse.

2.2.1.2   Calibrating and testing of regression models

The available data both for wells A, B, C and for wells E and D were subdivided into two subsets: (1) a training dataset (comprising 67% of all the data) and (2) a test dataset (comprising 33% of all the data). The training dataset was used to fit the regression model to experimental data, while the test dataset was used to provide an unbiased evaluation of the regression model fit on the training dataset.

For carbonate rocks of the heavy oil field, we used all well logs for input. For organic-rich shales of the Bazhenov Formation, the following set of input parameters was used: neutron porosity (NPHI), bulk density (ρ), photoelectric factor (PEF), radioactivity inferred from gamma-ray logging (GR), total porosity inferred from NMR logging (PHI_{NMR}), sonic velocities parallel and perpendicular to the bedding plane directions ($V_P^{\parallel}$, $V_P^{\perp}$, $V_S^{\parallel}$, and $V_S^{\perp}$), P- and S-wave acoustic impedances ($V_P^{\perp} \cdot \rho$ and $V_S^{\perp} \cdot \rho$), and electrical resistivity inferred from array induction tool application (R_T^{AT10} and R_T^{AT90}). The sonic velocities parallel and perpendicular to the bedding

plane directions were inferred from the standard interpretation of the cross-dipole sonic log data. The available electrical log data did not allow assessing the *in situ* electrical resistivity while accounting for anisotropy.

In our research, we have tuned hyperparameters of regression models using k-fold cross-validation method (Stone, 1974) on a train data set. The cross-validation was performed over the predefined grid of parameters. Cross-validation principally consists of the following steps:

- Firstly, we specify the grid of hyperparameters for regression models. Simultaneously, the configuration of k-folds is specified. We subdivided our train data into three k-folds.
- Secondly, on k–1 folds, optimal hyperparameters are found within the predefined ranges and intervals (grid-search) to fit the regression model. The resulting model is validated on the remaining fold. After that, another set of k–1 folds is used for regression model training. This procedure cyclically repeats k times. Mean squared error (MSE) was used as a performance measure to evaluate the model fit. On every iteration, found hyperparameters and evaluation scores are retained.
- The obtained results are summarized in the third step, and the retained hyperparameters are averaged to select the most optimal regression model.

The tuned hyperparameters for considering machine-learning algorithms are summarized in Table 4.

The determined optimal hyperparameters for regression models on the training data set were used for well-log based determination of rock thermal properties on the test dataset. As well as in Section 2.1.2.3, the performance of each algorithm was assessed via accuracy, precision, RMSE and R^2 between measured and predicted

values on a test dataset. Accuracy and precision are reported for a 0.95 confidence level.

Table 4. The tuned hyperparameters of the considered algorithms

Machine learning algorithm	Tuned hyperparameters
K-Nearest Neighbours	N – neighbors, metric, p order.
Fully-connected neural network	Hidden layer size, activation, learning rate, solver, alpha.
Gaussian Precess Regressor	Alpha, length scale, variance.
Random Forest	Max depth, n estimators, min samples split, min samples leaf.
AdaBoost	learning rate, n estimators, max depth.
Gradient Boosting	learning rate, n estimators, max depth, max features, min samples split, min samples leaf
Support vector regression	kernel, gamma, epsilon
Extra trees	max features, n estimators, max depth, min samples split, min samples leaf

The results of predicted rock thermal conductivity and volumetric heat capacity from well-logging data for carbonate rocks of a heavy oil field are summarized in Table 5. The predicted rock thermal conductivity for parallel and perpendicular directions to the bedding plane and the volumetric heat capacity of organic-rich shales are presented in Table 6.

Table 5. The results of prediction thermal conductivity and volumetric heat capacity on a test dataset for carbonate rocks of heavy oil field.

Machine learning algorithm	λ				C			
	R^2	RMSE $W \cdot m^{-1} \cdot K^{-1}$	P %	A %	R^2	RMSE $MJ \cdot m^{-3} \cdot K^{-1}$	P %	A %
Random Forest	0.88	0.12	9.6	0.5	0.29	0.09	8.5	-0.3
Gradient Boosting	0.86	0.12	10.4	0.6	0.30	0.08	8.1	-0.1
Extra trees	0.85	0.12	10.7	0.7	0.28	0.10	8.6	-0.5
Support vector regression	0.84	0.13	10.9	0.3	0.26	0.11	9.1	-0.1
Gaussian Precess Regressor	0.78	0.14	11.5	0.0	0.25	0.12	9.8	0.1
Fully-connected neural network	0.77	0.14	12.8	-0.1	0.25	0.12	9.7	0.0
AdaBoost	0.66	0.18	12.4	-0.9	0.24	0.13	10.2	0.1
K-Nearest Neighbours	0.62	0.19	12.9	-1.0	0.25	0.12	10.1	0.6

Table 6. The results of prediction thermal conductivity and volumetric heat capacity on a test dataset for organic-rich shales.

Machine learning algorithm	$\lambda_{\parallel}$				$\lambda_{\perp}$				C			
	R^2	RMSE $W\cdot m^{-1}\cdot K^{-1}$	P %	A %	R^2	RMSE $W\cdot m^{-1}\cdot K^{-1}$	P %	A %	R^2	RMSE $MJ\cdot m^{-3}\cdot K^{-1}$	P %	A %
Gradient Boosting	0.81	0.12	7.7	0.0	0.75	0.19	15.4	0.1	0.51	0.09	8.8	0.2
Random Forest	0.80	0.13	7.8	-0.1	0.74	0.20	15.8	0.6	0.54	0.08	8.4	0.1
Extra trees	0.80	0.13	7.9	-0.1	0.73	0.20	15.7	0.5	0.49	0.11	8.9	-0.2
Support vector regression	0.74	0.13	8.7	-0.1	0.69	0.21	16.2	0.8	0.48	0.12	9.0	-0.3
K-Nearest Neighbours	0.73	0.14	8.8	0.0	0.65	0.22	16.9	0.6	0.44	0.13	9.6	0.4
Fully-connected neural network	0.68	0.15	8.9	-0.2	0.70	0.20	16.0	0.4	0.49	0.15	8.9	0.1
Gaussian Precess Regressor	0.61	0.18	9.0	0.1	0.61	0.23	16.9	0.3	0.40	0.18	10.2	0.6
AdaBoost	0.58	0.22	10.1	-0.2	0.55	0.25	17.5	0.2	0.42	0.15	9.9	0.1

The presented results in Tables 5 and 6 show that among considered machine learning algorithms, the ensemble tree-based algorithms (gradient boosting, random forest, and extra trees methods) provided the lowest values on uncertainties when predicting thermal conductivity and volumetric heat capacity of rocks. AdaBoost and K-Nearest Neighbors algorithms, in most cases yielded the lowest performance according to calculated metrics.

Tables 6 demonstrates that thermal conductivity parallel to the bedding plane can be predicted with a precision of 7.7 % that is approximately twice less than prediction precision for thermal conductivity perpendicular to the bedding plane. This can be due to the more significant influence on the thermal properties perpendicular to the bedding plane of micro-cracking from core unloading. Another reason is rock heterogeneity. Since during thermal core logging along the perpendicular directions to the bedding plane we conduct only several measurements on one core sample, the obtaining values of thermal conductivity perpendicular to the bedding plane can be biased due to rock heterogeneity.

Compared to ensemble tree-based algorithms, the fully connected neural network architecture provided higher uncertainties on a test dataset for carbonates and organic-rich shales. Therefore, the application of ensemble tree-based algorithms seems preferable. However, other neural networks architectures (such as convolutional or recurrent neural networks) should also be considered.

2.2.2 Conclusions

The novel approach described in Section 2.1.1 for predicting rock thermal properties from sonic log data was extended by involving additional logs and multiple regression analysis using machine learning. The assessment of the effectiveness of diverse machine learning methods for determining rock thermal properties was performed. The vast experimental data from five wells from conventional and unconventional hydrocarbon reservoirs were considered within the cases study.

Testing diverse machine learning algorithms for predicting rock thermal properties revealed that ensemble tree-based algorithms tend to yield lower accuracy and precision values when predicting rock thermal conductivity and volumetric heat capacity. Thermal conductivity for perpendicular direction to the bedding can be less accurate predicted from well-logging data.

From a comparison of thermal property profiles predicted from well-logging data with experimental data, it can be concluded that volumetric heat capacity, thermal conductivity parallel and perpendicular to the bedding plane can be predicted with uncertainties of less than 9 %, 10 % and 16 %, respectively. Thus, the application of ensemble tree-based algorithms for predicting rock thermal properties accounting for thermal anisotropy is preferable.

2.3 Sensitivity study of regression models for predicting rock thermal properties

The sensitivity analysis of a regression model allows describing the severity of change of the model's output caused by the change of a given input. It is a highly effective instrument for analyzing interrelations between model parameters and model outputs. Moreover, sensitivity analysis is necessary to understand the tolerance of a given model to noise and the acceptable quality of input data.

The regression models established for well-log based determining rock thermal properties are constrained by the deposition environment and can be applied only for the analogous rock with similar well-logging data (Blackwell et al., 1989). A key aspect of predicting rock thermal properties is assessing prediction quality. However, there are many cases when the same well-logging was conducted with different logging tools that provide distinct measurement quality. Table 7 summarizes the technical specifications of four logging tools made by different producers.

There are cases when measurement precision is two (or even three) times lower for specific logging methods when different logging tools are used. Evidently, when the quality of logging data varies, the quality of well-log based predictions of rock thermal properties also varies. Therefore, the assessment of the quality of predicting thermal properties should consider the variations in the quality of well-logging data. Thus, the sensitivity analysis of regression models should be performed to understand the model behaviour when the quality of input data changes.

Table 7. The technical specifications of logging tools suggested by two producers.

Logging method	Producer	Precision*	Measurement range
Gamma ray logging		±5%	0 – 2000 API
Density logging		±0.01 g·cm^{-3}	1.04-3.05g·cm^{-3}
Neutron porosity logging	Schlumberger	0-20 p.u.: ±1 p.u. 30 p.u.: ±2 p.u. 45 p.u.: ±6 p.u.	0-60 p.u.
Sonic velocity logging		±6.6 us/m	131.0 – 1312.0 us/m
Gamma ray logging		±15%	0-2500 API
Density logging		±0.03 g·cm^{-3}	1.7 – 3.0 g·cm^{-3}
Neutron porosity logging	NefteGasGeophysica	±4 p.u.	0 – 40 pu
Sonic velocity logging		±15.0 us/m	120.0 – 500.0 us/m

*Confidence level was not given within the technical specifications and therefore is not reported here. The data on metrological characteristics of tools were inferred from service catalogs of the corresponding producer.

Due to the high predictive advantages of the neural network, a major part of publications related to sensitivity study of regression models developed using machine learning methods concern neural network models (Maosen et al., 2016). Among the variety of suggested methods, the partial derivative (Dimopoulos et al., 1995) and the input perturbation (Zeng and Yeung, 2003) algorithms have superior effectiveness than other sensitivity analysis methods. However, the partial derivative method of sensitivity study can be applied to neural network-based models, whereas the input perturbation method is universally applicable. Moreover, the input perturbation method technically models the actual situation that we can face when predicting rock thermal properties from well-logging data.

2.3.1 Workflow of the input perturbation method

The input perturbation method principally models the effect of random error on model behaviour. The workflow of the input perturbation method that was applied for sensitivity analysis of regression models used for determining rock thermal properties (Section 2.2.1) consisted of several steps.

In the first step, we assume that the regression model is already trained, and the prediction uncertainty was assessed on a test data. The sensitivity study is performed on the test dataset. Therefore, in the first step we specify the value of imposed uncertainty on our input data.

In the second step, we select one input feature and add so-called "white" random noise to it. All the rest input features are fixed. The absolute value of random noise is constrained by the specified in the first step uncertainty. The variance of the selected input feature can be represented as $x_i = x_i + \Delta x_i$, where x_i is the currently selected input variable, and Δx_i is the perturbation.

In the third step, we predict rock thermal property using the perturbated input data and assess the change of prediction quality via selected metrics. Within the case study, we assessed changes in prediction precision.

Steps two and three are cyclically repeated for all input features. The imposed uncertainty varied from 0 to 15% by 1% step.

2.3.2 Sensitivity study of the gradient boosting regression model for predicting rock thermal properties

To understand the tolerance of regression models of the gradient boosting algorithm established within Section 2.2.1 to noise and the acceptable quality of input well-log data sensitivity study was performed based on the input perturbation method.

The results of the sensitivity study of regression models of gradient boosting for determining thermal conductivity and volumetric heat capacity of carbonate rocks of a heavy oil field are presented in Figure 9.
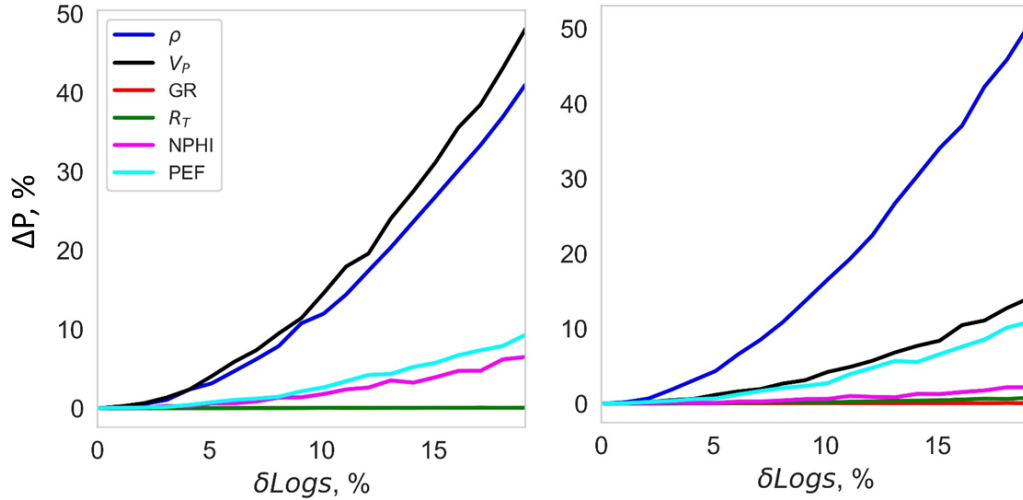
Figure 9. Results of sensitivity study of regression models of gradient boosting for determining thermal conductivity (left panel) and volumetric heat capacity (right panel) of carbonate rocks of the heavy oil field. The input well-logs are presented on the left panel. ΔP stands for relative change of prediction precision. *ΔLogs* stands for input well-log with imposed uncertainty.

As it may be seen from Figure 9, the perturbations in sonic and density logs cause the greatest relative changes in accuracy when predicting both thermal conductivity and volumetric heat capacity of carbonate rocks. Increase of uncertainty in sonic and density log data by 20% results in a relative change of prediction accuracy by more than 40% for thermal conductivity. Whereas for volumetric heat capacity, an increase of uncertainty in sonic velocity data by 20% leads to an increase of prediction accuracy by 12%. The perturbations in data on photoelectric factor, gamma-ray, neutron porosity and electrical resistivity less significantly affect prediction accuracy both for thermal conductivity and volumetric heat capacity.

Assuming that the acceptable prediction accuracy for thermal conductivity is 12% and for volumetric heat capacity is 10%, we can determine the acceptable

66

quality of input well-logging data. As reported in Table 5, the prediction accuracy on the test dataset for rock thermal conductivity and volumetric heat capacity were 10.4% and 8.1%, respectively. Thus, the limits for relative change of prediction accuracy for thermal conductivity and volumetric heat capacity are 15% ($1.6/10.4 \cdot 100\% \approx 15\%$) and 23% ($1.9/8.1 \cdot 100\% \approx 23\%$), respectively. Therefore, the admissible imposed uncertainty in sonic and density log data is about 12% when predicting rocks' thermal conductivity. The acceptable imposed uncertainty in the density log is about 13% when predicting rock volumetric heat capacity.

The sensitivity analysis is also helpful for understanding the importance of input features for determining rock thermal properties. The higher the relative change in prediction precision, the higher is the input feature's importance. The obtained results prove that porosity is the main factor conditioning dependencies between well-logging data and rock thermal properties. High contrast in the physical properties of the rock matrix and pore-filling fluids significantly changes the density, neutron and sonic log responses, and rock thermal conductivity (Popov et al. 2003). For this reason, density and sonic logs are the most important features at well-log based determination of rock thermal properties.

The results of the sensitivity study of regression models of gradient boosting for determining thermal conductivity and volumetric heat capacity of organic-rich shales are presented in Figure 10.
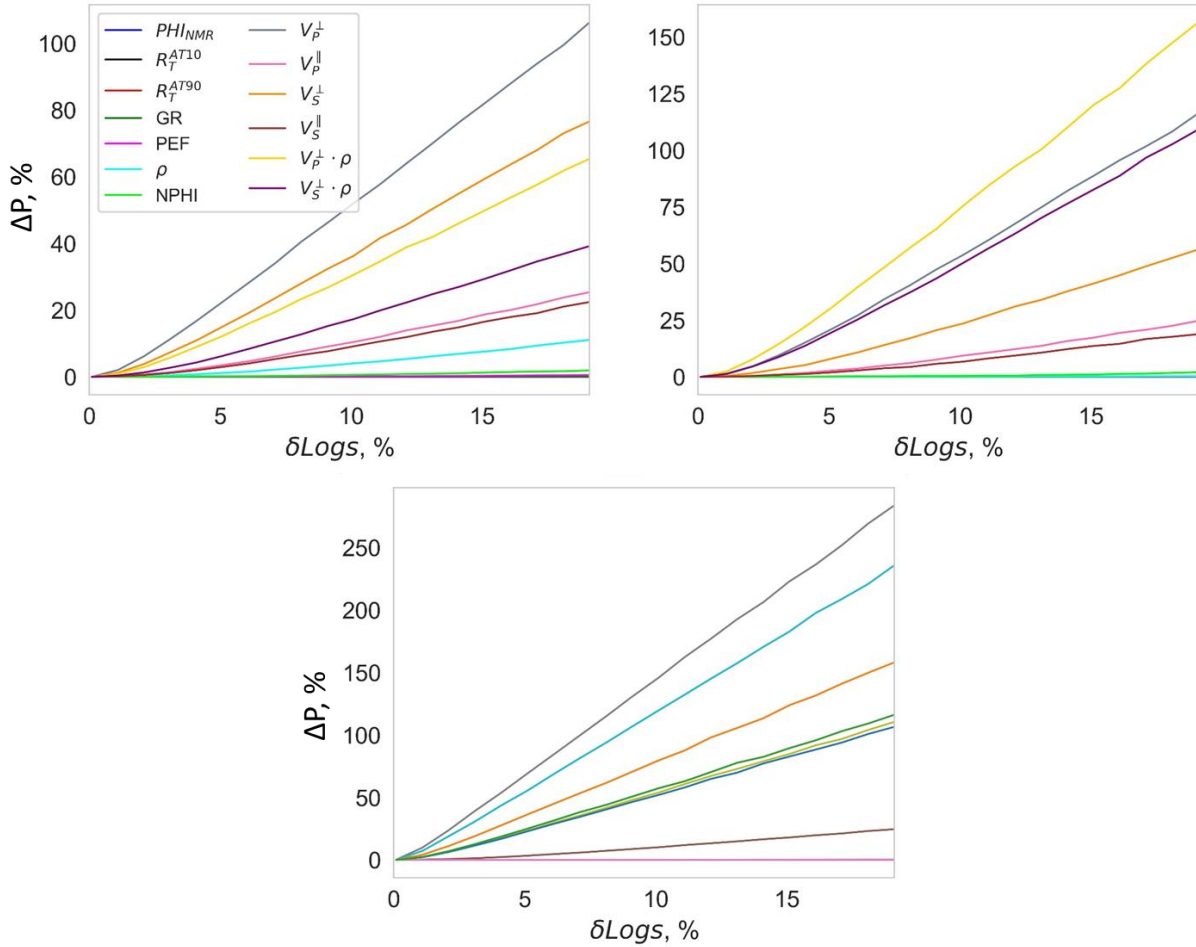
Figure 10. Results of sensitivity study of regression models of gradient boosting for determining thermal conductivity parallel (left panel) and perpendicular (right panel) to bedding plane and volumetric heat capacity (bottom panel) of carbonate rocks of heavy oil field.

The perturbations in the sonic log and data on the acoustic impedance of rocks cause the most remarkable relative changes in precision when predicting thermal conductivity for parallel and perpendicular directions to the bedding plane. For volumetric heat capacity of organic-rich shales, the most significant changes of prediction precision are observed when sonic and density log data are perturbated. The lowest effects on prediction precision are observed when perturbations are made in electrical log data and photoelectric factor both for thermal conductivity and volumetric heat capacity. According to the obtained results in Figure 10, it can be

concluded that the perturbations of neutron porosity and nuclear magnetic resonance porosity do not significantly affect prediction precision for thermal properties. It may be reasoned by the collinearity of these logs with sonic and density log data.

Increase of uncertainty in sonic log data and data on the acoustic impedance of rocks data by 20% results in a relative change of prediction precision by more than 60% for thermal conductivity parallel to the bedding plane. For thermal conductivity perpendicular to the bedding plane, a relative change of prediction precision by more than 60% is observed when uncertainty in sonic and density log data is about 7%. If uncertainty in sonic and density log data reaches 20%, the relative change of prediction precision is two times higher compared to the original one presented in Table 6. Therefore, the higher effect of input data perturbation on prediction precision is observed for thermal conductivity perpendicular to the bedding plane. For volumetric heat capacity, the increase of uncertainty in data on the acoustic impedance of rocks and sonic log data results in a relative change of prediction precision by more than 100%.

Following the same workflow for calculating the acceptable quality of predictions of thermal properties that was demonstrated for carbonate rocks, we could determine the limit values of uncertainty in input features.

The obtained results show that the acoustic impedance, density and sonic velocities have the highest relative importance values. The main reason for the strong correlation between the rock thermal properties and so-called porosity log data (neutron, sonic, and density logs) is a high contrast (exceeding 10:1 in some cases) between the corresponding physical properties of the rock matrix and organic matter, similar to the contrast in porous rocks between physical properties of the rock matrix and pore-filling fluid.

2.3.3 Conclusions

The sensitivity study of regression models of gradient boosting algorithm for predicting rock thermal properties was conducted using the input perturbations method. The obtained results revealed that the highest relative importance for predicting rock thermal properties have so-called porosity log data (sonic, density and neutron log).

For organic-rich shales, an essentially higher effect of input data perturbation on prediction precision is observed for thermal conductivity perpendicular to the bedding plane compared to thermal conductivity parallel to the bedding plane. Increase of uncertainty in sonic and density log by 20 % results in doubled prediction precision (30.8%) for thermal conductivity perpendicular to the bedding plane. Increase of uncertainty in sonic log data and data on the acoustic impedance of rocks data by 20% results in a relative change of prediction precision by more than 60% (which is about 12.3%) for thermal conductivity parallel to the bedding plane.

The obtained results are the basis for determining the acceptable quality of logging data for predicting rock thermal properties. The admissible prediction precision can vary depending on the applications. Therefore, imaginary threshold values for prediction uncertainties were specified, and corresponding calculations were performed to assess the acceptable quality of logging data.

Chapter 3. Determining thermal conductivity and volumetric heat capacity of anisotropic rocks based on theoretical modelling

In most cases, the methods described in Chapter 2 are applicable only for the analogous rock with similar lithological features and with providing same well-logging data. A theoretical model-based approach was implemented to predict rock thermal properties from well-logging data to overcome this limitation. For conventional theoretical thermal conductivity models, the data on volumetric fractions of rock-forming components and their thermal conductivities are required to calculate thermal conductivity. Concurrently, the well-logging suite used for constructing volumetric mineralogical models of rocks can vary from well to well. Another possibility of the theoretical model-based approach is the ability to reconstruct rock thermal properties with different saturation degrees.

In this Chapter, I will describe a novel approach to predict thermal properties by combining well-logging data and theoretical modelling.

3.1. Approach for determining thermal properties accounting for thermal anisotropy via theoretical modelling

To account for the effect of the rock structure on rock thermal conductivity, some theoretical models include specific parameters known as a correction factor (see, e.g. Asaad, 1955). It was shown that the absolute values of the correction factor could depend on the degree of compactness and cementation of rocks (see, e.g., Schoen 2015). Thus, if thermal anisotropy of rocks has a structural nature, we assume that the correction factor can encompass the effect of rock structure along directions of principal axes of thermal conductivity and, therefore, predictions of thermal conductivity accounting for thermal anisotropy from well-logging data combined with theoretical modelling are accessible.

3.1.1 Workflow

The novel approach for determining rock thermal conductivity and volumetric heat capacity of sedimentary rocks consists of several principal steps.

In the first step, lithological differentiation of geological profile and volumetric mineralogical model of rocks within the reference (interval where core samples are available) and target (interval where rock samples are not available and rock thermal properties are inferred from well-logging data) intervals is constructed. Volumetric mineralogical model of a rock can be obtained via inversion o standard logs or via pulsed neutron gamma-ray logging (Serra, 1986).

In the second step, for each lithological type of rock the directions of principal axes of thermal conductivity are determined. As described in Section 2.1.1, they can be inferred from results of thermal core logging along several distinct scanning lines (Popov et al., 2016). Moreover, these directions can be determined through a set of geomechanical tests of standard core plugs (Kim et al., 2012).

In the third step, measurements of rock thermal conductivity along directions of principal axes for each lithological type are performed with optical scanning technique at atmospheric pressure and temperature. Simultaneously, measurements of rock volumetric heat capacity are conducted.

In the fourth step, the thermal conductivity of rock-forming minerals and fluids and correction factors for the appropriate theoretical model are determined by minimising the divergence between the measured and predicted rock thermal conductivity. The theoretical thermal conductivity model is calibrated separately for each lithological type and principal axes direction of thermal conductivity. Additionally, the volumetric heat capacity of rock-forming components are determined via minimization of the divergence between the measured and predicted volumetric heat capacity.

After that, rock thermal properties are determined within non-coring intervals using the volumetric mineralogical model of a target interval, established correction factors along directions of principal axes of thermal conductivity and data on thermal properties of rock-forming components.

Additionally, the dependencies of rock thermal conductivity and volumetric heat capacity pressure and temperature are determined. It can be performed through a set of laboratory investigations, or some of these dependencies can be inferred from literature data.

In the fifth step, thermal property predictions are corrected for in situ temperature and pressure using the dependencies established in the fourth step. The data on in situ temperature can be inferred from temperature logging, and data on in situ pressure can be inferred from the results of the formation test. As well as in Section 2.1, these corrections are distinct for each principal axes of thermal conductivity.

3.1.2 Case study: thermal properties of organic-rich shales of the Bazhenov Formation accounting for thermal anisotropy from well-logging and theoretical modelling

The suggested approach for determining rock thermal properties on the basis of theoretical modelling was tested on data from three wells (A, B, C) drilled through the Bazhenov Formation (Chapter 2). The volumetric mineralogical model for the investigating wells was inferred from high-definition spectroscopy and nuclear magnetic resonance log data. The Bazhenov Formation rocks include nine rock-forming components: illite, kaolinite, bound water, chalcedony, albite, calcite, dolomite, kerogen, and oil.

3.1.2.1 Theoretical models of thermal properties

As it was mentioned, the suggested approach implies the use of theoretical models that contain so-called correction factors and, therefore, enable the determination of the rock thermal conductivity while accounting for structural thermal anisotropy. We investigated three theoretical models of effective thermal conductivity for specific to organic-rich shales:

1. The Lichtenecker-Asaad model (Asaad, 1955), which was adopted in this study for organic-rich shales:

$$\lambda_{\text{eff}} = \lambda_{\text{m}}^{1-f \cdot (V_{\text{Ker}}+V_{\text{fl}})} \cdot \left(\lambda_{\text{Ker}}^{V_{\text{Ker}}} \cdot \lambda_{\text{fl}}^{V_{\text{fl}}}\right)^{f} \tag{4}$$

2. The Krischer and Esdorn model (Krischer and Esdorn, 1956):

$$\lambda_{eff} = \left(\frac{1-b}{\sum_{i=1}^{N} V_i \lambda_i} + \frac{b}{(\sum_{i=1}^{N} \frac{V_i}{\lambda_i})^{-1}}\right)^{-1} \tag{5}$$

3. The Lichtenecker-Rother model (Lichtenecker and Rother, 1931):

$$\lambda_{eff} = \left(\sum_{i=1}^{N} V_i \lambda_i^{\alpha}\right)^{\frac{1}{\alpha}} \tag{6}$$

where λ_{eff}, λ_{ker}, λ_{fl}, and λ_s represent the effective rock thermal conductivity, kerogen thermal conductivity, fluid thermal conductivity, and rock matrix thermal conductivity, respectively; V_{ker}, V_{fl}, and V_i represent the kerogen volume fraction, fluid volume fraction, and volume fraction of the ith component, respectively; and f, b (varies from 0 to 1), and α (varies from -1 to 1) are correction factors in the corresponding theoretical models. The thermal conductivity of fluid is calculated via the weighted geometric mean model.

It is worth noting that the abovementioned models with different values of the correction factors can cover a wide range of theoretical models of thermal conductivity. For instance, the Lichtenecker-Asaad model transforms into the

weighted geometric-mean model if the correction factor "f" equals 1. The Lichtenecker-Rother model transforms into the weighted geometric-mean model if "α" equals 0. The Lichtenecker-Rother model and the Krischer-Esdorn model turn into the weighted arithmetic mean model when the correction factors equal 1. The Lichtenecker-Rother and Krisher-Esdorn models can also turn into harmonic mean models (if b = 0 and α = -1). When "α" equals 0.5, the Lichtenecker-Rother model transforms into a root mean square (Roy et al., 1981). In the study, we do not fix a correction factor in advance; it is an unknown variable that is defined during the calibration stage.

Since volumetric heat capacity is a scalar physical property, the weighted arithmetic mean model is applied to determine the volumetric heat capacity from well-logging data:

$$C = \sum_{i=1}^{N} V_i C_i \tag{7}$$

where C is the rock volumetric heat capacity, V_i is the volume fraction of component i, and C_i is the volumetric heat capacity of component i.

3.1.2.2   Calibrating theoretical models of thermal properties

The available data were subdivided into two random datasets: (1) a training dataset (comprising 66% of all the data) and (2) a test dataset (comprising 34% of all the data). Theoretical model calibration requires data on rock thermal properties, volumetric fractions of rock-forming mineralogical components, and thermal properties of rock-forming mineralogical components. The data on the rock thermal properties were inferred from the results of thermal core logging, and the data on the volumetric fractions were inferred from the well-logging data. The data on the thermal properties of rock-forming minerals are inferred from data available in the

literature. Table 8 summarizes the available data on the thermal properties of minerals and fluids used in the volumetric models of rocks.

Table 8. Literature data on the thermal properties of minerals and fluids (at atmospheric pressure and temperature).

Mineral/fluid	λ_{eff}, W·m⁻¹·K⁻¹	ρ, g·cm⁻³	c, kJ·kg⁻¹·K⁻¹	C, MJ·m⁻³·K⁻¹	
				min	max
Calcite	3.13[a], 3.59[b]	2.71[d], 2.72[b], 2.72-2.94[e]	0.815 [b] 0.79[f]	2.14	2.44
Dolomite	5.66-6.28[a], 5.51[b]	2.87[d], 2.86[b], 2.86-2.93[e]	0.870 [b] 0.93[f]	2.46	2.72
Chalcedony	3.17[a], 3.25[b]	2.65[d]	0.735 [b] 0.94	1.85	1.98
Albite	1.63-2.32[a], 1.94-2.35[b]	2.62 [d], 2.61[b], 2.63[e]	0.70 [b] 0.71[f]	1.83	1.87
Illite	1.80[c]	2.90 [d] 2.60-2.90[e]	0.79[h]	2.05	2.29
Kaolinite	2.69[c]	2.66 [d] 2.61-2.68[e]	0.97[i]	2.53	2.60
Oil	0.11-0.15[g]	0.88-0.97[j]	1.73-1.81 [j]	1.52	1.75
Water	0.59-0.61[j]	1.00[j]	4.19[j]	4.19	4.19

[a]Popov et al. 1987; [b]Horai, 1971; [c]Brigaud and Vasseur (1989); [d]Deer et al., 1992; [e]Fertl and Frost, 1980; [f]Cermak and Rybach, 1982; [g]Schoen, 2015; [h]Skauge et al. (1983); [i]Waples and Waples (2004); [j]Clauser (2006). Rock volumetric heat capacity was calculated as a product of density and specific heat capacity.

The model calibration implies the (1) application of reliable data to the thermal properties of rock-forming mineral components, (2) determination of correction factors for theoretical models in the directions parallel and perpendicular to the bedding plane, and (3) minimization of the mean relative discrepancy between measured and calculated rock thermal properties. Unfortunately, experimental data on the thermal properties of kerogen vary with kerogen porosity and differ for different oil fields. Therefore, the thermal properties of the kerogen were determined by optimization and not experimentally. To solve this problem, we applied a constrained genetic minimization algorithm (Storn and Price, 1997). Since volumetric fractions of minerals were available for the Bazhenov Formation, the possible range of mineral thermal properties was taken directly from Table 8.

The results of the theoretical model calibration accounting for thermal anisotropy (Table 9) indicated that:

- For the Bazhenov Formation, the rock thermal conductivity component parallel to the bedding plane can be predicted via the theoretical model more accurately than the component perpendicular to the bedding plane. This can be due to the more significant influence on the thermal properties perpendicular to the bedding plane of micro-cracking from core unloading.

- Among the considered theoretical models of rock thermal conductivity, the Lichtenecker-Rother model yields the lowest prediction uncertainty and the highest values of R^2 between measured and predicted values.

- The Lichtenecker-Rother model yields the most physically adequate values of thermal properties of the rock components (especially for kerogen and lithological components of the Domanic Formation). For example, through optimization of the Lichtenecker-Asaad and Krischer and Esdorn models with Bazhenov Formation data, we obtained kerogen thermal conductivities of 0.13 and 0.14, respectively, which are more typical for movable oil than that suggested by the Lichtenecker-Rother model.

Based on these points, we can conclude that the Lichtenecker-Rother model for predicting rock thermal conductivity from the well-logging data is preferable.

3.1.2.3 Predicting rock thermal properties from well-logging data based on theoretical modelling

Rock thermal properties were predicted on a test dataset via the Lichtenecker-Rother model, the established values of the correction factor for parallel and perpendicular direction to the bedding plane and thermal properties of rock-forming

components (Table 10). For comparison, the predictions of thermal properties using the gradient boosting method are also included and analyzed within this Section.

Table 9. Calculated values of the thermal properties of the rock-forming components for the training dataset of the Bazhenov Formation.

Theoretical model	Thermal conductivity of minerals/fluids parallel to the bedding plane (N = 326), $W \cdot m^{-1} \cdot K^{-1}$												
	Calcite	Dolomite	Kerogen	Chalcedony	Illite	Kaolinite	Albite	Oil	Correction factor	R^2	RMSE, $W \cdot m^{-1} \cdot K^{-1}$	P,%	A,%
Lichtenecker-Asaad	3.13	5.51	0.13	3.25	1.80	2.65	2.2	0.11	0.17	0.62	0.23	12.8	-4.1
Lichtenecker-Rother	3.13	5.51	0.29	3.25	1.80	2.65	2.2	0.14	0.39	0.59	0.24	12.7	-0.6
Krischer and Esdorn	3.13	5.51	0.14	3.25	1.80	2.65	2.2	0.11	0.95	0.56	0.25	13.1	-0.8
	Thermal conductivity of minerals/fluids perpendicular to the bedding plane (N = 296), $W \cdot m^{-1} \cdot K^{-1}$												
Lichtenecker-Asaad	3.13	5.51	0.13	3.25	1.80	2.65	2.2	0.11	0.44	0.57	0.29	21.7	-4.1
Lichtenecker-Rother	3.13	5.51	0.29	3.25	1.80	2.65	2.2	0.14	-0.27	0.58	0.27	19.1	-0.4
Krischer and Esdorn	3.13	5.51	0.14	3.25	1.80	2.65	2.2	0.11	0.79	0.55	0.28	19.9	0.05
	Volumetric heat capacity of minerals/fluids (N = 326), $MJ \cdot m^{-3} \cdot K^{-1}$												
Weighted arithmetic mean	2.40	2.46	1.61	1.85	2.01	2.20	1.83	1.52	-	0.05	0.13	12.3	1.6

Table 10. Prediction results of the rock thermal properties on the test datasets.

Model*	Thermal conductivity								Volumetric heat capacity				
	$\lambda_{||}$				$\lambda_\perp$								
	R^2	RMSE $W \cdot m^{-1} \cdot K^{-1}$	P %	A %	R^2	RMSE $W \cdot m^{-1} \cdot K^{-1}$	P %	A %	Model	R^2	RMSE $MJ \cdot m^{-3} \cdot K^{-1}$	P %	A %
GB	0.79	0.14	7.7	0.8	0.79	0.19	15.4	1.1	GB	0.52	0.09	8.8	0.2
LR	0.62	0.18	10.4	0.1	0.50	0.30	19.9	1.5	AM	0.10	0.13	11.4	2.3

*GB stands for the gradient boosting method, LR stands for the Lichtenecker-Rother model, AM stands for the weighted arithmetic mean model.

Figure 11 plots the thermal property predictions and experimental values of the rock thermal properties for the test datasets.
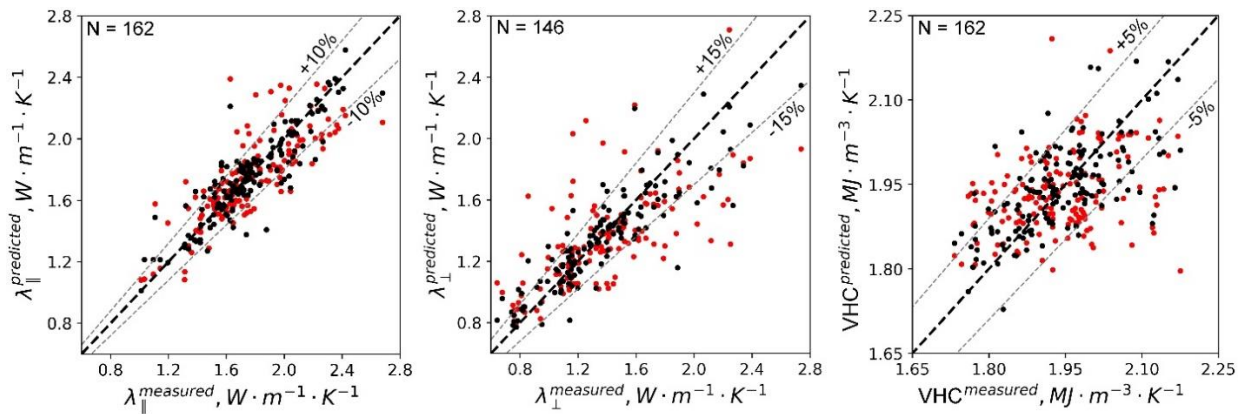
Figure 11. Experimental data of the rock thermal properties compared to the thermal properties predicted from well-logging data of training datasets for the Bazhenov Formation. Black dots present results with the gradient boosting method, red dots results via theoretical model. The dashed black line (y=x) shows a perfect prediction.

The results obtained for the case studies show that theoretical models provide a less accurate prediction of rock thermal properties from well-logging data than the machine-learning algorithm for organic-rich shales. There are several sources of uncertainties that cause relatively high errors when dealing with theoretical models of rock thermal properties. First, the volumetric mineralogical models resulting from the initial geophysical data processing are constructed within a set of assumptions, such as vertical and lateral continuity, a constant ratio of bound water to dry clay, etc. Moreover, the models are interpretative, implying their subjective nature. Consequently, volumetric mineralogical models increase the uncertainties of the data on the volume fractions of rock-forming components that are used for predicting thermal properties based on the theoretical model of thermal properties.

Another aspect refers to the imperfections of theoretical models of thermal conductivity. As already mentioned, the rocks thermal conductivity depends on many factors, such as mineralogical composition, porosity, saturation, intergranular contacts, and the shape of minerals. Therefore, the implementation of only one, the

so-called correction factor, can be insufficient, at least in some cases. Thus, the improvement in theoretical models of thermal conductivity is important.

For a detailed uncertainty analysis, boxplots of the relative discrepancies between the measured and predicted values are plotted in Figure 12.
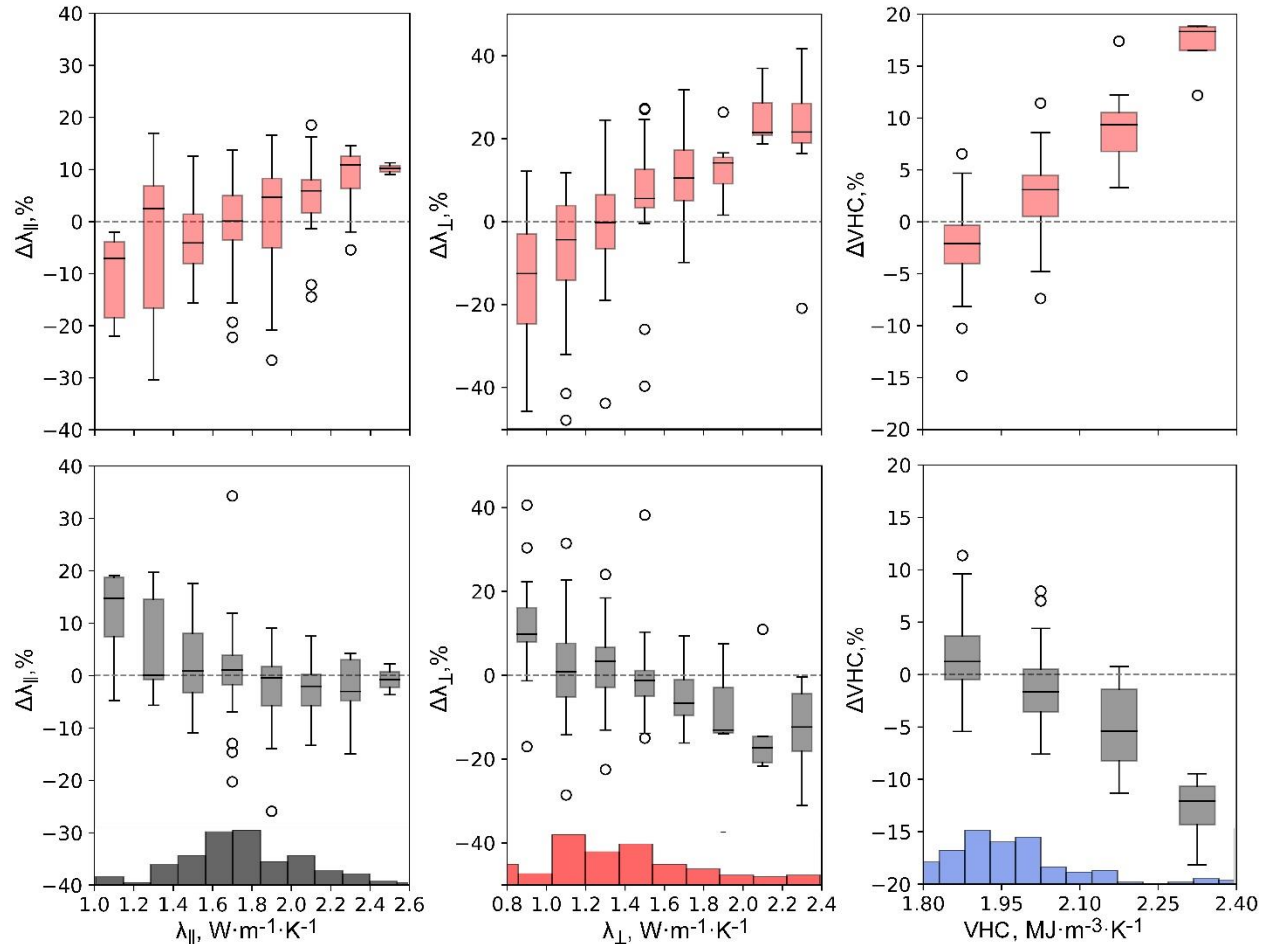
Figure 12. Boxplots of the relative discrepancies between the measured and predicted values of rock thermal properties for the Bazhenov Formation. Above, predictions based on the theoretical models; below, predictions based on the gradient boosting algorithm. Histograms of thermal properties from the test dataset are also shown.

It may be deduced that systematic underestimation is observed when predicting rock thermal conductivity on the basis of a theoretical model for low thermal conductivities (0.8-1.2 $W \cdot m^{-1} \cdot K^{-1}$) for the Bazhenov Formation. In most cases, the gradient boosting algorithm provides less biased predictions of thermal properties

compared to the predictions on the basis of the theoretical models. There is a systematic overestimation in the prediction of thermal conductivity for the Bazhenov Formation for high thermal conductivities (2.4–2.8 W·m^{-1}·K^{-1} for the parallel thermal conductivity component and 2.0–2.4 W·m^{-1}·K^{-1} for the perpendicular thermal conductivity component). Analysis of the data showed that this bias is caused by the silicification of some intervals resulting in the occurrence of highly high-conductive quartz.

Based on results presented in Figures 11 and 12, we can conclude that the gradient boosting method is more effective for predicting rock thermal properties than the theoretical models because of its high sensitivity to the non-linear and implicit dependencies of the rock thermal properties and well-logging data. However, in case of rocks that are low porous or have low organic matter content, the correlations between thermal and other physical properties can diminish and the quality of predictions will be unacceptable. Moreover, the application of gradient boosting requires training datasets, which are not always available. Therefore, for cases when core samples are absent and only well-logging data are available or the rocks are low porous (or which have low organic matter content), predictions of rock thermal properties can be performed with sufficient precision based on theoretical models. Another benefit of the application of the theoretical modelling approach is an opportunity of transition from one saturation state to another. In case of lateral variations of rock saturation, the regression model-based approach requires determining corrections to rock thermal properties for different saturations on the basis of special experimental investigations (see, e.g., Popov et al., 2017), whereas the theoretical model-based approach does not.

Applied theoretical thermal conductivity models contain correction factors that encompass the effect of structural peculiarities on rock thermal conductivity. The possible way to enhance theoretical models in application to organic-rich shales includes an arrangement of comprehensive experimental study and analysis of

results to understand how the correction factor depends on geological features of source rocks and the implementation of additional correction parameter that will account for textural peculiarities.

3.1.3 Conclusions

An approach for determining the thermal properties of rocks accounting for thermal anisotropy via theoretical modelling was suggested and tested. The approach provides simultaneous determination of the rock thermal conductivity and volumetric heat capacity. Predictions of thermal conductivity accounting for thermal anisotropy are accessible due to applications of theoretical models of thermal conductivity that contain correction factors encompassing the effect of rock structure. Like the approach suggested in Section 2.1, this approach also accounts for the influence of *in situ* thermobaric conditions on thermal properties, differentiating the effect on distinct thermal conductivity tensor components.

Within the case study the experimental dataset on rock thermal properties inferred from continuous thermal core logging and volumetric mineralogical models inferred from high definition spectroscopy and nuclear magnetic resonance log from three wells drilled through anisotropic organic-rich shales were the basis for the approach development and testing. The results obtained during the case study show that rock thermal conductivity components can be predicted from well-logging data with uncertainties of less than $\pm11\%$ for thermal conductivity parallel to the bedding plane and less than $\pm20\%$ for thermal conductivity perpendicular to the bedding plane (for a 0.95 confidence level). Volumetric heat capacity can be predicted from well-logging data with an uncertainty of less than $\pm12\%$ (for a 0.95 confidence level).

From comparison study of prediction results obtained with gradient boosting method and Lichtenecker-Rother model, it can be concluded that the gradient boosting method is more effective for predicting rock thermal properties than the

83

theoretical models because of its high sensitivity to the non-linear and implicit relations between the rock thermal properties and well-logging data.

3.2. Approach for assessing uncertainty in a correction factor of Krischer-Esdorn model

An essential aspect of theoretical modelling of rock thermal conductivity is assessing the prediction quality of a model. The prediction quality of the theoretical model is principally determined by uncertainties in input parameters (thermal conductivity of rock matrix and pore fluid, structural parameters, and volume fraction of rock-forming components). One of the most commonly used ways to assess the theoretical model's prediction quality is a comparison of measured and predicted values of rock thermal conductivity. However, the assessment results are true only for considered data (that have given uncertainties) and can vary if uncertainties in input parameters change.

Therefore, when predicting rock thermal conductivity from well-logging data on the basis of theoretical modelling, particular calculations are required to assess the prediction quality accounting for uncertainties in input parameters. A key for the problem solution is the sensitivity study of the theoretical model. It allows understanding the influence of uncertainties in input parameters on prediction uncertainty. However, very often, there is a lack of data (or the data is absent) on uncertainty in the correction factor of the theoretical model of rock thermal conductivity. The uncertainty in correction factor can be determined via special experimental investigations on the collection of core samples provided that the uncertainty in thermal conductivity of matrix, pore fluid, and porosity are known (Stolyarov et al., 2007). Concurrently, not always there is an opportunity to conduct such investigations and, thus, an effective approach for assessing uncertainties in data on correction factor is required.

A new effective approach was developed and suggested to assess the uncertainty in the correction factor of theoretical models. An example is given for the Krischer-Esdorn model.

3.2.1 Workflow

The workflow of assessment of the correction factor uncertainty implies that the thermal conductivity of rock-forming components and correction factor are known. The approach consists of several principal steps.

In the first step, the prediction uncertainty of the theoretical thermal conductivity model is assessed via a comparison of predicted and measured thermal conductivity values. Prediction accuracy and precision are calculated (using formulas 2 and 3, Section 2.1.2) to evaluate the prediction uncertainty.

In the second step, based on the partial derivative method, the sensitivity study of the theoretical model is performed. The result of the sensitivity study are determined sensitivity coefficients of dependency of prediction uncertainty from uncertainties in input parameters.

In the third step, using the prediction uncertainty evaluated in the first step and evaluated coefficients of dependency of prediction uncertainty from uncertainties in input parameters, the uncertainty in correction factor is determined with:

$$\delta\lambda_{eff} = K_1 \cdot \delta\lambda_{matrix} + K_2 \cdot \delta\lambda_{fluid} + K_3 \cdot \delta\phi + K_4 \cdot \delta a \qquad (8)$$

$$\delta a = \frac{\delta\lambda_{eff} - K_1 \cdot \delta\lambda_{matrix} - K_2 \cdot \delta\lambda_{fluid} - K_3 \cdot \delta\phi}{K_4} \qquad (9)$$

where $\delta\lambda_{eff}$ is prediction uncertainty that is calculated in the first step; K_1, K_2, K_3, K_4 are coefficients of dependency of prediction uncertainty from uncertainties in corresponding input parameters that are inferred from sensitivity study of a model; $\delta\lambda_{matrix}$ is uncertainty in data on thermal conductivity of rock matrix; $\delta\lambda_{fluid}$ is uncertainty in data on thermal conductivity of pore-filling fluid; $\delta\phi$ is uncertainty in porosity; δa is uncertainty in correction factor.

3.2.2 Case study: assessing the uncertainty in correction factor of Krischer-Esdorn model established for clayey rocks of the Tumen Formation

The suggested approach for assessing the uncertainty in correction factor of theoretical model of thermal conductivity suggested by Krisher and Esdorn (Krischer and Esdorn, 1956) was tested on data from two wells (A and C, Section 2.1.2).

3.2.2.1 Geological setting and field data

The Tumen Formation is of the Jurassic age and was formed under coastal-marine conditions. From high-definition spectroscopy data and NMR data, the investigating clayey rocks are principally composed of illite, kaolinite, albite, orthoclase, siderite, siliceous minerals (mainly chalcedony), bound and free water (Figure 13).
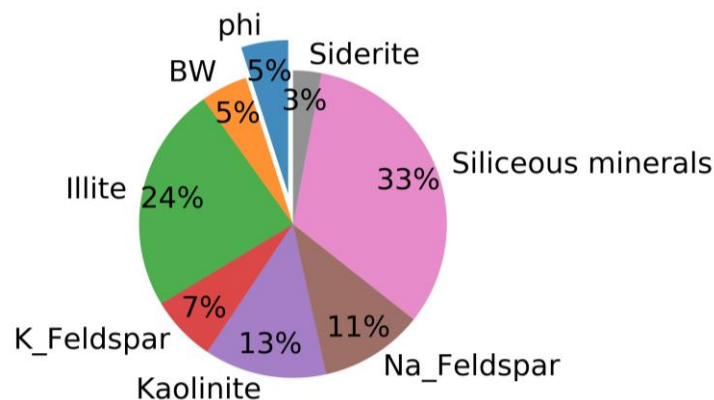
Figure 13. Pie chart of average volume fractions of rock-forming components of the investigating rocks inferred from high definition spectroscopy and NMR log data.

According to NMR log data, the porosity varies from 1% to 10%, with mean value of 4.5% and a standard deviation of 3%. The clayey minerals due to oriented alignment condition the stratified structure. Thus, the considering clayey rocks can be treated as transversely isotropic medium with a vertical axis of symmetry.

3.2.2.2 Thermal core logging results for the clayey rocks of the Tumen Formation

The continuous thermal core logging was conducted on 507 full-sized core samples from wells A and C (57 m in total). Scanning lines were chosen parallel and perpendicular to the bedding plane on the flat surfaces of the sawed core samples. The continuous profiles of the thermal conductivity components parallel and perpendicular to the bedding plane directions are plotted in Figure 14.
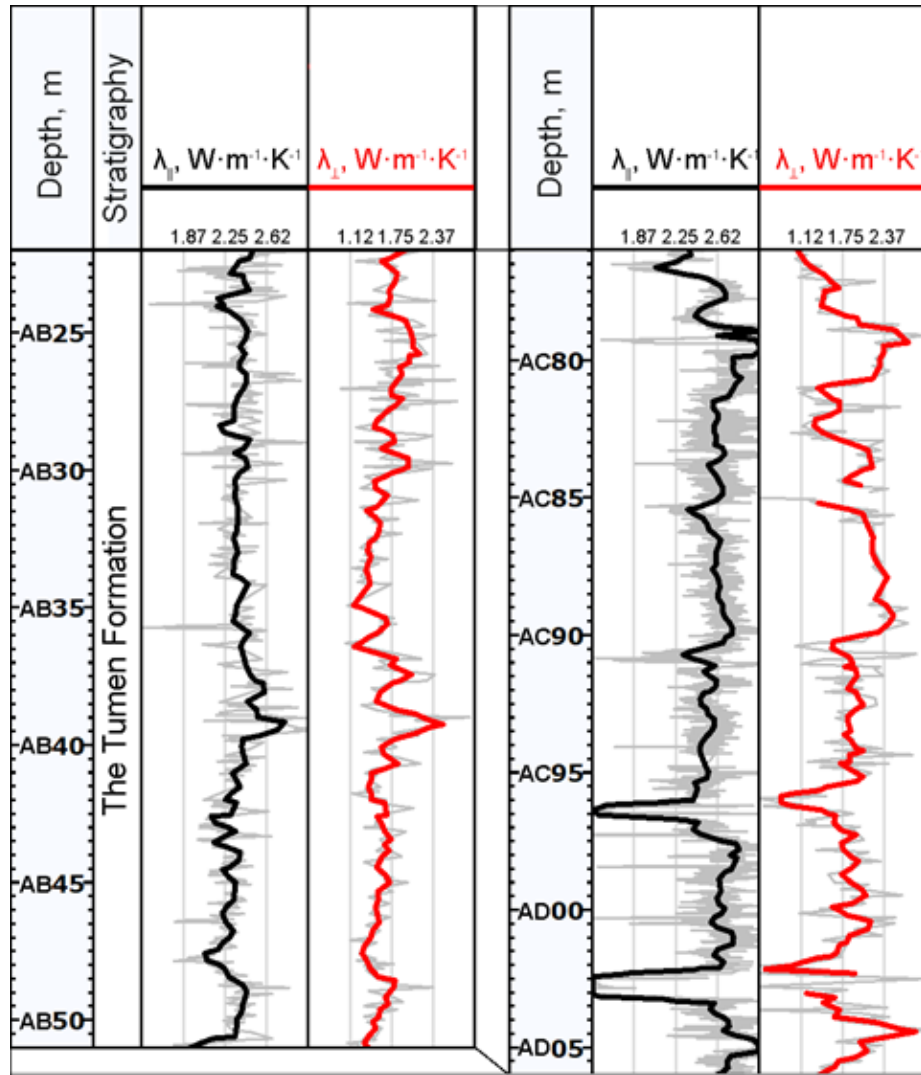
Figure 14. Results of rock thermal property measurements for wells A (left) and C (right). λ stands for rock thermal conductivity; subscripts $\parallel$ and $\perp$ stand for the thermal conductivity components in the directions parallel and perpendicular to the bedding plane, respectively; grey lines represent the original profiles of the rock thermal properties; black, red and blue lines represent averaged thermal property profiles in a moving 0.5 window.

A high content of clayey minerals (especially illite) conditions a systematic thermal anisotropy of the investigating rocks (Figure 15).
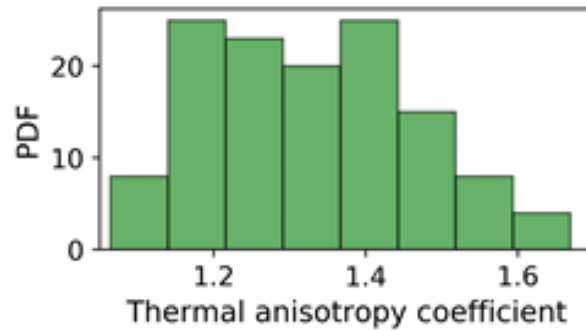
Figure 15. Histogram of thermal anisotropy coefficient inferred from thermal core logging for wells A and C.

3.2.2.3 Results of predicting rock thermal conductivity from well-logging data based on Krischer-Esdorn model

The available data on rock thermal properties and volumetric fractions of rock-forming components were subdivided into two random datasets: (1) a training dataset (comprising 66% of all the data) and (2) a test dataset (comprising 34% of all the data). Following the workflow described in Section 3.1.1 for determining rock thermal conductivity from well-logging data based on theoretical modelling, we performed calibration of the Krischer-Esdorn model on the training dataset and predicted rock thermal conductivity on the test dataset. During model calibration, the data on thermal conductivity of rock minerals were inferred from Table 8. Additionally, the data on thermal conductivity of orthoclase and siderite were inferred from Popov et al. (1987). Since investigating rocks exhibit a high degree of thermal anisotropy (Figure 15), the correction factor of the Krischer-Esdorn model was determined both for parallel and perpendicular directions to the bedding plane. According to laboratory investigations, considering clayey rocks are characterized by negligible permeability and, thus, during model calibrating, 100% water saturation of pore space was implied.

The results of model calibration for parallel and perpendicular directions to the bedding plane are presented in Table 11. The results of predicting thermal conductivity on the test dataset are presented in Table 12.

Table 11. Calculated values of the thermal properties of the rock-forming components for the training dataset of the clayey rocks.

Thermal conductivity of minerals/fluids parallel to the bedding plane (N = 110), $W \cdot m^{-1} \cdot K^{-1}$

Siderite	Orthoclase	Chalcedony	Illite	Kaolinite	Albite	Correction factor	R^2	RMSE, $W \cdot m^{-1} \cdot K^{-1}$	P,%	A,%
3.08	2.17	3.25	1.80	2.65	2.2	0.38	0.78	0.09	7.4	0.2

Thermal conductivity of minerals/fluids perpendicular to the bedding plane (N = 79), $W \cdot m^{-1} \cdot K^{-1}$

| 3.08 | 2.17 | 3.25 | 1.80 | 2.65 | 2.2 | 0.66 | 0.68 | 0.13 | 14.2 | 0.9 |

Table 12. Prediction results of the rock thermal properties on the test datasets.

$\lambda_{\parallel}$, (N = 132)				$\lambda_{\perp}$, (N = 53)			
R^2	RMSE, $W \cdot m^{-1} \cdot K^{-1}$	A, %	P, %	R^2	RMSE, $W \cdot m^{-1} \cdot K^{-1}$	P, %	A, %
0.73	0.09	8.0	0.0	0.64	0.15	15.0	1.2

The prediction uncertainty is assessed for a 0.95 confidece level. Figure 16 plots the experimental data on rock thermal conductivity and predicted thermal conductivities for the test dataset.
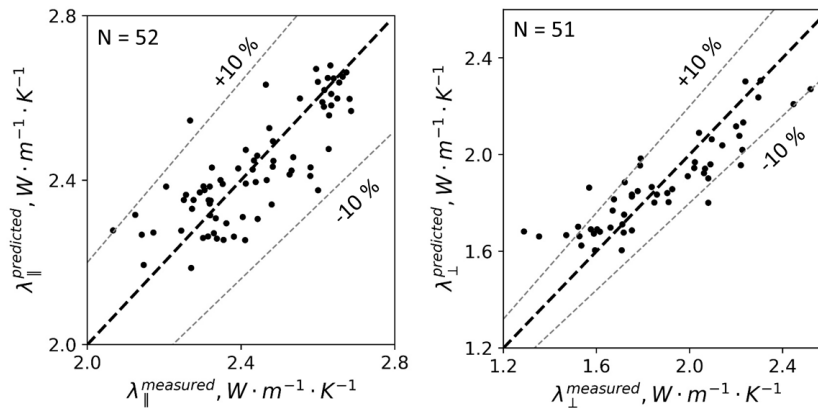
Figure 16. Experimental data of the rock thermal conductivity compared to the predicted thermal conductivity from well-logging data on test datasets. The dashed black line (y=x) shows perfect prediction. N stands for number of points.

3.2.2.4 Sensitivity study of Krischer-Esdorn model and assessment of uncertainty in the correction factor

The partial derivative method of the sensitivity analysis uses the Taylor expansion to approximate the uncertainty of the function output with respect to the uncertainties in input parameters. The Taylor expansion for input perturbations of a function can be written as:

$$f(x + \Delta x) - f(x) = \frac{\partial f(x)}{\partial x} \Delta x + \frac{1}{2} \cdot \frac{\partial^2 f(x)}{\partial x^2} (\Delta x)^2 + \frac{1}{6} \cdot \frac{\partial^3 f(x)}{\partial x^3} (\Delta x)^3 + \cdots \approx \frac{\partial f(x)}{\partial x} \Delta x \qquad (10)$$

where Δx is a very small non-zero positive number. Because the Δx is very small, the second and subsequent terms are negligible and as a result, the uncertainty of the function's output is approximated by the first term of the Taylor expansion.

To assess the influence of relative uncertainties in input parameters on relative uncertainty of the output, the equation 10 is rewritten as:

$$\delta f = \frac{\Delta f(x)}{f(x)} = \frac{\partial f(x)}{\partial x} \cdot \frac{1}{f(x)} \cdot \frac{1}{x} \cdot \delta x \qquad (11)$$

where δf is relative uncertainty in the output of the function, Δf stands for $f(x+\Delta x) - f(x)$, δx is relative uncertainty in the input parameter. The ratio of derivative of the function with respect to the input parameter to the product of x and function output $f(x)$ is denoted as a sensitivity coefficient.

The Krischer-Esdron model for a two-component system is written the following way:

$$\lambda_{eff} = \left(\frac{1-a}{(1-phi) \cdot \lambda_{matrix} + phi \cdot \lambda_{fluid}} + \frac{a}{\left(\frac{1-phi}{\lambda_{matrix}} + \frac{phi}{\lambda_{fluid}} \right)^{-1}} \right)^{-1} \qquad (12)$$

where phi is porosity, λ stands for thermal conductivity, a is a correction factor.

Partial derivatives of the Krisher-Esdorn model with respect to the thermal conductivity of rock matrix, pore-filling fluid, porosity and correction factor a are:

$$\frac{\partial \lambda_{eff}}{\partial \lambda_{matrix}} = -\frac{\frac{(1-a)\cdot(1-\phi)}{\left(\lambda_{fluid}\cdot\phi+\lambda_{matrix}\cdot(1-\phi)\right)^2}+\frac{a\cdot(1-\phi)}{\lambda_{matrix}^2}}{\left(\frac{1-a}{\lambda_{fluid}\cdot\phi+\lambda_{matrix}\cdot(1-\phi)}+a\cdot\left(\frac{\phi}{\lambda_{fluid}}+\frac{1-\phi}{\lambda_{matrix}}\right)\right)^2} \tag{13}$$

$$\frac{\partial \lambda_{eff}}{\partial \lambda_{fluid}} = -\frac{\frac{a\cdot\phi}{\left(\lambda_{fluid}\right)^2}+\frac{\phi\cdot(1-a)}{\left(\lambda_{fluid}\cdot\phi+\lambda_{matrix}\cdot(1-\phi)\right)^2}}{\left(\frac{1-a}{\lambda_{fluid}\cdot\phi+\lambda_{matrix}\cdot(1-\phi)}+a\cdot\left(\frac{\phi}{\lambda_{fluid}}+\frac{1-\phi}{\lambda_{matrix}}\right)\right)^2} \tag{14}$$

$$\frac{\partial \lambda_{eff}}{\partial \phi} = -\frac{a\cdot\left(\frac{1}{\lambda_{fluid}}-\frac{1}{\lambda_{matrix}}\right)-\frac{(1-a)\cdot(\lambda_{fluid}-\lambda_{matrix})}{\left(\lambda_{fluid}\cdot\phi+\lambda_{matrix}\cdot(1-\phi)\right)^2}}{\left(\frac{1-a}{\lambda_{fluid}\cdot\phi+\lambda_{matrix}\cdot(1-\phi)}+a\cdot\left(\frac{\phi}{\lambda_{fluid}}+\frac{1-\phi}{\lambda_{matrix}}\right)\right)^2} \tag{15}$$

$$\frac{\partial \lambda_{eff}}{\partial a} = -\frac{-\frac{1}{\lambda_{fluid}\cdot\phi+\lambda_{matrix}\cdot(1-\phi)}+\frac{\phi}{\lambda_{fluid}}+\frac{1-\phi}{\lambda_{matrix}}}{\left(\frac{1-a}{\lambda_{fluid}\cdot\phi+\lambda_{matrix}\cdot(1-\phi)}+a\cdot\left(\frac{\phi}{\lambda_{fluid}}+\frac{1-\phi}{\lambda_{matrix}}\right)\right)^2} \tag{16}$$

According to Chorpa et al. (2018) and Fuchs et al. (2018), the high effectiveness of the Lichtenecker model is observed in the calculation of effective thermal conductivity of low-porous rocks with minerals, which have low thermal conductivity contrast. Thus, the thermal conductivity of rock matrix for the investigating clayey rocks is calculated using the Lichtenecker model using data on average volumetric composition that was inferred from high-definition spectroscopy and thermal conductivities of minerals. The Lichtenecker model is written as:

$$\lambda_{eff} = \prod_{i=1}^{N} \lambda_i^{V_i} \tag{17}$$

where λ_i is thermal conductivity of i-th component and V_i is volume fraction of the i-th component.

To assess the uncertainty of the determined correction coefficients for parallel and perpendicular directions to the bedding plane, data on uncertainty in thermal conductivity of rock matrix, pore-filling fluid, and porosity are required.

The uncertainty in data on porosity and pore-filling fluid is taken from technical specifications of the utilized measurement tools. Data on porosity is inferred from

nuclear magnetic resonance log data, and according to technical specifications of the applied logging tool, the uncertainty on porosity is ±2.0%. The uncertainty on thermal conductivity of water is ±2.5%.

To assess the uncertainty in the thermal conductivity of the rock matrix, the sensitivity study of the Lichtenecker model was performed. The partial derivatives of the Lichtenecker model with respect to the thermal conductivity of i-th component and its volume fractions are calculated as:

$$\frac{\partial \lambda_{eff}}{\partial \lambda_i} = V_i \cdot \lambda_i^{V_i-1} \cdot \prod_{j=1}^{N} \lambda_j^{V_j} \ (i \neq j) \tag{18}$$

$$\frac{\partial \lambda_{eff}}{\partial V_i} = ln(V_i) \cdot \prod_{i=1}^{N} \lambda_i^{V_i} \tag{19}$$

As reported by Popov et al. (1987), the uncertainty in data on rock-forming minerals that are involved in this study can be ±2.5%. According to technical specifications of the high-definition spectroscopy tool, the uncertainty in data on volume fractions of minerals is ±3.0%. The uncertainty in thermal conductivity of rock matrix is calculated as:

$$\delta\lambda_{matrix} = K_{\lambda_{Illite}} \cdot \delta\lambda_{Illite} + K_{\lambda_{Orthoclase}} \cdot \delta\lambda_{Orthoclase} + K_{\lambda_{Kaolinite}} \cdot \delta\lambda_{Kaolinite} +$$
$$K_{\lambda_{Albite}} \cdot \delta\lambda_{Albite} + K_{\lambda_{Chalcedony}} \cdot \delta\lambda_{Chalcedony} + K_{\lambda_{Siderite}} \cdot \delta\lambda_{Siderite} + K_{V_{Illite}} \cdot \delta V_{Illite} +$$
$$K_{V_{Orthoclase}} \cdot \delta V_{Orthoclase} + K_{V_{Kaolinite}} \cdot \delta V_{Kaolinite} + K_{V_{Albite}} \cdot \delta V_{Albite} + K_{V_{Chalcedony}} \cdot$$
$$\delta V_{Chalcedony} + K_{V_{Siderite}} \cdot \delta V_{Siderite} \tag{20}$$

where K is the sensitivity coefficient for the corresponding input parameter of the Lichtenecker model. The calculated uncertainty in data on matrix thermal conductivity from equation 20 for investigated clayey rocks is 6.1% for a 0.95 confidence level.

In the calculations of the sensitivity coefficients, the average values of rock porosity and thermal conductivity of rock matrix in equations 13 – 16 are assigned within the case study. Correction factors were determined in Section 3.2.2.3 and are taken from Table 11. Figure 17 shows the influence of uncertainties in input parameters of the Krisher-Esdorn model on thermal conductivity components for

parallel and perpendicular directions to the bedding plane and the importance of input parameters within the case study is ranked both for parallel and perpendicular directions to the bedding plane the following way.
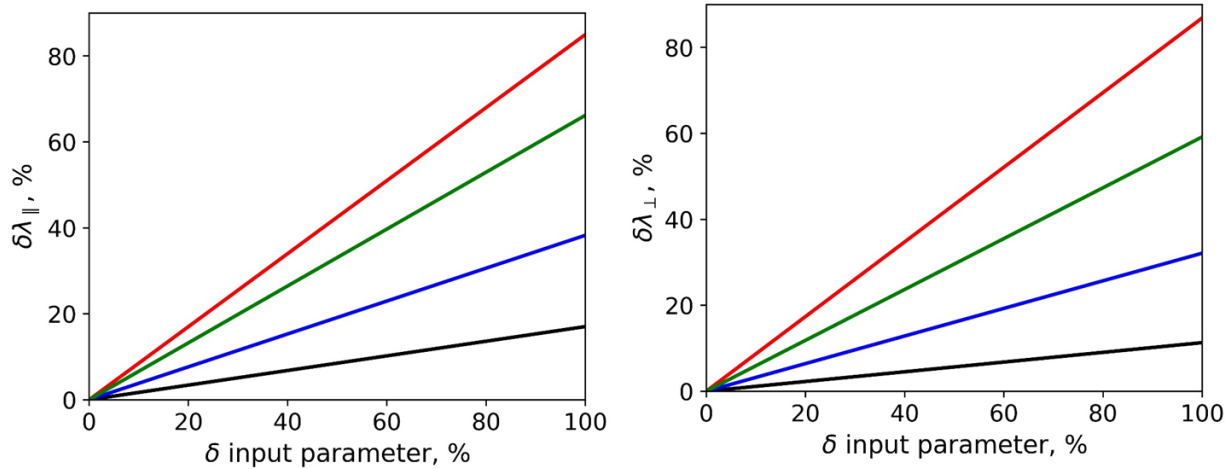
Figure 17. Results of assessing influence of uncertainty in thermal conductivity of rock matrix (red lines), porosity (green line), thermal conductivity of pore fluid (blue line), and correction factor (black line) on rock thermal conductivity for parallel (left panel) and perpendicular (right panel) directions to the bedding plane.

Following the workflow (Section 3.2.1), the assessment of uncertainty in data on correction factors by means of equation 9. For assessment of uncertainty in data on correction factor were involved (1) the sensitivity coefficients for each input parameter obtained during sensitivity study of Krisher-Esdorn model, (2) the data on uncertainty in thermal conductivity of rock matrix, porosity, the thermal conductivity of pore fluid, and (3) the prediction uncertainty of Krischer-Esdorn model (Table 12). The calculated uncertainties in correction factors (via equation 9) for parallel and perpendicular directions to the bedding plane are 15% and 37%, respectively.

3.2.3 Conclusions.

A new approach for assessing uncertainty in the correction factor of the Krischer-Esdorn model was suggested and tested. The approach relies on the

application of the partial-derivative method, and requires integrating results of predicted rock thermal conductivity from well-logging data on the basis of theoretical modelling of thermal conductivity.

The approach was tested on data from the Tumen Formation that is composed of clayey rocks. From the sensitivity study, it can be concluded that for investigated rock the uncertainty in correction factor has the lowest influence on uncertainty in effective thermal conductivity compared to the influence of uncertainties in other input parameters (thermal conductivity of rock matrix, porosity, thermal conductivity of pore-fluid). The calculated uncertainties in correction factors for parallel and perpendicular directions to the bedding plane are 15% and 37%, respectively. The obtained results enable accounting for variations in the quality of input data from well to well while assessing the quality of predicting rock thermal conductivity from well-logging data.

The developed approach is not applicable only to the Krischer-Esdorn model, but it can be used for assessing uncertainty in correction factors of Lichtenecker-Rother and Lichtenecker-Asaad models.

Chapter 4. Well-log based technique (WLBT) for determining rock thermal properties accounting for thermal anisotropy at *in situ* pressure, temperature and saturation

An important aspect of well-log based predictions of rock thermal properties accounting for thermal anisotropy is the development of a well-defined and clear workflow that could encompass a variety of conditions. Moreover, the integration of opportunities that were disclosed due to the implementation of modern experimental bases for problem solution is very often not a trivial task.

In this Chapter, by integrating regression and theoretical model-based approaches described in Chapters 2 and 3, we propose an enhanced technique for the well log-based determination of rock thermal properties accounting for rock thermal anisotropy. The technique's novelty, which allows us to account for the pressure, temperature and saturation effects, is supported and evidenced by a Russian patent (Popov et al., 2019a).

4.1. Workflow of WLBT for thermal property prediction

The developed enhanced technique for determining rock thermal properties accounting for thermal anisotropy from well-logging data consists of the following principal steps:

1. Analysing and processing of the available input data.
2. Determining directions ij of the principal axes of anisotropy (2D anisotropy is considered for sedimentary rocks).
3. Selecting regression or theoretical models of the rock thermal properties and determining model parameters.
4. Determining the rock thermal properties in a target depth interval from well-logging data at atmospheric pressure and temperature.
5. Determining the rock thermal properties in the target depth interval at *in situ* temperature and pressure.

The detailed schema of the proposed algorithm is presented in Figure 18.
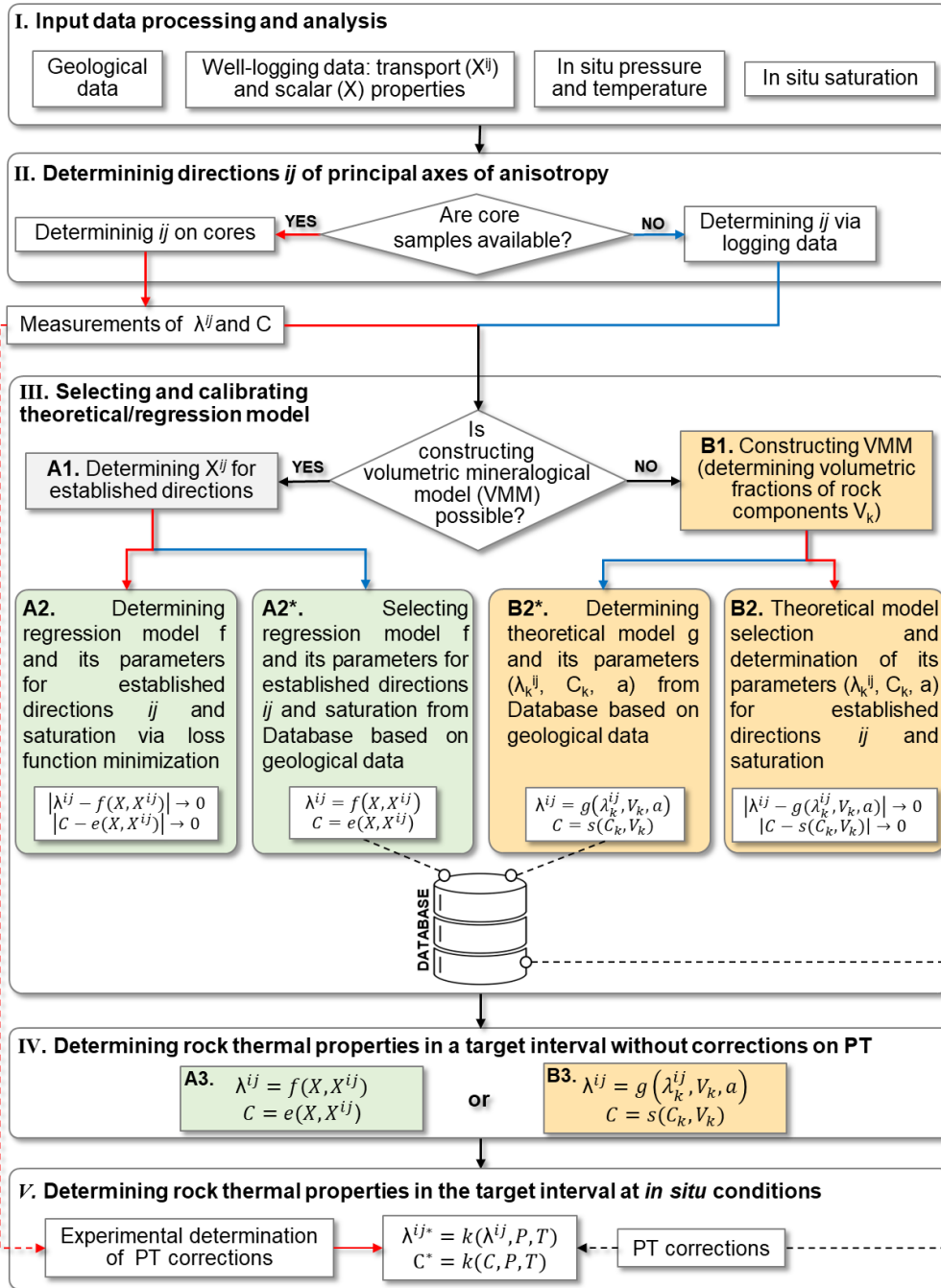
Figure 18. Workflow for well log-based determination of rock thermal properties accounting for rock thermal anisotropy (Shakirov et al., 2021). Red and blue arrows indicate cases when "core samples are available" and "core samples are absent", respectively. λ^{ij} is the thermal conductivity in the *ij* directions; C is the volumetric heat capacity. V_k is a volumetric fraction of the k-th rock-forming component, $\lambda_k{}^{ij}$ is the thermal conductivity of the k-th component for the *ij* direction, and C_k is the volumetric heat capacity of the k-th component. "a" is a correction factor. P and T stand for pressure and temperature, respectively.

Preliminary, target intervals for predicting rock thermal properties are defined. In step I, the available geological and geophysical data are analysed. The main characteristics of the target intervals to be evaluated are the (1) lithological composition of the rocks composing the target interval, (2) formation peculiarities (porosity type, shaliness type, physical properties of the rock-forming mineral, cementation degree, etc.), (3) in situ pressure and temperature, (4) in situ saturation, and (5) quality of the available well-logging data. If there are reference intervals for predicting the rock thermal properties, the same characteristics of the reference intervals are evaluated from the geological and geophysical data. Requirements for the "reference interval" are as follows: (1) drilled with coring, (2) composed of similar (to the target interval) rocks, and (3) is investigated with the same well log suite.

In step II, the directions ij of the principal axes of the rock thermal conductivity are determined. If core samples of the reference interval are available and the orientation of these samples are known relative to in-situ formations (Figure 18, step II, red arrow), the directions ij are determined experimentally via a special procedure: the optical scanning measurements are performed on selected core samples with sequential rotation of scanning line directions, as described by Popov et al. (2016). Since the directions ij are considered to be the same for the thermal conductivity, sonic velocity and geomechanical characteristics of the same rocks (Kim et al., 2012), the ij directions can be determined via a set of geomechanical tests. If core samples are not available (Figure 18, step II, blue arrow), the directions ij are determined via analysis of sonic log data (see, e.g., Hornby et al., 2003) or electric log data (Faivre et al., 2002; via a high-definition resistivity formation micro imager). The directions ij are determined for each lithology presented in the target interval.

After that, when core samples are available, continuous thermal logging of core samples extracted from the reference interval is performed to obtain the principal components of thermal conductivity and volumetric heat capacity in the ij directions.

There are two possible variants of step III. If the available geological and geophysical data allow constructing a volumetric mineralogical model (VMM) of both the reference and the target intervals, then the enhanced theoretical model-based approach can be realized. Otherwise, the enhanced regression model-based approach can be utilized. The adopted variant depends on the available data and prediction precision, which vary in each case. Moreover, these approaches can be combined: for some part of the target interval, the rock thermal properties are determined via a theoretical model-based approach, while those of the other part are determined via a regression model-based approach.

The approach based on the regression model starts by evaluating the transport physical properties (sonic velocity and electrical resistivity) inferred from well-logging data along the principal axis directions ij of thermal conductivity (Figure 18, step III, block A1). After that, the regression models, their parameters for the ij directions and the corresponding fluid saturation of rocks are determined. If core samples recovered from the reference interval were available in the previous steps and continuous thermal core logging was conducted, then a regression models and their parameters are determined using experimental data via minimization of the misfit between the measured and calculated rock thermal properties (Figure 18, step III, A2). If core samples were not available, then the regression model and its parameters are selected from the database (Figure 18, step III, A2*). For database, we imply local or published representative databases that contain among other things information for assessing the similarity of being investigated and previously investigated rocks (such as mineralogical composition, petrophysical characteristics, pore fluid, anisotropy, etc.), data on rock thermal properties, other rock properties and/or well-logging data, and regression models (regression equations, machine

learning models, etc.) between thermal properties and well-logging data. The regression models for predicting rock thermal properties are developed on an individual basis within stratigraphic units and / or for each rock type. The regression models can be simple (linear or multiple regressions) and advanced (decision tree-based, neural network-based, etc.).

The approach based on the theoretical model starts with constructing a VMM that can be inferred from special well-logging methods (such as high-definition spectroscopy) or standard well-logging data (Serra, 1986). If core samples and core logging were available from the previous steps, then a VMM of the reference interval is also constructed. After that, a theoretical model (selection of the theoretical model of thermal conductivity is discussed in Section 2.2) of the rock thermal conductivity is selected, and its parameters are determined. Also, the volumetric heat capacity of the rock-forming components (pore fluids, minerals, etc.) is determined. If core samples extracted from the reference interval and thermal core logging were available, then the theoretical model of the rock thermal conductivity, thermal properties of the rock-forming components, and correction factors are determined via minimization of the divergence between the measured and predicted rock thermal properties (Figure 18, step III, B2). The theoretical model of thermal conductivity is calibrated separately for each principal axis direction ij of thermal conductivity. If core samples were not available, the theoretical model of thermal conductivity, thermal properties of the rock-forming components and correction factors are selected from the database (Figure 18, step III, B2*).

In step IV, the rock thermal properties are determined by accounting for the in situ saturation without corrections of the pressure and temperature from well-logging data (Figure 18) using established parameters of the regression or theoretical model for the predetermined directions ij.

In step V (Figure 18), the thermal properties of the rocks composing the target interval are determined at in situ pressure and pressure using data on the formation

conditions and the dependencies of rock thermal properties on temperature and pressure. If core samples recovered from the reference interval are available, the pressure and temperature dependencies can be determined experimentally by taking into account the principal axis directions ij of thermal conductivity (Popov et al., 2012; Wang et al., 2018). Otherwise, the dependencies of the rock thermal properties on the temperature and pressure can be inferred from data available in the literature.

As the basis of the developed WLBT for determining rock thermal properties from well-logging data, the high effective thermal core logging technique is suggested based on the application of an optical scanning instrument (Popov E. et al., 2019). Popov et al. (2016) gave a comprehensive description of the theoretical background, the specimen requirements and the measurement procedure.

4.2. Testing of WLBT for determining thermal properties of organic-rich shales of the Domanic Formation accounting for thermal anisotropy from well-logging data

To demonstrate evidence that the developed technique can be universally applied for predicting thermal properties of sedimentary rocks from well-logging data accounting for thermal anisotropy, a test was performed on data from organic-rich shales of the Domanic formation.

4.2.1. Analysis and processing of the available input data

The suggested technique was tested on data from two wells (F and G) drilled through the Domanic formation. The lithological and petrophysical characteristics of the rocks are given in Table 13. The Domanic Formation sedimented under relatively deep shelf conditions. More detailed information about the geological peculiarities of the Domanic Formations was given by Liang et al. (2015).

Table 13. Lithological and petrophysical characteristics of the rocks in the case study.

Dominant mineral composition		Organic matter		Reservoir properties	
Mineral	Mean mass content, % (SD)	Kerogen type	Mean TOC, % (SD)	Porosity, % (SD)	ln(Permeability), mD (SD)
Silicate minerals (SiO$_2$)	16.4 (22.1)				
Carbonate minerals	78.1 (25.8)	II-III	7.5 (3.4)	1.5 (0.6)	-3.1 (2.4)
Clayey minerals	1.4 (2.7)				

*SD stands for standard deviation, TOC stands for total organic carbon. Kerogen typing was performed according to Tissot and Welte (1984). ln stands for natural logarithm. For specific depth points, sum of mineral content, organic matter and porosity yields 100%.

For the investigated wells only a standard well logging suite was available that included data on bulk density (ρ), neutron porosity (NPHI), P- and S-wave velocities, photoelectric factor (PEF), and gamma-ray spectrometry data (uranium, thorium, and potassium). Figures 19 and 20 present results of well-logging.
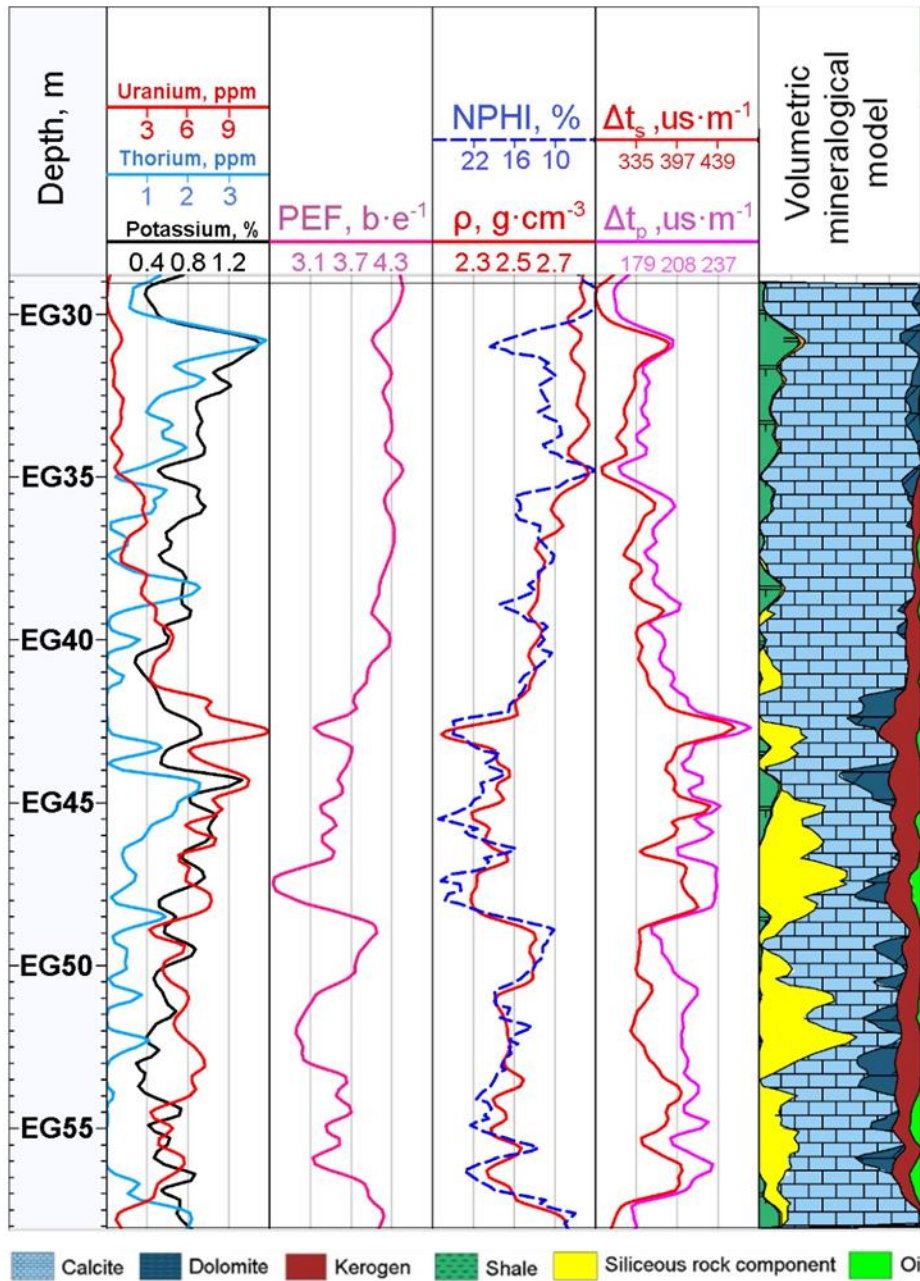
Figure 19. Well logs for well F. Log symbols were defined in the text above.
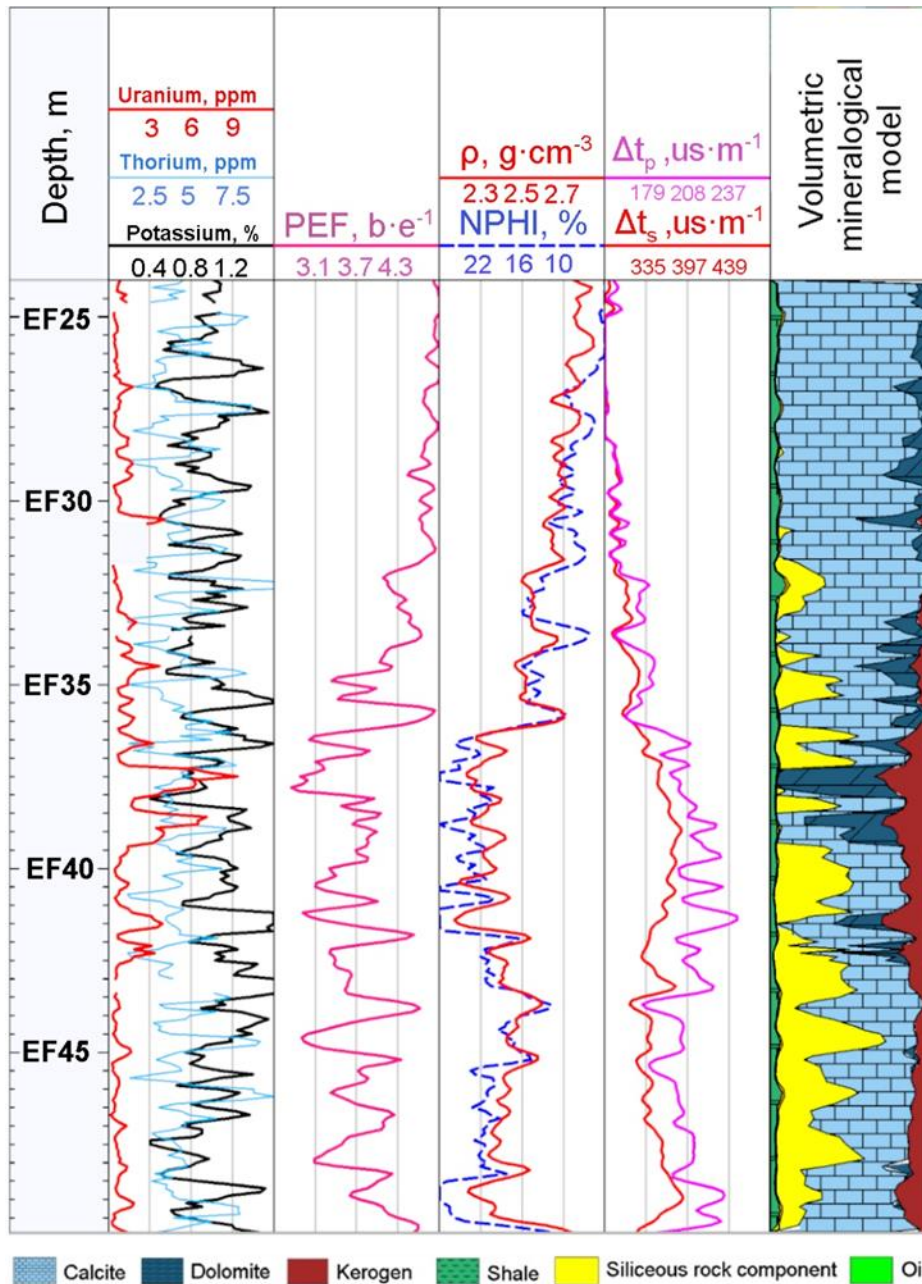
Figure 20. Well logs for well G.

The presented volumetric-mineralogical models in Figures 19 and 20 were inferred by inversion of standard well-logging data (Serra, 1986). There were no available hydrodynamic tests for the wells F and G. Therefore, we need to assume *in situ* pressure and temperature conditions for the Domanic Formation data from neighbouring wells. The approximate average *in situ* pressure and temperature of the Domanic Formation are 32 MPa and 60 °C, respectively. Accurate assessment of in

situ saturation for the investigated formation is complicated because it exhibits low permeability and porosity (Table 13). Hence, we assumed that the Domanic Formation is fully saturated by oil.

A set of editing steps was applied before using the well-logging data. Logging data from different tools were shifted to common depth points, the data from cavernous intervals were eliminated, and environmental corrections were applied. The core depths were shifted to the logging depths.

4.2.2. Thermal core logging results for highly heterogeneous rocks of the Domanic Formation

Thermal core logging was conducted on full-sized core samples recovered from both investigated wells. Figure 21 plots the typical full-sized core samples of the Domanic Formation. The total length of the core samples under study was 61 m. Due to the stratified structure of core samples, scanning lines were chosen parallel and perpendicular to the bedding plane on the flat surfaces of the sawed core samples.

Figure 21. Photographs of typical core samples of the Domanic Formation.

The full-sized core samples from well G were not sawed and, therefore, only the parallel component of thermal conductivity was measured. Statistical assessments of the variations in rock thermal conductivity for parallel and perpendicular to the bedding plane directions, coefficient of thermal anisotropy ($K_T = \lambda_{\parallel} \cdot \lambda_{\perp}^{-1}$), and coefficient of thermal heterogeneity ($\beta = (\lambda_{max}-\lambda_{min}) \cdot \lambda_{avr}^{-1}$) are summarized in Table 14. The Domanic Formation rocks exhibit a high degree of thermal anisotropy and heterogeneity. For the Domanic Formation, the kerogen distribution is not uniform, with patches of thin kerogen layers.

Table 14. Results of thermal property measurements ацк the studied core samples.

Well	$\lambda_{\parallel}$, W·m^{-1}·K^{-1} Mean (SD) (min-max)	λ_{L}, W·m^{-1}·K^{-1} Mean (SD) (min-max)	K_T Mean (SD) (min-max)	β Mean (SD) (min-max)	C, MJ·m^{-3}·K^{-1} Mean (SD) (min-max)	Number of core samples	The total length of core samples under study (m)
F	2.17 (0.39) (0.83-4.49)	1.90 (0.39) (0.34-3.64)	1.29 (0.58) (0.61-5.62)	0.38 (0.27) (0.06-2.04)	2.01 (0.11) (1.76-2.33)	266	24
G	2.30 (0.37) (1.17-3.57)	-	-	0.51 (0.36) (0.06-1.82)	1.94 (0.12) (1.65-2.25)	302	37

Continuous profiles of the thermal conductivity components parallel and perpendicular to the bedding plane directions and the volumetric heat capacity of full-diameter core samples recovered from two wells are presented in Figure 22. For general trend analysis, the original profiles of thermal properties were averaged in a 0.5 m moving window to obtain a vertical resolution comparable with the vertical resolution of the well-logging tools.
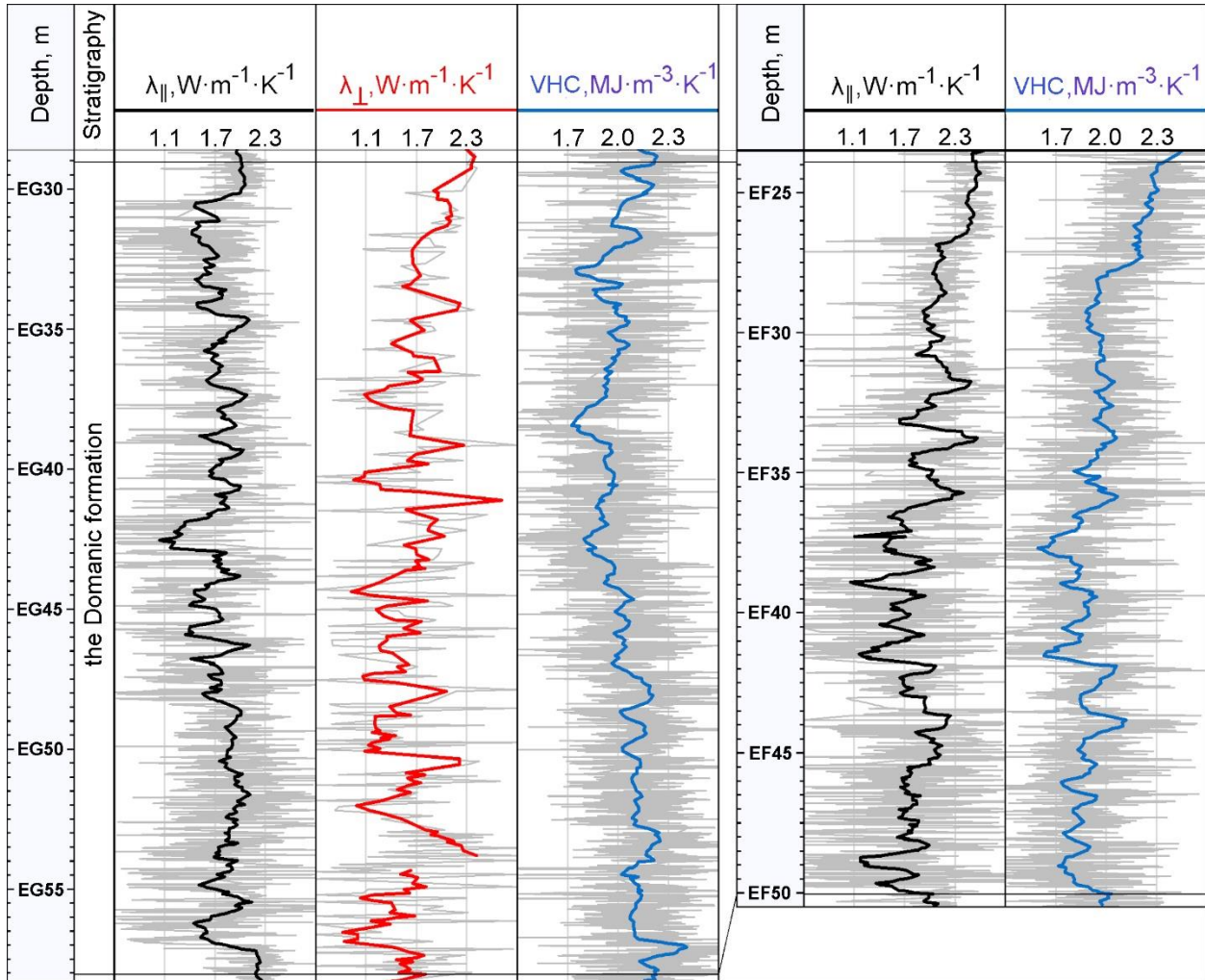
Figure 22. Results of rock thermal property measurements for wells F (left) and G (right). λ stands for rock thermal conductivity, subscripts ‖ and ⊥ stand for the thermal conductivity components in the directions parallel and perpendicular to the bedding plane, respectively; grey lines represent the original profiles of the rock thermal properties. Black, red and blue lines represent averaged thermal property profiles in a moving 0.5 window.

Thin layering is a distinguishing characteristic of the Domanic Formation, which results in significant vertical variations of rock thermal conductivity. For this reason, the implementation of the thermal core logging technique is the best way to detect the detailed variations in rock thermal properties. We consider the determination of rock thermal properties from well-logging data based on regression analysis and theoretical modelling for the investigated geological formation.

106

4.2.3. Calibrating gradient boosting regression model

The well-logging data were used as input data, while the rock thermal properties were used as the variables to predict. For the multiple regression analysis, we used a gradient boosting method (Friedman, 1999). The available data were subdivided into two random datasets: (1) a training dataset (comprising 66% of all the data) and (2) a test dataset (comprising 34% of all the data). The training dataset was used to fit a regression model to experimental data, while the test dataset was used to provide an unbiased evaluation of the regression model fit on the training dataset.

The input parameters were the neutron porosity (NPHI), bulk density (ρ), photoelectric factor (PEF), P- and S-wave sonic velocities (V_P and V_S), gamma-ray spectra inferred from K, Th, and U, and P and S-wave acoustic impedances ($V_P \cdot \rho$ and $V_S \cdot \rho$).

Before the gradient boosting training, we assessed the relative importance of each log in predicting rock thermal properties on the training data by means of the ranking method proposed by Chen et al. (2007), known as the noise-based perturbation. The results of the importance ranking for the Domanic Formation are presented in Figure 23.

The results show that the neutron porosity, acoustic impedance, and sonic velocities have the highest relative importance. The main reason for the strong correlation between the rock thermal properties and so-called porosity logs data (neutron, sonic, and density logs) is the high contrast (exceeding 10:1 in some cases) between the physical properties of the rock matrix and organic matter. This is similar to the contrast in porous rocks between the physical properties of the rock matrix and pore-filling fluid. In most cases, the relation between thermal properties and photoelectric factor is weak because it is mainly determined by mineralogical composition. The relation between thermal properties and natural radioactivity is

generally indirect. Uranium is adsorbed by kerogen (Balushkina et al., 2014), and many factors control the quantitative accumulation of uranium in organic-rich shales (e.g., Khaustova et al., 2019).
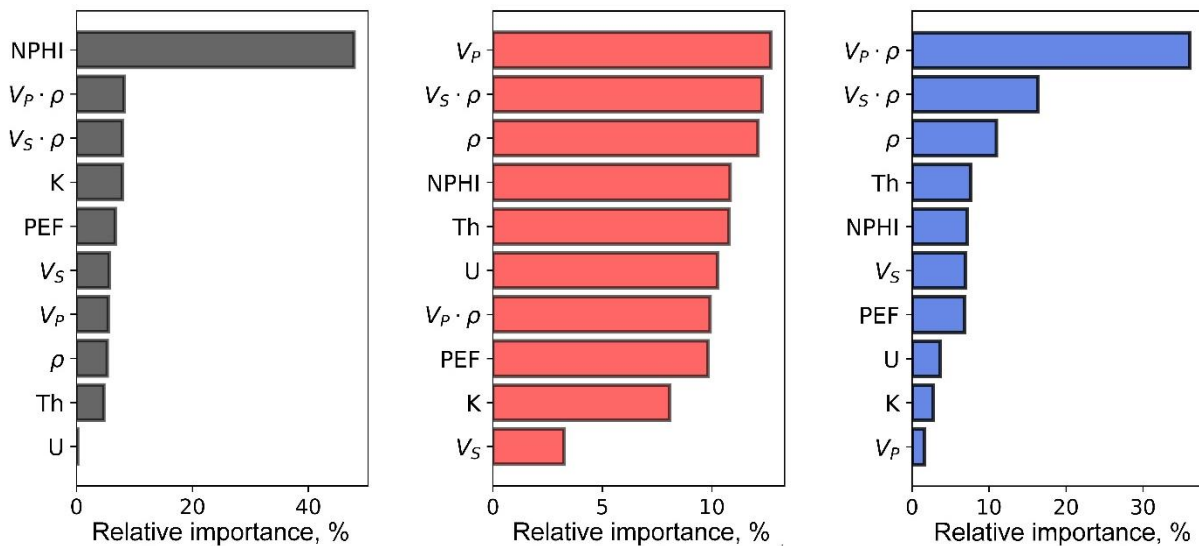
Figure 23. Well log importance during predicting rock thermal properties assessed via noise-based perturbation importance ranking method for the Domanic Formations. Black corresponds to thermal conductivity parallel to the bedding plane, red coloured diagram corresponds to thermal conductivity perpendicular to the bedding plane, and blue coloured diagram corresponds to rock volumetric heat capacity.

After the analysis of the importance of the well-logging parameters, we performed a regression analysis of the thermal properties and well-logging data using the gradient boosting method. We performed several iterations of regression model training, eliminating the worst (according to relative feature importance) input parameter on each iteration. Assessing the results of thermal property prediction on the training dataset, we established that the optimal threshold limit value for relative importance for predicting the thermal properties is 5%.

The gradient boosting algorithm was applied using the k-fold cross-validation method (Stone 1974). We used five k-folds. In the regression of the training dataset, we tuned the following set of hyperparameters: (1) learning rate, (2) number of boosting stages (number of estimators), and (3) maximum depth of the individual

108

regression estimators (max depth). The cross-validation was performed over the predefined grid of hyperparameters. The mean squared error was used to evaluate the model fit. The results of the hyperparameter tuning for gradient boosting of the training datasets of the Bazhenov and Domanic Formations are presented in Table 15.

Table 15. Results of hyperparameter tuning for gradient boosting of the training datasets.

Thermal property	Optimal parameters	RMSE	R^2	P,%	A,%	N
$\lambda_{\parallel}$, $W\cdot m^{-1}\cdot K^{-1}$	learning rate = 0.17 number of estimators = 115 max depth = 6	0.10	0.80	-0.1	5.1	313
$\lambda_{\perp}$, $W\cdot m^{-1}\cdot K^{-1}$	learning rate = 0.15 number of estimators = 109 max depth = 3	0.19	0.56	2.1	10.9	137
C, $MJ\cdot m^{-3}\cdot K^{-1}$	learning rate = 0.17 number of estimators = 105 max depth = 5	0.06	0.78	-0.5	2.9	313

The obtained correlation coefficients ($r = (R^2)^{0.5}$) between the measured and predicted values of the rock thermal properties are statistically significant according to Student's t-test for the 0.95 confidence level ($r^{critical} = 0.16$ for N = 137, $r^{critical} = 0.13$ for N = 296, $r^{critical} = 0.12$ for N = 313, and $r^{critical} = 0.11$ for N = 326). For test data, statistically significant correlation coefficients indicate the satisfactory quality of model fit.

4.2.4. Calibrating theoretical models of thermal properties

The same training and testing datasets were used for calibrating and assessing theoretical models of rock thermal properties. As well as for the Bazhenov Formation (Section 3.1.2), we investigated the effectiveness of three theoretical models for predicting the thermal conductivity of the Domanic Formation: Lichtenecker-Asaad model (equation 4), Krischer-Esdorn model (equation 5), and Lichtenecker-Rother model (equation 6).

The Domanic Formation present six components: shale, siliceous rock, limestone, dolostone, kerogen, and oil. For lithological components, we assumed that they consist of one main and secondary minerals and that physical properties are mainly determined by the physical properties of the dominant mineral. The dominant mineral in shale, siliceous rock, limestone and dolostone are illite, silicates (mainly chalcedony), calcite and dolomite, respectively.

Theoretical model calibration requires data on rock thermal properties, volumetric fractions of rock-forming mineralogical components, and thermal properties of rock-forming mineralogical components. The data on the rock thermal properties were inferred from the results of thermal core logging, and the data on the volumetric fractions were inferred from the well-logging data. The data on the thermal properties of rock-forming minerals were inferred from Table 8.

The model calibration implies the (1) application of reliable data to the thermal properties of rock-forming mineral components, (2) determination of correction factors to theoretical models in the directions parallel and perpendicular to the bedding plane, and (3) minimization of the mean relative discrepancy between measured and calculated rock thermal properties.

For the Domanic Formation rocks, the data on the volumetric fractions of the lithological rock-forming components were available. Thus, we assigned the upper constraint of the possible range for a given thermal property that was assumed equal to the value of the dominant mineral. The results of the model (Table 16) reveal that:

- The rock thermal conductivity parallel to the bedding plane can be predicted by the theoretical models more accurately than thermal conductivity perpendicular to the bedding plane.
- Among the considered theoretical models of rock thermal conductivity, the Lichtenecker-Rother model yields the lowest prediction uncertainty and the highest values of R^2 between measured and predicted values.

110

- The rock components have different values of thermal conductivity along different directions. This can be observed at the lithological scale.

Table 16. Calculated values of thermal properties for rock-forming components for the training dataset of the Domanic Formation.

Theoretical model	Thermal conductivity of lithological components parallel to the bedding plane (N = 313), $W \cdot m^{-1} \cdot K^{-1}$										
	Limestone	Dolostone	Organic matter	Siliceous rock component	Shale	Oil	Correction factor	R^2	RMSE, $W \cdot m^{-1} \cdot K^{-1}$	P,%	A,%
Lichtenecker-Asaad	2.42	2.58	0.60	2.43	1.90	0.13	0.05	0.54	0.16	8.1	-0.3
Lichtenecker-Rother	2.44	3.33	0.53	3.08	1.80	0.14	0.48	0.64	0.14	6.9	0.3
Krischer-Esdorn	2.49	3.50	0.31	3.22	1.87	0.11	0.95	0.61	0.14	6.9	0.1
	Thermal conductivity of minerals/fluids perpendicular to the bedding plane (N = 137), $W \cdot m^{-1} \cdot K^{-1}$										
Lichtenecker-Asaad	2.09	2.58	0.15	2.38	1.51	0.13	0.36	0.26	0.25	12.9	0.6
Lichtenecker-Rother	2.06	3.25	0.18	2.37	1.46	0.13	0.35	0.31	0.24	12.3	0.2
Krischer-Esdorn	2.07	3.15	0.10	2.53	1.10	0.11	0.90	0.33	0.23	12.1	0.3
	Volumetric heat capacity of lithological components (N = 313), $MJ \cdot m^{-3} \cdot K^{-1}$										
Weighted arithmetic mean	2.09	2.20	1.64	1.98	1.80	1.53	-	0.42	0.09	4.4	-1.2

The obtained results coincide with results that were obtained for the Bazhenov formation (Section 3.1.2). Based on these points, the Lichtenecker-Rother model was used for predicting rock thermal conductivity from well-logging data.

4.2.5. Predicting rock thermal properties from well logging data on a test dataset

Rock thermal properties were predicted on a test dataset with both the gradient boosting and theoretical models of rock thermal properties. We assessed the prediction uncertainty from the comparison of predicted values and experimental data of the rock thermal properties (Table 17). Figure 24 plots the thermal property predictions and experimental values of the rock thermal properties for the test datasets.

Table 17. Prediction results of the rock thermal properties on the test dataset.

| | Thermal conductivity | | | | | | | | Volumetric heat capacity | | | | |
| | $\lambda_{\parallel}$ | | | | $\lambda_{\perp}$ | | | | | | | | |
Model*	R^2	RMSE $W \cdot m^{-1} \cdot K^{-1}$	P %	A %	R^2	RMSE $W \cdot m^{-1} \cdot K^{-1}$	P %	A %	Model	R^2	RMSE $MJ \cdot m^{-3} \cdot K^{-1}$	P %	A %
GB	0.80	0.10	5.1	0.1	0.56	0.19	10.9	2.1	GB	0.78	0.06	2.9	0.5
LR	0.59	0.15	6.6	1.8	0.25	0.24	12.8	0.7	AM	0.44	0.10	4.8	0.6

*GB stands for the gradient boosting method, LR stands for the Lichtenecker-Rother model, AM stands for the weighted arithmetic mean model.
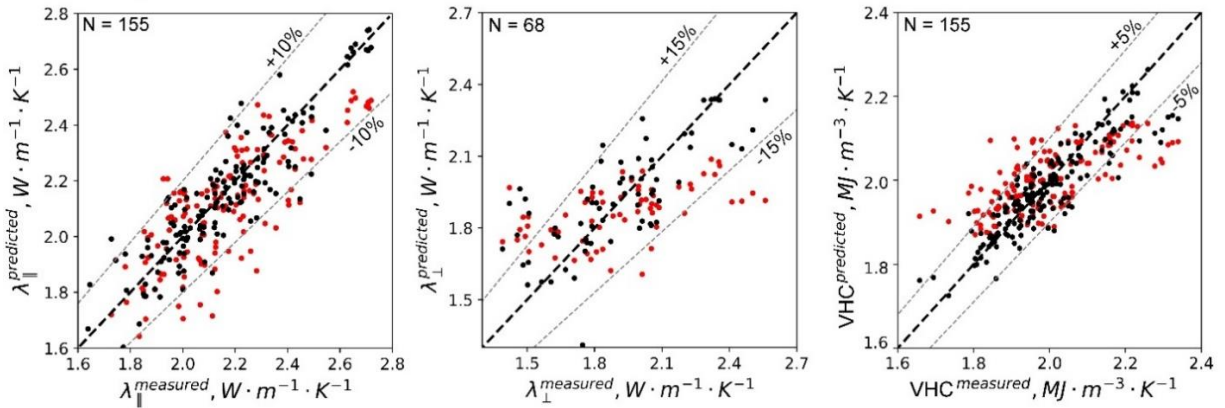
Figure 24. Experimental data of the rock thermal properties compared to the thermal properties predicted from well-logging data of training datasets for the Domanic Formation. Black dots present results with the gradient boosting method, red dots results via theoretical model. The dashed black line (y=x) shows a perfect prediction.

Compared to theoretical models, the gradient boosting algorithm provides more precise predictions of thermal conductivity and volumetric heat capacity from well-logging data. This is evidenced by the higher values of R^2 between the measured and predicted values and lower values of RMSE and P.

As well as for the Bazhenov Formation, the results presented in Table 17 and Figure 24 revealed that theoretical models of thermal properties provide less accurate predictions from well-logging data than the gradient boosting algorithm for organic-rich shales.

Boxplots of the relative discrepancies between the measured and predicted values for a detailed uncertainty analysis are plotted in Figure 25.
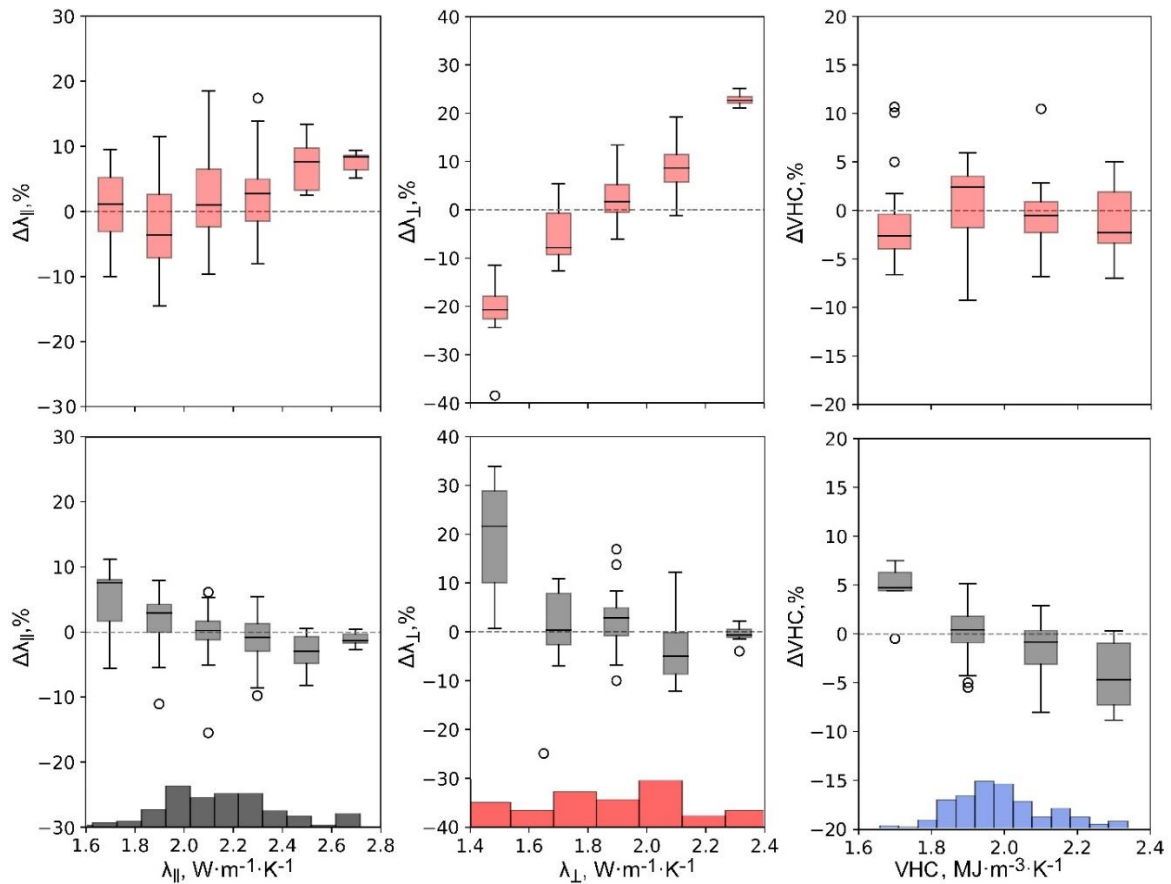
Figure 25. Boxplots of the relative discrepancies between the measured and predicted values of rock thermal properties for the Domanic Formation. Above, predictions based on the theoretical models; below, predictions based on the gradient boosting algorithm. Histograms of thermal properties from the test dataset are also shown.

As well as for the Bazhenov Formation, there is a systematic underestimation of rock thermal conductivity when predicting via the Lichtenecker-Rother model for within the range of low thermal conductivities (1.4-1.6 $W \cdot m^{-1} \cdot K^{-1}$) of the Domanic Formation rocks. In general, the gradient boosting algorithm yields less biased thermal properties predictions than the theoretical models of thermal properties. A high level of bias is observed in the prediction of the thermal conductivity perpendicular to the bedding plane with both the Lichtenecker-Rother model and the gradient boosting algorithm. This bias can be conditioned by the effect of the imposed fracturing that occurred due to the unloading of core samples.

4.2.6. Corrections for in situ temperature and pressure

Following the workflow (Figure 18), the predicted rock thermal properties require correction for *in situ* temperature and pressure. As we did not measure rock thermal properties at high temperature and pressure in this study, we use data available in the literature to account for *in situ* conditions.

Recent investigations of rock samples from the Domanic Formations (Gabova et al., 2020) have revealed that the average decrease in thermal conductivity (λ_l) for Domanic Formation rocks at 60 °C is ~4%.

Temperature corrections for thermal conductivity should be performed to account for thermal anisotropy since there are different dependencies of thermal conductivity on pressure and temperature for components parallel and perpendicular to the bedding plane directions (as shown by Wang et al., 2018). In literature, there are still no reliable experimental data on the dependencies of thermal conductivity on temperature accounting for the thermal anisotropy of the rocks from the Domanic Formation. Thus, we assumed that the temperature corrections for thermal conductivity parallel and perpendicular to the bedding plane are both 4%.

There is no data in the literature on dependencies of thermal conductivity of the Domanic Formation rocks from pressure. Therefore, we can only assume that for Domanic Formation rocks and the Bazhenov Formation rocks (Section 2.1.2.4), the necessary pressure correction does not exceed 5%.

Following Waples D. and Waples S. (2004) research results, we imply a negligible effect of pressure volumetric heat capacity (for the in situ pressure of the Domanic Formations, the increase in pressure is less than approximately 1%). The temperature effect on volumetric heat capacity can be inferred from Savest and Oja (2013). According to their results, the correction to volumetric heat capacity for oil shales at temperature 60 °C amounts approximately to 5%.

4.3. Comparison of the WBLT for determining rock thermal properties and Deming approach

Among the few approaches so far proposed to account for the thermal anisotropy, one of the most commonly used was suggested by Deming (1994). There are many studies that apply this approach for the investigations of basin thermal structures and variations of heat flow density (see, e.g. Corry and Brown, 1998; Tanikawa et al., 2016). A comparison of the technique proposed in this study and the Deming correction approach was performed to assess their effectiveness.

4.3.1. Workflow of the Deming correction approach

The Deming approach relies on the application of the theoretical model of Lichtenecker. The thermal anisotropy of a certain component is assumed as a main factor resulting in thermal anisotropy of a rock. For a two-component porous rock thermal conductivity for parallel and perpendicular directions to the bedding plane are given by:

$$\lambda_\parallel = \lambda_{matrix\,\parallel}^{1-\phi} \cdot \lambda_{fluid}^{\phi} \tag{21}$$

$$\lambda_\perp = \lambda_{matrix\,\perp}^{1-\phi} \cdot \lambda_{fluid}^{\phi} \tag{22}$$

where $\lambda_\parallel$ is effective thermal conductivity of a rock for parallel direction to the bedding plane, $\lambda_\perp$ is effective thermal conductivity of a rock for perpendicular direction to the bedding plane, $\lambda_{matrix\parallel}$ and $\lambda_{matrix\perp}$ are thermal conductivity of a rock matrix for parallel and perpendicular directions, respectively, λ_{fluid} is thermal conductivity of a fluid and ϕ stands for porosity.

Thermal conductivity of rock matrix for parallel and perpendicular directions can be determined from minimization of the discrepancy between measured and predicted thermal conductivity for corresponding directions.

4.3.2. Case study: predicting rock thermal conductivity accounting for thermal anisotropy based on the Deming approach and the novel WLBT for determining rock thermal properties

The object of investigation is the same that was described within Section 3.2. The data for clayey rocks is considered in the case study. The results of determining rock thermal conductivity on the basis of the Krischer-Esdorn model are presented in Section 3.2.2.3.

4.3.2.1 Calibrating the Lichtenecker model via the Deming approach

From correlation analysis of high-definition spectroscopy data and the thermal anisotropy coefficients inferred from thermal core logging, we established that there are statistically significant correlations between the coefficient of thermal anisotropy and the volume fraction of illite and kaolinite (Figure 26).
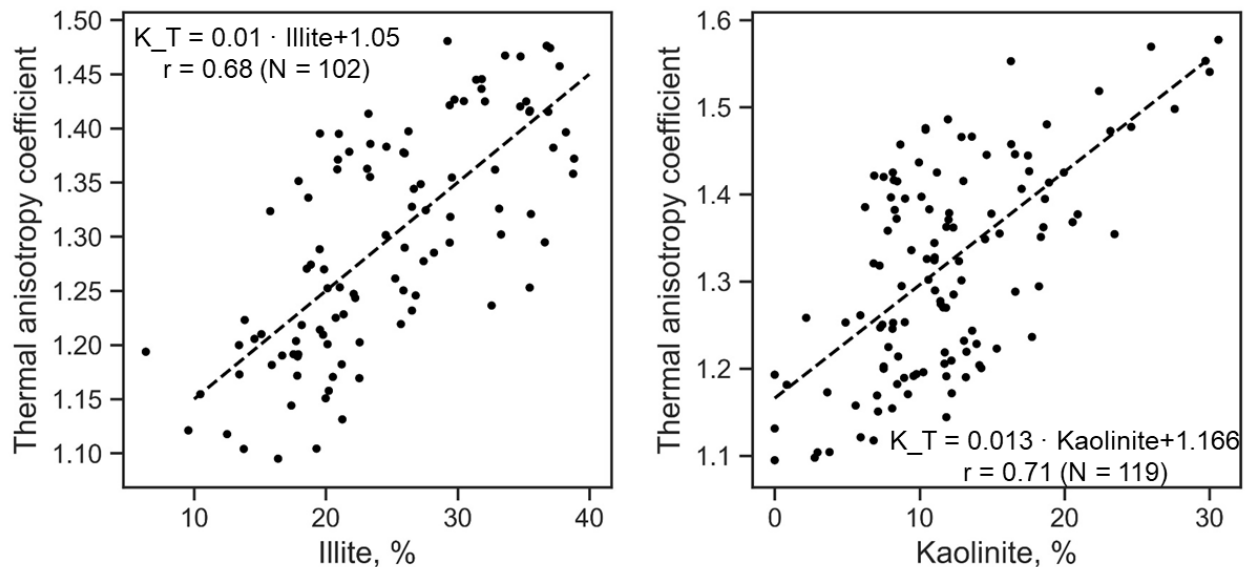
Figure 26. Cross-plots between thermal anisotropy coefficient and illite volume fraction (left panel) and thermal anisotropy coefficient and kaolinite volume fraction (right panel). The dashed lines represent the regression trend.

Thus, we assumed three-component media composed of isotropic rock matrix, anisotropic clayey minerals and pore-filling fluid. The rock matrix is composed of

orthoclase, albite, siliceous minerals, and siderite and its thermal conductivity of was calculated using data on volume fractions of minerals (inferred from high-definition spectroscopy) and data on thermal conductivity of those minerals (Section 3.1.2.2, Table 8) with the Lichtenecker model. Due to extremely low permeability, the pore space of the investigating rocks was considered fully water-saturated. The Lichtenecker model can be rewritten the following way:

$$\lambda_{\parallel} = \lambda_{matrix}^{V_{matrix}} \cdot \lambda_{clay\parallel}^{V_{clay}} \cdot \lambda_{fluid}^{\phi} \tag{23}$$

$$\lambda_{\perp} = \lambda_{matrix}^{1-\phi} \cdot \lambda_{clay\perp}^{V_{clay}} \cdot \lambda_{fluid}^{\phi} \tag{24}$$

To determine the thermal conductivity of clayey component, the constrained genetic minimization algorithm (Storn and Price, 1997) was applied. The available data were subdivided into the same random training (66% of all data) and test datasets (34% of all dataset) that were presented in Section 3.2. From minimization of the discrepancy between predicted and measured values of thermal conductivity on a training dataset it was established that thermal conductivity of clayey component for parallel and perpendicular directions to the bedding plane is 2.57 W·m^{-1}·K^{-1} and 1.21 W·m^{-1}·K^{-1}, respectively. The calculated values of R2, RMSE, accuracy and precision for the training dataset are summarized in Table 18.

Table 18. Prediction results of the rock thermal properties on the training datasets.

$\lambda_{\parallel}$				$\lambda_{\perp}$			
R^2	RMSE, W·m^{-1}·K^{-1}	P, %	A,%	R^2	RMSE, W·m^{-1}·K^{-1}	P, %	A, %
0.25	0.15	12.4	0.9	0.56	0.18	20.1	-0.1

4.3.2.2 *Training gradient boosting regression models for determining rock thermal conductivity accounting for thermal anisotropy*

The well-logging data were used as input data, while the data on rock thermal conductivity for parallel and perpendicular directions to the bedding plane were used as the variables to predict. The available well-logging data include radioactivity, density, photoelectric factor, neutron porosity, P-wave and S-wave velocities for

parallel and perpendicular directions to the bedding plane (that were inferred from cross-dipole sonic log data). Additionally, as input data, the calculated acoustic impedances ($V_P \cdot \rho$, $V_S \cdot \rho$) were used. The initial dataset was subdivided the same way (exactly the same depth points) as it was done in Section 4.3.2.1.

For the multiple regression analysis, we used a gradient boosting method (Friedman, 1999). The training dataset was used to fit the regression model to experimental data, while the test dataset was used to provide an unbiased evaluation of the regression model fit on the training dataset.

The gradient boosting algorithm was applied using the k-fold cross-validation method (Stone 1974). We used three k-folds. In the regression of the training dataset, we tuned the following set of hyperparameters: (1) learning rate, (2) number of boosting stages (number of estimators), (3) maximum depth of the individual regression estimators (max depth), and the fraction of samples to be used for fitting the individual base learners (subsample). The cross-validation was performed over the predefined grid of hyperparameters. A mean squared error was used to evaluate the model fit.

The results of the hyperparameter tuning for gradient boosting on the training datasets are presented in Table 19. The obtained correlation coefficients ($r = (R^2)^{0.5}$) are statistically significant according to Student's t-test for the 0.95 confidence level ($r^{critical} = 0.17$ for N = 128, $r^{critical} = 0.21$ for N = 92).

Table 19. Results of hyperparameter tuning for gradient boosting of the training datasets.

Thermal conductivity	Optimal parameters	RMSE	R^2	P,%	A,%	N
$\lambda_{\parallel}$, $W \cdot m^{-1} \cdot K^{-1}$	learning rate = 0.1 number of estimators = 60 max depth = 3 subsample = 0.2	0.04	0.92	5.1	0.1	128
$\lambda_{\perp}$, $W \cdot m^{-1} \cdot K^{-1}$	learning rate = 0.13 number of estimators = 30 max depth = 3 subsample =5	0.06	0.96	11.6	0.1	92

4.3.2.3   *Predicting rock thermal conductivity based on the Deming approach and the gradient boosting regression models*

The values of thermal conductivity of the clayey component for parallel and perpendicular directions to the bedding plane were used to predict rock thermal conductivity on a test dataset. As well as for the training dataset, the matrix thermal conductivity for the test dataset was calculated using data on volume fractions of minerals (inferred from high-definition spectroscopy) and data on thermal conductivity of that minerals via the Lichtenecker model (equations 23 and 24). The trained gradient boosting regression models were used for predicting thermal conductivity for parallel and perpendicular directions to the bedding plane on a test dataset. The results of thermal conductivity predictions based on the Deming approach and the novel WLBT technique are presented in Table 20.

Table 20. Prediction results of the rock thermal properties on the test dataset.

Model*	$\lambda_{\parallel}$				$\lambda_{\perp}$			
	R^2	RMSE $W \cdot m^{-1} \cdot K^{-1}$	P %	A %	R^2	RMSE $W \cdot m^{-1} \cdot K^{-1}$	P %	A %
Deming	0.1	0.15	12.7	-0.9	0.56	0.18	20.8	0.1
GB	0.93	0.07	6.06	0.2	0.73	0.14	15.4	0.3

*GB stands for the gradient boosting method; Deming stands for predictions that are based on the Deming approach.

Figure 27 shows measured and predicted values of rock thermal conductivity for parallel and perpendicular directions to the bedding plane.
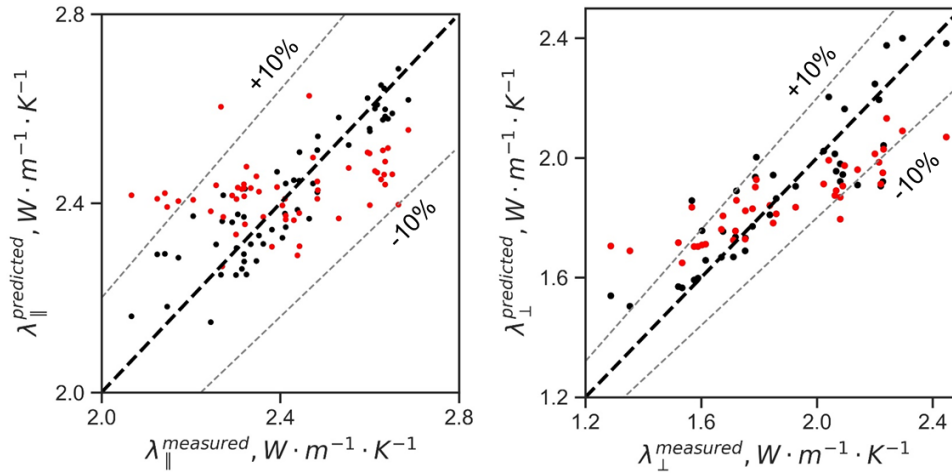
Figure 27. Experimental data of the rock thermal conductivity compared to the thermal conductivity predicted from well-logging data of test datasets for the investigating clayous rocks. Black dots present results with the gradient boosting method, red dots results via the Deming approach. The dashed black line (y=x) shows perfect prediction.

The Deming correction approach provided less precise predictions of rock thermal conductivity both for parallel and perpendicular directions. WBLT provided essentially more accurate predictions based on both theoretical model-based approach (see Table 20) and regression model-based approach (the gradient boosting regression models in our case) according to higher values of R^2 between the measured and predicted values and lower values of RMSE and precision. Concurrently, comparing Table 20 and Table 17 it can be concluded that, thermal conductivity predictions for both parallel and perpendicular directions that were made based on the Krischer-Esdorn model and the gradient boosting regression models are of relatively similar quality (according to the obtained metrics).

For a detailed uncertainty analysis, the boxplot of the relative discrepancies between the measured and predicted values is depicted in Figure 28. From the analysis of the obtained boxplots it can be concluded that the Deming correction approach yields systematic errors for low and high thermal conductivities both for parallel and perpendicular directions. The gradient boosting regression models yield systematic errors within the range of 2-2.2 W·m^{-1}·K^{-1} for thermal conductivity

parallel to the bedding plane and within the range of 1.2-1.6 W·m^{-1}·K^{-1} for thermal conductivity perpendicular to the bedding plane.

The obtained results demonstrate that WBLT is significantly more effective compared to the approach suggested by Deming. The higher effectiveness of the WLBT is conditioned by the application of enhanced theoretical models of thermal conductivity, advanced machine-learning techniques, and integration of thermal core logging data.
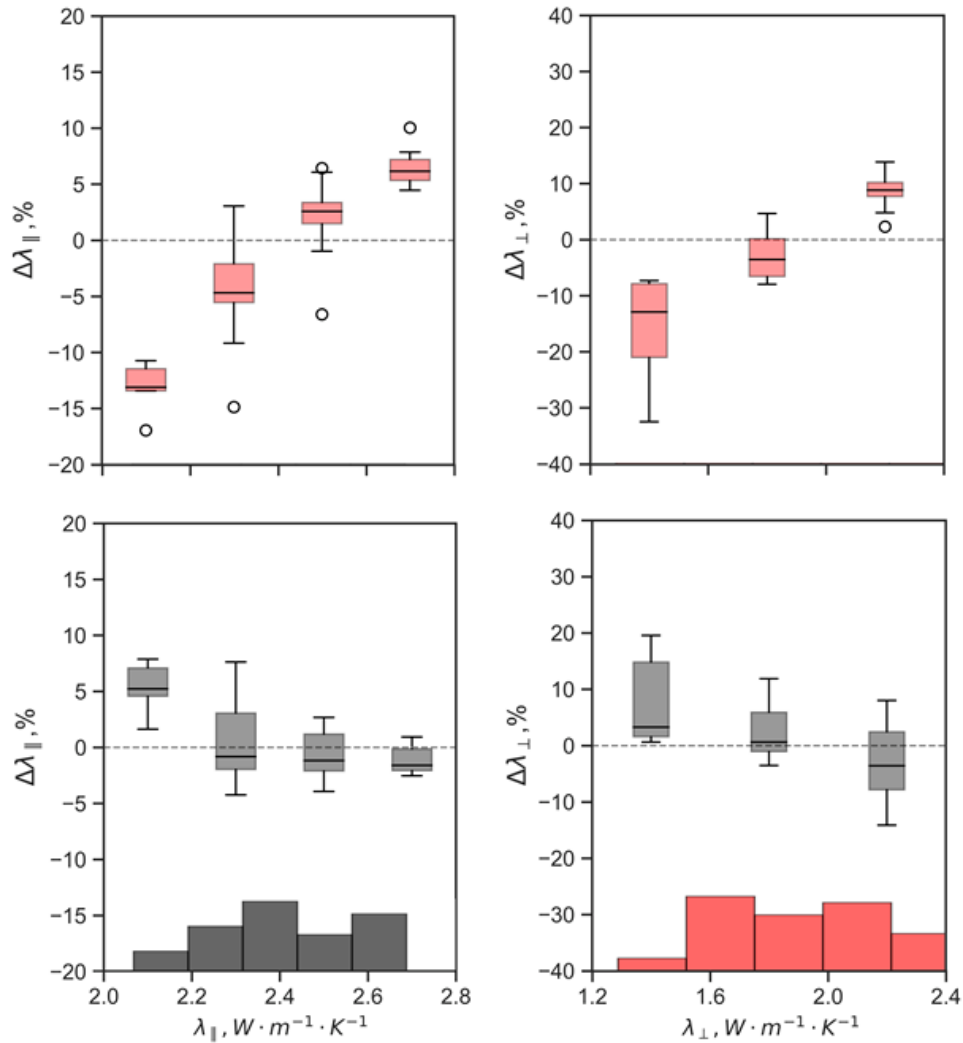
Figure 28. Boxplots of the relative discrepancies between the measured and predicted values of rock thermal conductivity for the investigating clayous rocks. The upper panel represents the boxplots for predictions that are made via the Deming correction approach. The lower panel represents the boxplots for predictions that are made via the gradient boosting regression models. Histograms of thermal conductivities for the test dataset are also shown.

4.4. Conclusions

The developed approaches (Chapters 2 and 3) for predicting rock thermal properties accounting for thermal anisotropy, rock heterogeneity and *in situ* thermobaric conditions were unified and presented within the novel, well-defined technique, referred to as WLBT. This technique's workflow relies on the application of advanced thermal core logging technique that provides continuous non-contact non-destructive profiling of thermal conductivity (principal components of thermal conductivity) and volumetric heat capacity on full-diameter cores, core plugs, and broken cores. WLBT implies the application of advanced machine-learning techniques or enhanced theoretical modelling depending on the available input data.

WLBT was tested for organic-rich shales of the Domanic Formation. From the comparison of the experimental and predicted data on rock thermal properties, it can be concluded that novel WLBT provided uncertainties in data on thermal conductivity for parallel direction less than 7%, for perpendicular direction – less than 13% and uncertainties in data on volumetric heat capacity is less than 5%.

A comparison study between WLBT and the commonly used Deming approach was conducted within the case study on rocks of the Tumen Formation. The prediction results revealed that WLBT provides more precise predictions of thermal conductivity for both parallel and perpendicular directions to the bedding plane. The higher effectiveness of WLBT is conditioned by application of enhanced theoretical models of thermal conductivity, of advanced machine-learning techniques and integration of the thermal core logging data. Thus, testing of the WLBT technique indicated its universal applicability.

Chapter 5. Results of implementing WLBT for determining rock thermal properties during investigations of oil fields

Information about the actual heat flow and rock thermal properties is necessary for modelling sedimentary basins and oil- and gas-bearing systems (Hantschel & Kauerauf, 2009). It was shown that uncertainties in these data lead to a severe reduction of modelling (Chekhonin et al., 2020). There are many biases of the previously used methods that lead to unreliable data on heat flow density (Popov et al., 2019b).

In this Chapter I present two case studies of geothermal investigations of prospecting and appraisal wells located in Russia. The performed investigations were conducted by means of the modern methodological and experimental basis of thermal petrophysics. The performed geothermal investigations demonstrated that the WLBT for determining rock thermal properties is a critical component for reliable determining vertical variations of heat flow density.

5.1 Determining vertical variations of rock thermal properties and heat flow density along Bazhenovskaya 1 well

In this Section, I describe the results of implementing WLBT for predicting rock thermal conductivity in a geothermal study of the southwest part of Lyaminsk oil and gas region, West Siberian basin.

5.1.1. Object of study

The investigated well is located in the southwest part of the Lyaminsk oil and gas region of the West Siberian basin near the Khanty-Mansyisk city, Russia (Figure 29). The area understudy occurs in the Elisarov downfold. According to the results of structural-facial zoning, the investigated area is classified as a transitional zone of the Bazhenov Formation into the Tutleim Formation.

Well drilling was started and completed in 2018. The well is almost vertical. The maximum well inclination does not exceed 1º 80'. The final depth of the well is 3202.8 m. The geological profile of the investigating well includes the Vikulov, Frolov, Tutleim, Abalak, and Tymen formations as well as pre-Jurassic deposits

(Table 21). The total length of cored intervals is 643.8 m with 89.3% core recovery (574.98 m).

Figure 29. Geographic location of the Bazhenovskaya well №1 (retrieved from https://www.crru.ru). The large yellow point indicates the location of well.

Table 21. Characteristics of the rocks from the investigating well based on the analysis of the recovered cores.

№	Rock type	Age	Logging depth, m	N*
1	Interbedding of siltstones, argillites and quartz sandstones.	K_1vk	1735-1786.9	310
			2131.6-2196.6	626
2	Argillites with rare thin layers of marl.	K_1fr	2416.6-2462.6	247
			2720.1-2770	376
3	Bituminous argillites with pyritization and fractures in the upper part. Bituminous clayey rocks with pyritization in the lower part.	K_1tt_2	2770-2791.33	147
	Bituminous clayey carbonate thin bedded rocks with pyritization. In some cases with siliceous components.	$J_3 - K_1tt_1$	2802.12-2827.92	157
4	In the upper part – thin bedded argillites with rare layers lenses of sandstone and siltstone. In the lower part – interbedding of siltstone and argillite.	$J_{2-3}ab$	2828-2846.6	147
6	Inhomogeneous interbedding of argillite and siltstone with rare layers of coal and sandstones in the upper part. Inhomogeneous interbedding of argillite, siltstone and sandstone with thin layers of coal and marl in the middle part. In the lower part – interbedding of sandstone, conglomerate and sandy gravelstone with thin layers of argillite and coal.	J_2tm	2847-3030	1324
7	3030-3032.5 – crust of weathering composed of gravelstone, argillite, coal and siliceous-clayey rocks. 3032.5-3202.8 – pre-Jurassic formation composed of (1) in the upper part - rhyolite, rhyolite-rhyodacite tuffs, (2) in the middle part – siltstone, argillite, and sandstone, and (3) in the lower part – rhyolite and rhyolite-rhyodacite tuffs.	P-T	3030-3202.8	768

*N – number of recovered core samples.

5.1.2. Results of measuring rock thermal properties and temperature logging

The following set of experimental investigations was conducted:

- Continuous thermal core logging with optical scanning technique of all recovered full-sized cores.

- Additional measurements of rock thermal properties on a representative collection of standard core plug at different saturations with the optical scanning laser setup.

- Measurements of rock thermal properties at elevated temperatures on a representative collection of standard plugs with the optical scanning laser device, DTC-300 instrument and DCS 214 Polyma (NETZSCH).

Representative collections of core samples for additional measurements were selected based on results of the continuous thermal core logging of full-sized cores and its lithological description.

During thermal core logging, the total relative measurement uncertainty did not exceed ±2.5% for thermal conductivity (with measurement precision not exceeding ±1.5%), ±4% for thermal diffusivity, and ±5% for the volumetric heat capacity (measurement uncertainties are reported for 0.95 confidence level). Figure 30 shows the distributions of the average rock thermal conductivity components for parallel and perpendicular directions to the bedding plane, rock volumetric heat capacity, thermal anisotropy coefficient, and heterogeneity factor for the investigated depth intervals of the Vikulov Formation (1753-2055 m depth) and the Frolov Formation (2105-2770 m depth).
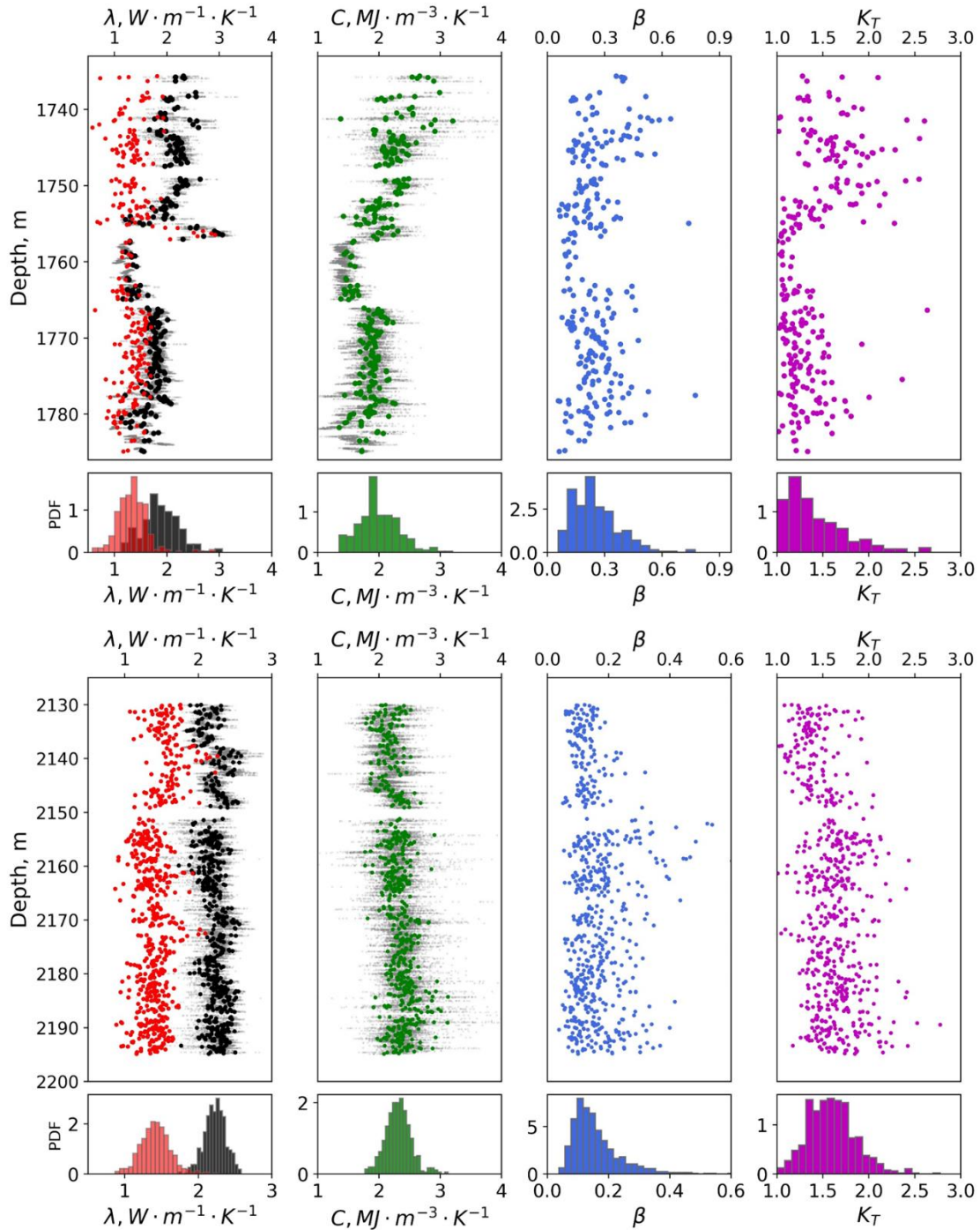
Figure 30. Results of continuous thermal core logging for depth intervals of the Vikulov (upper panel) and Frolov formations (lower panel). Black coloured dots represents thermal conductivity parallel to the bedding plane, red coloured dots represent thermal conductivity perpendicular to the bedding plane, green colored dots represent volumetric heat capacity, blue coloured dots represent thermal heterogeneity factor, and purple coloured dots represent thermal anisotropy coefficient. Grey coloured dots represent high-resolution profiles (with 1-mm spatial resolution) of thermal conductivity and volumetric heat capacity.

126

To correct the continuous thermal core logging results for *in situ* saturation, measurements of rock thermal properties (with the optical scanning laser setup) and porosity on 40 core plugs were conducted. Measurements on standard core plugs were conducted at "as received" dried and saturated states. These measurements enabled establishing the dependence of the relative increase of thermal properties after full water saturation from rock porosity. An example of the assessment of relative increase of thermal conductivity after saturating core samples is presented in Figure 31.
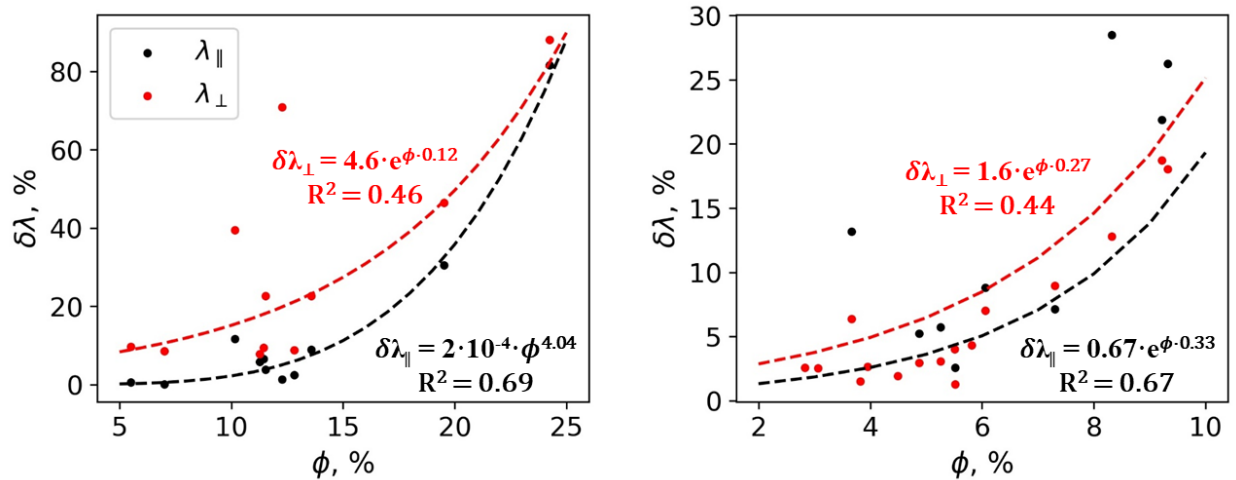
Figure 31. The dependency of relative increase of thermal conductivity after water saturation from porosity for the Vikulov and Frolov formations (left panel) and for the Abalak and Tyumen formations (right panel). Red colored dots and regression trend represent data for thermal conductivity perpendicular to the bedding plane. Black colored dots and regression trend represent data for thermal conductivity parallel to the bedding plane.

The results of temperature logging are given in Figure 32. The precision of temperature measurements did not exceed ±0.007 °C. The industrial partner conducted the temperature logging. Since drilling was suspended for at least six months, the registered temperature gradient can be considered as in equilibrium. Figure 32 (right panel) plots the results of the temperature gradient calculations for each 50 m depth interval with a 10 cm step.
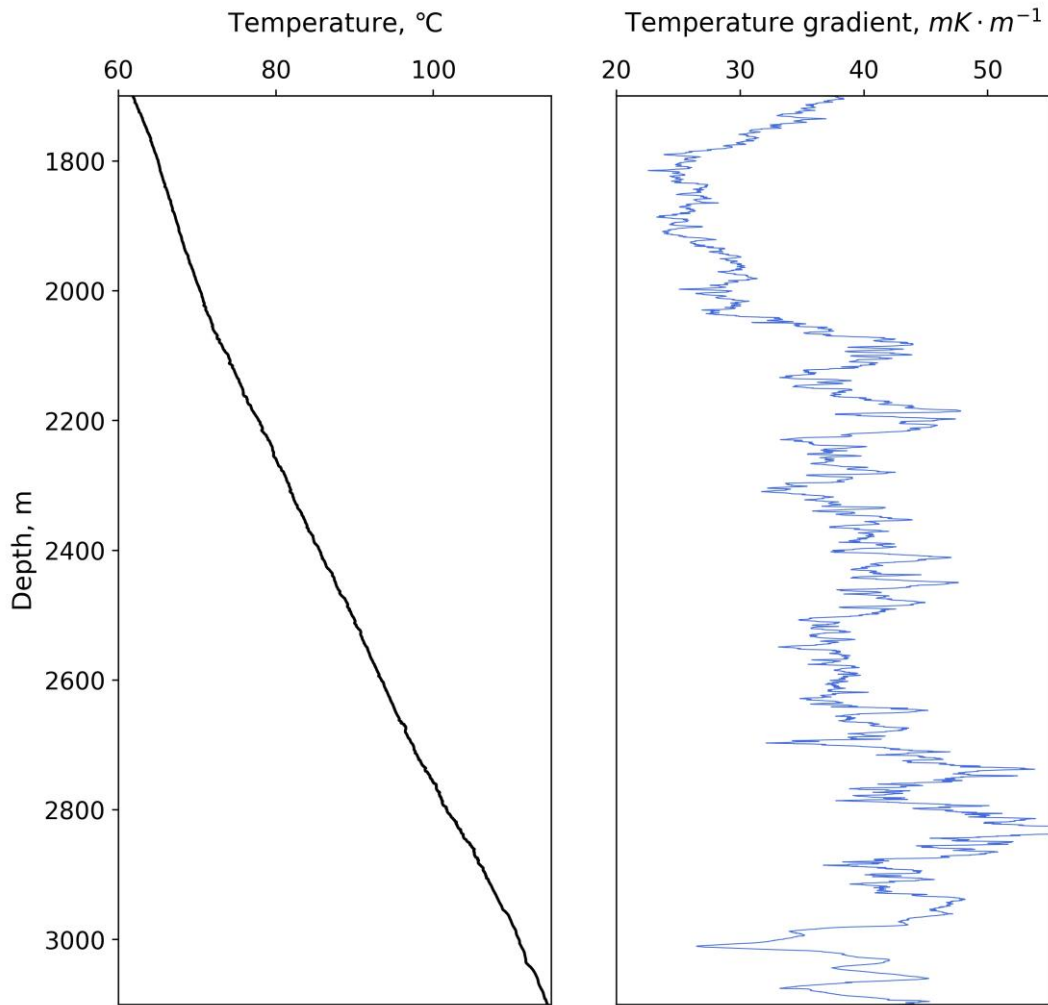
Figure 32. The temperature and temperature gradient along the well.

5.1.3. Results of application of WLBT for determining rock thermal conductivity within non-coring intervals

The target intervals for predicting rock thermal properties from well-logging data within non-coring intervals were the Vikulov and Frolov formations. According to the results of thermal core logging, these formations exhibit a considerable degree of thermal anisotropy (Figure 33).
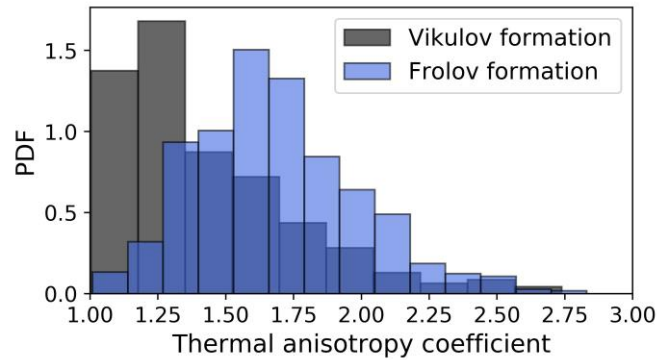
Figure 33. The histogram of thermal anisotropy coefficient for the Vikulov (black colour) and the Frolov (blue colour) formations.

The oriented bedded texture of argillites in the Frolov Formation condition higher degree of thermal anisotropy than the Vikulov Formation rocks. The rocks from the Vikulov and Frolov Formations at *in situ* conditions are water-saturated according to results of interpreting well-logging data and analysis of recovered core samples. The directions of principal axes of thermal conductivity tensor for the investigating rocks coincide with parallel and perpendicular directions to the bedding plane according to results of thermal core logging of full-sized cores and standard core plugs. Hence, during thermal core logging, the scanning lines were parallel and perpendicular to the bedding plane.

The rock thermal properties for the Vikulov Formation were determined using theoretical modelling.

The Lichtenecker-Rother model was used for predicting rock thermal conductivity. A two-component medium (rock matrix and pore-filling fluid) was considered for the Vikulov Formation rocks. The application of the Lichtenecker-Rother model requires data on thermal conductivity of rock matrix, thermal conductivity of the pore-filling fluid, porosity, and the correction factor "α" (see formula 6, Seciton 3.2.2.). The thermal conductivity of water was assumed 0.6 W·m⁻¹·K⁻¹ and data on rock porosity was inferred by standard processing and interpreting

the density log data. The data on thermal conductivity of matrix and the correction factor were inferred with a procedure that is articulated in the following steps.

In the first step, we used the results of measurements of rock thermal properties on standard core plugs. Since results of measurements were available for dried and water-saturated states, we solved for each core sample the system of equations:

$$\begin{cases} \lambda_{eff}^{dry} = \left((1 - \phi) \cdot \lambda_{matrix}^{\alpha} + \phi \cdot \lambda_{air}^{\alpha}\right)^{\frac{1}{\alpha}} \\ \lambda_{eff}^{water} = \left((1 - \phi) \cdot \lambda_{matrix}^{\alpha} + \phi \cdot \lambda_{water}^{\alpha}\right)^{\frac{1}{\alpha}} \end{cases} \tag{25}$$

where λ_{eff} ^{dry} is effective thermal conductivity for dried core plug, λ_{eff} ^{water} is effective thermal conductivity for water-saturated core plug, ϕ is porosity, λ_{matrix} is the thermal conductivity of rock matrix, λ_{air} is the thermal conductivity of air, λ_{water} is thermal conductivity of water and α is a correction factor. The modelling implies several assumptions:

- rock matrix is isotropic;
- anisotropy of rocks is conditioned by the oriented laminated texture of rocks (structural nature of anisotropy).
- the correction factor α encompasses the effect structural and textural peculiarities of rocks on rock thermal conductivity;
- the correction factor α does not depend on saturation type.

Firstly, this system of equations was solved for the parallel component of thermal conductivity. Secondly, this system of equations was solved for the perpendicular component of thermal conductivity but with already known values of matrix thermal conductivity. This is justified by the more significant influence of micro fracturing of rocks on the perpendicular component of thermal conductivity. Figure 34 illustrates the distribution of matrix thermal conductivity and correction factor for parallel and perpendicular directions.
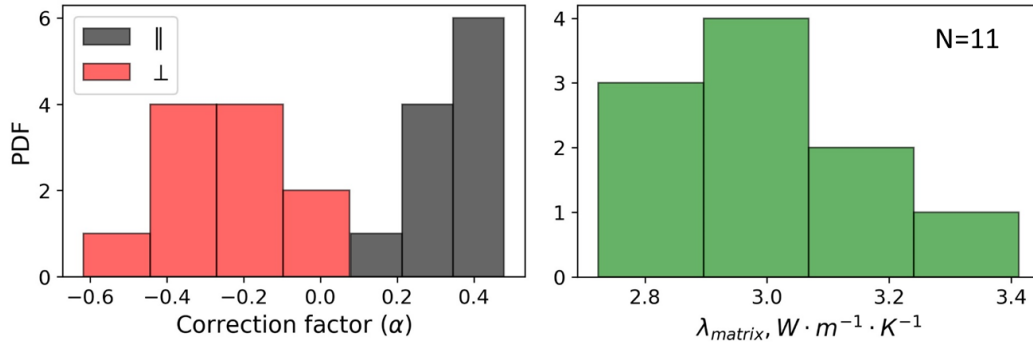
Figure 34. The histogram of the determined correction factors for parallel (black colour) and perpendicular (red colour) directions to the bedding plane and thermal conductivity of rock matrix (right panel).

As a result, the possible ranges for matrix thermal conductivity and the correction factors (for parallel and perpendicular directions to the bedding plane) were established.

In the second step, the average values of matrix thermal conductivity and correction factors were determined for the investigating rocks by solving the system of equations:

$$
\begin{cases}
\lambda_{\parallel} = \left((1 - \phi)\lambda_{matrix}^{\alpha_{\parallel}} + \phi\lambda_{fluid}^{\alpha_{\parallel}} \right)^{\frac{1}{\alpha_{\parallel}}} \\
\lambda_{\perp} = \left((1 - \phi)\lambda_{matrix}^{\alpha_{\perp}} + \phi\lambda_{fluid}^{\alpha_{\perp}} \right)^{\frac{1}{\alpha_{\perp}}}
\end{cases}
\tag{26}
$$

where $\lambda_{\parallel}$ and $\lambda_{\perp}$ are thermal conductivity parallel and perpendicular to the bedding plane, respectively, that were inferred from continuous thermal core logging. The matrix thermal conductivity and correction factors are determined by means of constrained minimization of the mean discrepancy between measured and predicted thermal conductivity values simultaneously for parallel and perpendicular directions. The constraints for matrix thermal conductivity and correction factors (for parallel and perpendicular directions) are taken from the previous step (see Figure 35). The possible range for thermal conductivity of pore-filling fluid was set from 0.0024 to 0.6 W·m⁻¹·K⁻¹ since at the time of thermal core logging of full-sized

131

cores, the pore-filling fluid was a mixture of air and water. According to minimization results, the average matrix thermal conductivity is 3.11 $W \cdot m^{-1} \cdot K^{-1}$, the average values of $\alpha_\parallel$ and $\alpha_\perp$ are 0.08 and -0.06, respectively, and thermal conductivity of pore-filling fluid is 0.12 $W \cdot m^{-1} \cdot K^{-1}$. The results of predicted thermal conductivity of rocks within the reference interval and assessment of prediction quality are presented in Figure 35.
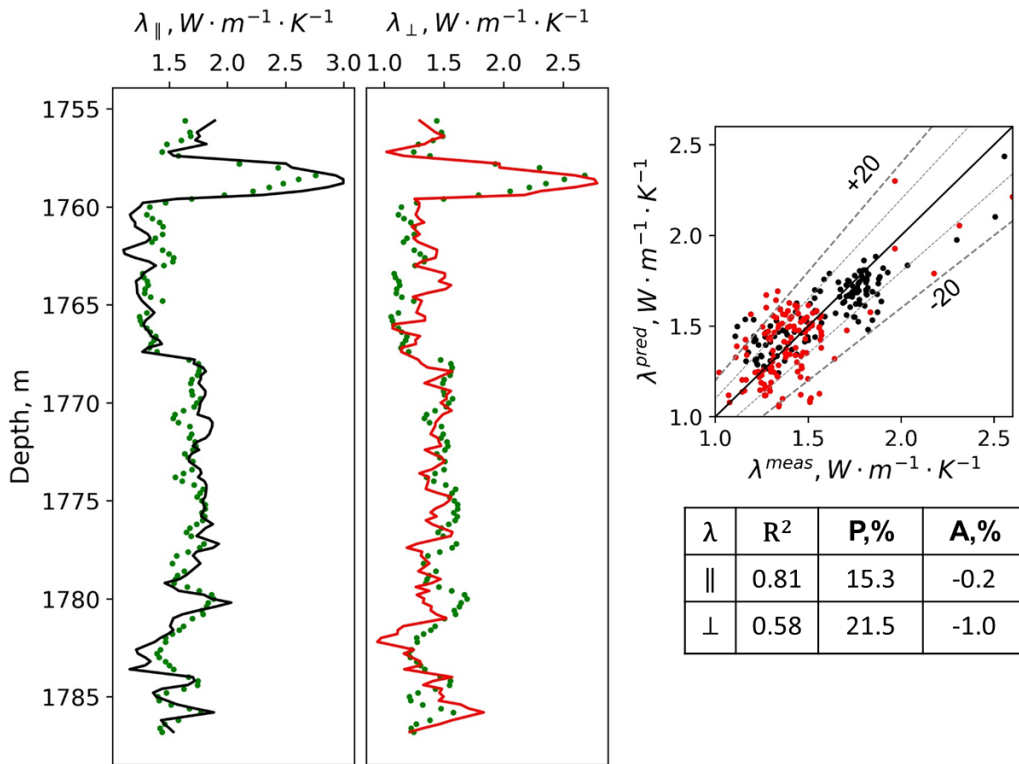
Figure 35. The results of predicting the thermal conductivity of rocks and assessment of prediction quality for the Vikulov Formation. Black and red curves (left panel) represent measured values of thermal conductivity for parallel and perpendicular directions to the bedding plane, respectively. Green dots represent the predicted thermal conductivity. Prediction quality is reported for a 0.95 confidence level.

The rock thermal properties for the Frolov formation were determined using gradient boosting. The density and gamma-ray logs were used to predict the thermal conductivity of non-cored depth intervals.

In the first step, the initial 1-mm profiles of thermal conductivity were averaged within a 0.5 m moving window to obtain a vertical resolution comparable with the vertical resolution of the logging tools. In addition, the core depths were matched with logging depths using the results of gamma-spectrometry. The available dataset (that is composed of data on rock thermal conductivity and well-logging data) was subdivided into the random train (80% of the whole dataset) and test subsets (20% of the entire dataset). The optimal hyperparameters of the gradient boosting regression model were determined via the cross-validation method (three folds were used). The results of the assessment of prediction quality for thermal conductivity parallel to the bedding plane are summarized in Table 22.

Table 22. Results of the gradient boosting regression model training and testing.

Subset	R^2	P, %	A, %
train	0.25	6.7	0.7
test	0.4	6.5	0.2

Figure 36 plots predicted and measured values of thermal conductivity for training and test subsets.
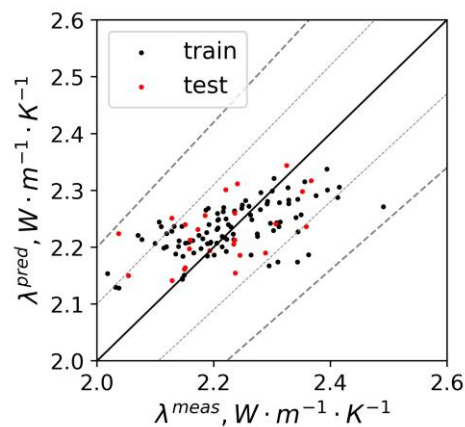
Figure 36. The cross-plot of measured and predicted values of thermal conductivity parallel to the bedding plane.

Due to the fracturing of core samples from the Frolov Formation did not allow to correctly upscale the initial data on thermal conductivity perpendicular to the bedding plane to logging scale. Thus, the relation between thermal conductivity parallel to the bedding plane and perpendicular to the bedding plane was analyzed. Figure 37 plots the dependency of thermal anisotropy coefficient from thermal conductivity perpendicular to the bedding plane.
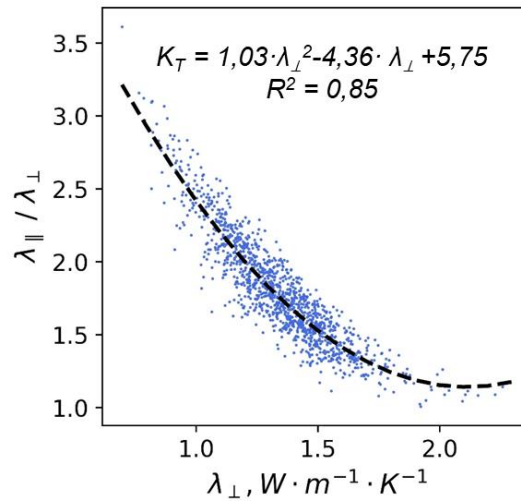
Figure 37. The cross-plot of thermal anisotropy coefficient and thermal conductivity perpendicular to the bedding plane.

The obtained determination coefficient for the regression equation in Figure 37 is statistically significant (at 0.95 confidence level) and, therefore, can be used to determine thermal conductivity perpendicular to the bedding plane from data on thermal conductivity parallel to the bedding plane.

Figure 38 plots the results of well-log based prediction of rock thermal conductivity for parallel and perpendicular directions at normal temperature and pressure.
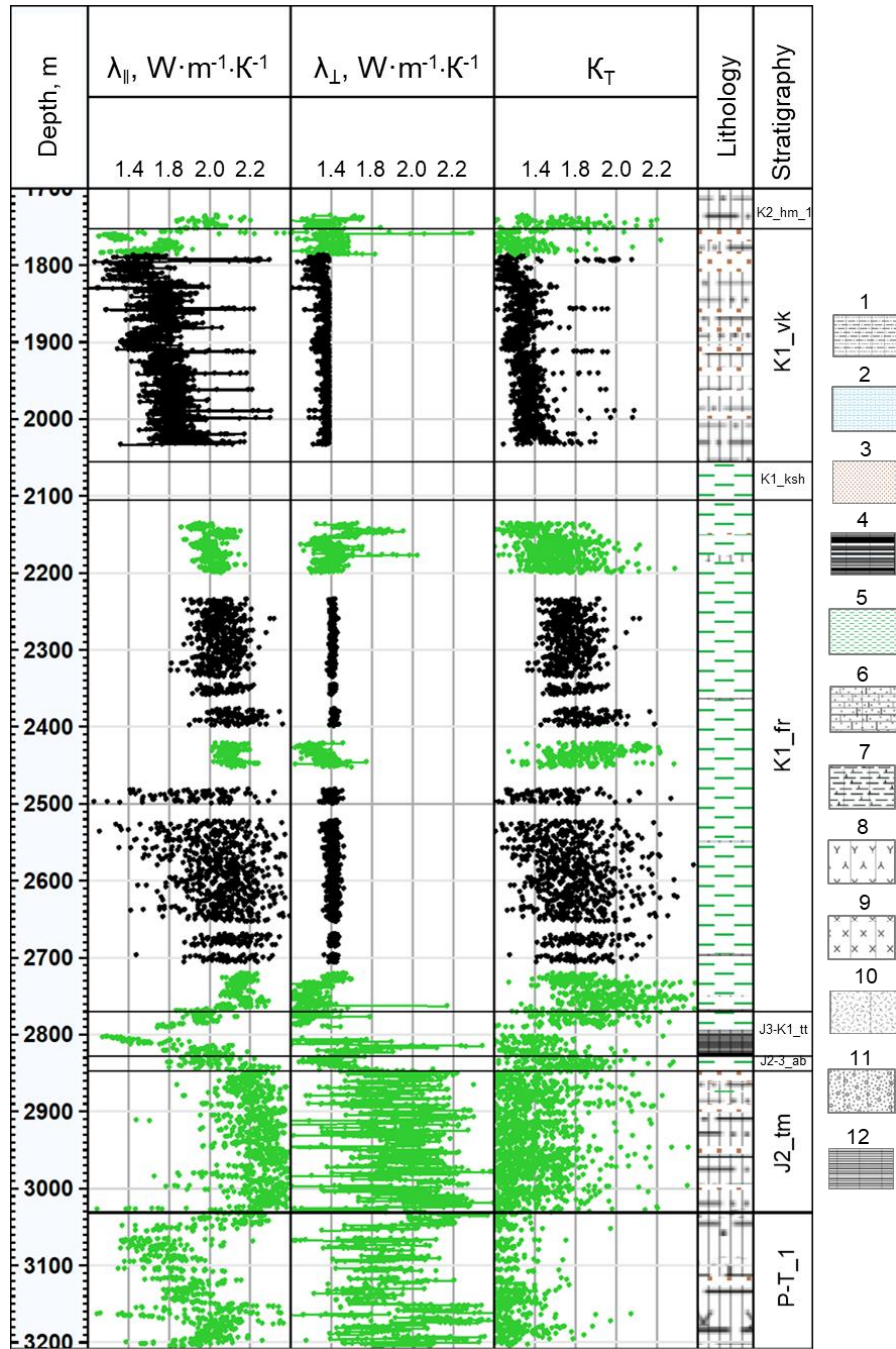
Figure 38. Results of well-log based prediction of rock thermal conductivity for parallel and perpendicular directions to the bedding plane at atmospheric conditions (Popov et al., 2021a). Green coloured dots represent experimental data and black coloured dots represent the predicted data on rock thermal conductivity. Lithology: 1 – interbedding of argillites and siltstone, 2 – marl, 3 – sandstone, 4 – bituminous argillite, 5 – argillites, 6 – limy sandstone, 7 – metarhyolites, 8 – metaplagiogranite, 9 – rhyolite, 10 – tuff, 11 – sandy gravelite, 12 – argillite with coals.

135

5.1.4. Determining vertical variations of heat flow density

Determining the heat flow density with the Fourier equation requires data on equivalent thermal conductivity of rocks along perpendicular direction provided that the vertical component of the temperature gradient is registered (Popov and Mandel, 1998).

The equivalent thermal conductivity of rocks was determined considering the following factors:

- results of thermal core logging measurements of thermal conductivity components for parallel and perpendicular to the bedding plane directions for 4102 full-sized core samples;
- results of additional measurements of the rock thermal properties on 40 standard core plugs drilled out full-size core samples and selected using the results of thermal core logging;
- results of well-log based predictions of rock thermal conductivity;
- experimental data on micro- and macro-anisotropy of rocks obtained from the thermal property measurements on 4102 full-size core samples and 40 core plugs;
- results of thermal property measurements on selected full-sized core samples and core plugs saturated with formation fluid model;
- ageing of core samples during core storage due to decompression effect;
- effects of *in situ* temperature and pressure separately for thermal conductivity tensor components.

Figure 39 plots the results of determining temperature gradient, equivalent thermal conductivity of rocks and the heat flow density within 14 depth intervals that were recognized from the analysis of vertical variations of thermal conductivity and the temperature gradient.
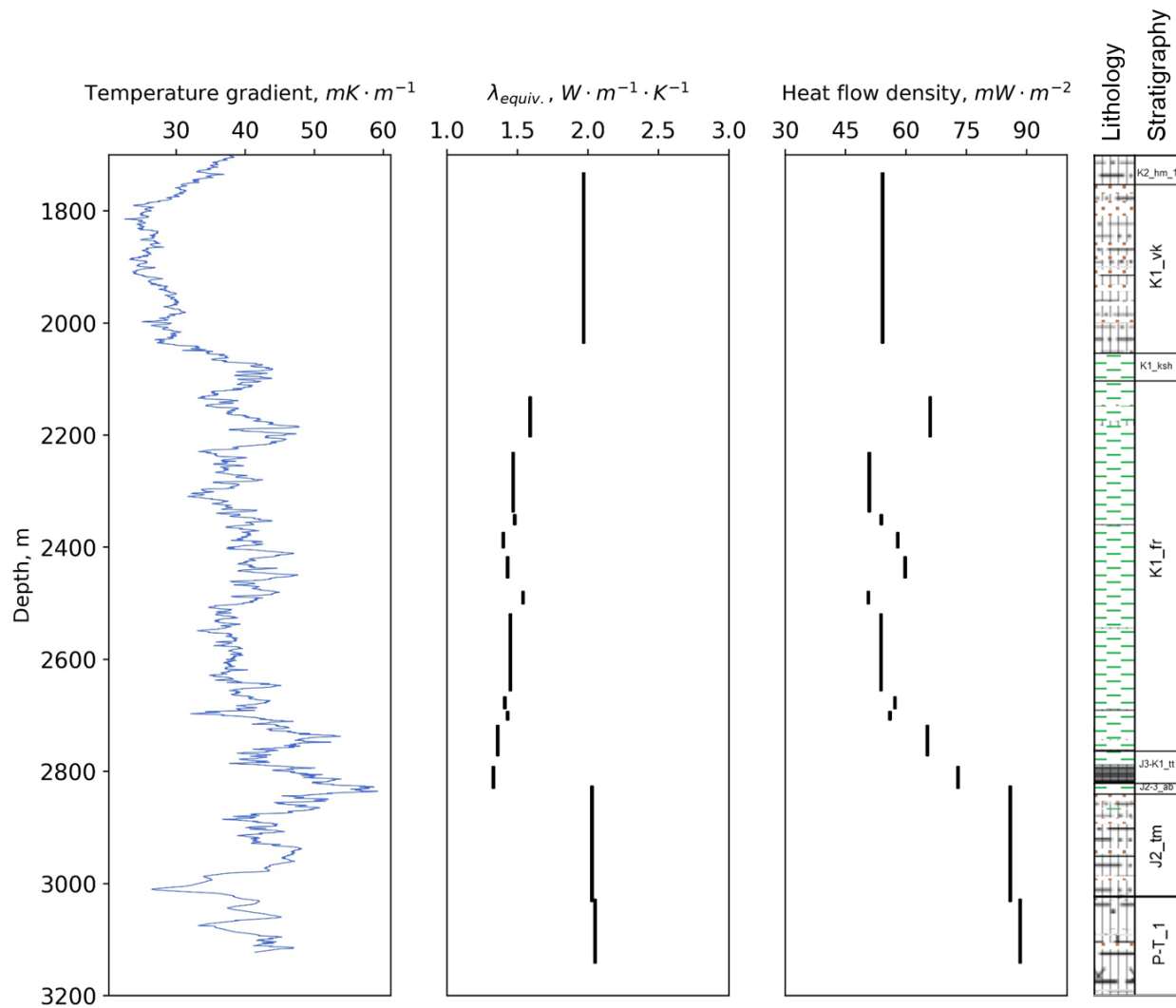
Figure 39. Results of determining temperature gradient, equivalent thermal conductivity of rocks and the heat flow density within 14 depth intervals. Lithology legend was given in Figure 38 (Popov et al., 2021a).

The obtained results manifest the significant vertical variations of heat flow density along the investigated well. Within the 1736-2821 m interval, the average heat flow density is 56.3 mW·m$^{-2,}$ and within 2828-3121 m interval, the average heat flow density is 87.1 mW·m^{-2}, i.e. it increases by 55%.

The terrestrial heat flow that was registered in the investigated well is in agreement with the data determined in the nearly located super-deep well SG6 and in the En-Yahinskaya super-deep well SG-7 (Popov et al., 2008, 2012). Based on

the comparison of the previous data on heat flow density in the investigated are (Duchkov et al., 1987; Kurchikov et al., 1987) with the new data, the relative difference amounts to 45% (previously the heat flow density was 55-65 mW·m^{-2}).

5.2 Determining vertical variations of rock thermal properties and heat flow density along Baleikinskaya 10 well

In this Section I described the results of implementing the WLBT for predicting rock thermal conductivity of the Baleikinskoye oil field.

5.2.1. Object of study

The studied well belongs to the group of wells drilled in the framework of the development of the unconventional Domanik resources in the Volga-Urals region (Peterson et al., 1983; Bazhenova, 2017; Ulimshek, 2003; Vashkevich et al., 2018). The well was drilled on the territory of the Baleikinskoye field that had been discovered in 2006 in the Orenburg region of the Russian Federation (Figure 40). Drilling was started on 6 December 2013 and finished on 22 April 2014. The drilling depth was 3827 m. The maximum tilt angle of the well is 1º 80' at a depth of 1360 m. The structural casing, the conductor, and the production strings are cemented up to the wellhead, eliminating the possibility of vertical inter-string flows that can distort the temperature field of rocks.
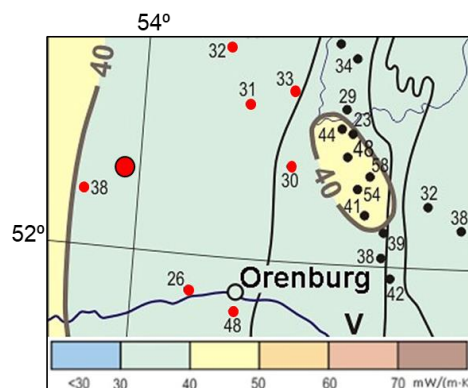
Figure 40. Geographic location of the Baleikinskaya well on the heat flow map (Popov et al., 2021b). The large red point indicates the well's location.

138

The borehole was drilled through Quaternary, Paleozoic, and Upper Proterozoic sediments (Table 23). The Quaternary sediments are represented by clay, argillaceous sand, and conglomerate. The Paleozoic group is represented by the deposits of Permian, Carboniferous, and Devonian systems. the Upper Proterozoic by the Vendian-Riphean formations. The Upper-Middle Permian sedimentary rocks are characterized by alternating shales, siltstone, and sandstones with subordinate interlayers of carbonate rocks. The Lower Permian and Carboniferous formations are represented by carbonate rocks (irregularly sulfated dolomite and limestone). There is a powerful sulfate-halogen formation in the upper part of the Lower Permian sediments (743.0-1192.0 m), which forms a regional seal. Limestones prevail in the Upper-Middle Devonian series. Sandstones and gravelstone represent the Lower Devonian series of the Paleozoic group and the Upper Proterozoic sediments. In the depth interval of 3371.9 to 3452.0 m, the borehole crossed the Domanik Formation.

5.2.2. Results of measuring rock thermal properties and temperature logging

The temperature logging was conducted in December 2017. The precision of temperature measurements did not exceed ±0.007 °C. Industrial partner conducted the temperature logging. Drilling was finished 12.5 months before temperature logging. At the time of temperature logging, the current well bottom was 3610 m. Spacing of temperature measurements was 0.1 m. There was a cement plug below the current bottom at a depth of 3610 m, thus being unavailable for the survey. The quality of the temperature logs throughout the investigating well can be evaluated as good.

The results of temperature logging are given in Figure 41. The results of temperature logging merge in one curve for three different measurements. For the general characterization of vertical variations of the temperature gradient, Figure 41

(right panel) plots the results of the temperature gradient calculations for each 50 m depth interval with a 10 cm step.

Table 23. Characteristics of the rocks from the investigating well based on the analysis of the recovered cores.

№	Rock type	Age	Logging depth, m	N*
1	In the upper part anhydrite-dolomite rock, in the middle and lower parts - limestone	P_{1ar}	1348.50 - 1366.10	135
2	Biclastic limestones with rare inclusions of anhydrite and porous intervals	C_{1t}	2612.29 - 2629.20	145
			2657.00 - 2665.74	73
3	Biclastic limestones that are (1) with rare dolomitized intervals, (2) porous, (3) cavernous, (4) oil-saturated in some intervals, (5) with a rare interbedding of argillites.	D_{3zv}	2737.30 - 2746.02	78
			2754.90 - 2763.60	65
			2794.90 - 2812.50	143
4	Biclastic limestones that are porous, fractured, with rare interbedding of argillites.	D_{3fm}	2916.90 - 2934.34	143
6	In the upper part – quartz sandstones and argillites; in the middle part – limestones and argillites; and in the lower part – marlstones.	D_{3p}-D_{2ml}	3506.40 - 3539.30	272
7	Interbedding of quartz sandstones and shally siltstone.	D_{2ar}	3585.38 - 3597.40	92
8	Biclastic limestones with oil saturated intervals and thin layers of sandstones.	D_{2vb}-D_{2af}	3619.20 - 3630.68	89
9	Biclastic limestones that are unevenly oil-saturated.	D_{2af}	3650.00 - 3667.08	93
10	In the upper part – organogenic limestone; in the middle and lower parts – quartz sandstones and argillites.	D_{2bs}-D_{1kv}	3756.70 - 3776.31	148
11	Argillites, sandstones and gravelites.	V-R	3782.64 - 3812.12	223
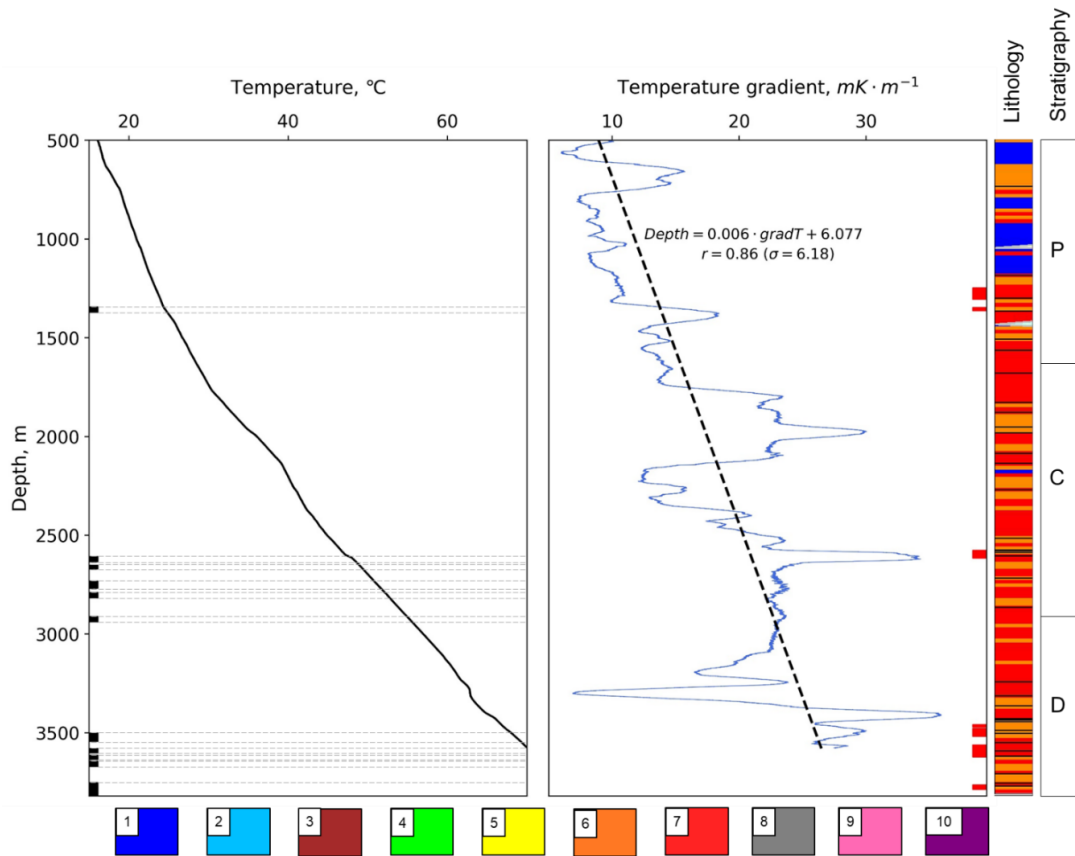
Figure 41. Temperature (black curve) and temperature gradient (blue curve) distributions along the well (Popov et al., 2021b). Black dots on the left panel represent intervals of drilling with coring. Red dots on the right panel represent bad-hole quality intervals (cavernous intervals; diameters of caverns exceed 10 cm). A dashed black line on the right panel represents the regression trend for temperature gradient with depth (the correlation coefficient and the standard deviation are given below the regression equation). Lithology legend: 1 – sandstone, 2 – carbonate-rich sandstone, 3 – bituminous argillite, 4 – clayey sand-stone, 5 – silty argillite, 6 – limestone, 7 – dolomite, 8 – dolomite limestone, 9 – limy dolomite, 10 – anhydrite.

Measurements of rock thermal properties on full-sized cores, sawed along their vertical axis, were conducted using a field lamp device of optical scanning (Popov et al., 2016). The total relative measurement uncertainty did not exceed ±2.5% for the thermal conductivity (with a measurement precision not exceeding 1.5%), ±4% for the thermal diffusivity, ±5% for the volumetric heat capacity (measurement uncertainties are reported for 0.95 confidence level).

For each of 1699 full-sized core samples recovered from the well, a series of measurements of the thermal properties were conducted in the core storage via the

continuous thermal core logging by scanning for two mutually perpendicular directions (Popov E. et al., 2020). The core sample lengths ranged from 31 to 404 mm with an average length of 99 mm (Figure 42).
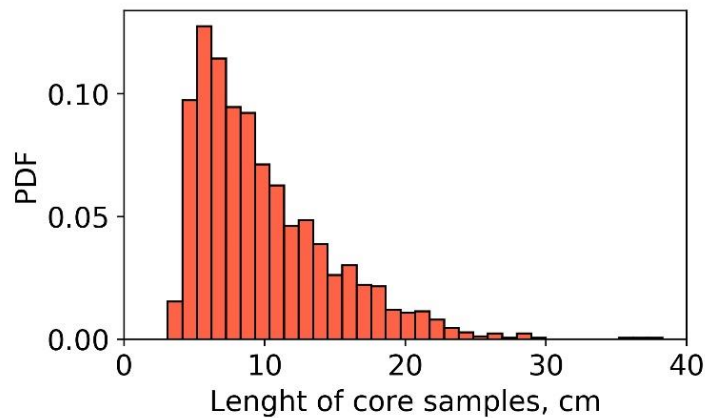
Figure 42. Distribution histogram for the length of full-sized cores under study (Popov et al., 2021b).

The measurements were performed on a flat surface of core samples, sawed along their vertical axis (volumetric ratio of the sawed parts was 1:2). The core samples have been stored at normal pressure and temperature for about a year after being recovered from the borehole. Figure 43 presents the distributions of the average rock thermal conductivity components for parallel and perpendicular directions, rock volumetric heat capacity, thermal anisotropy coefficient, and heterogeneity factor for the investigated depth intervals.
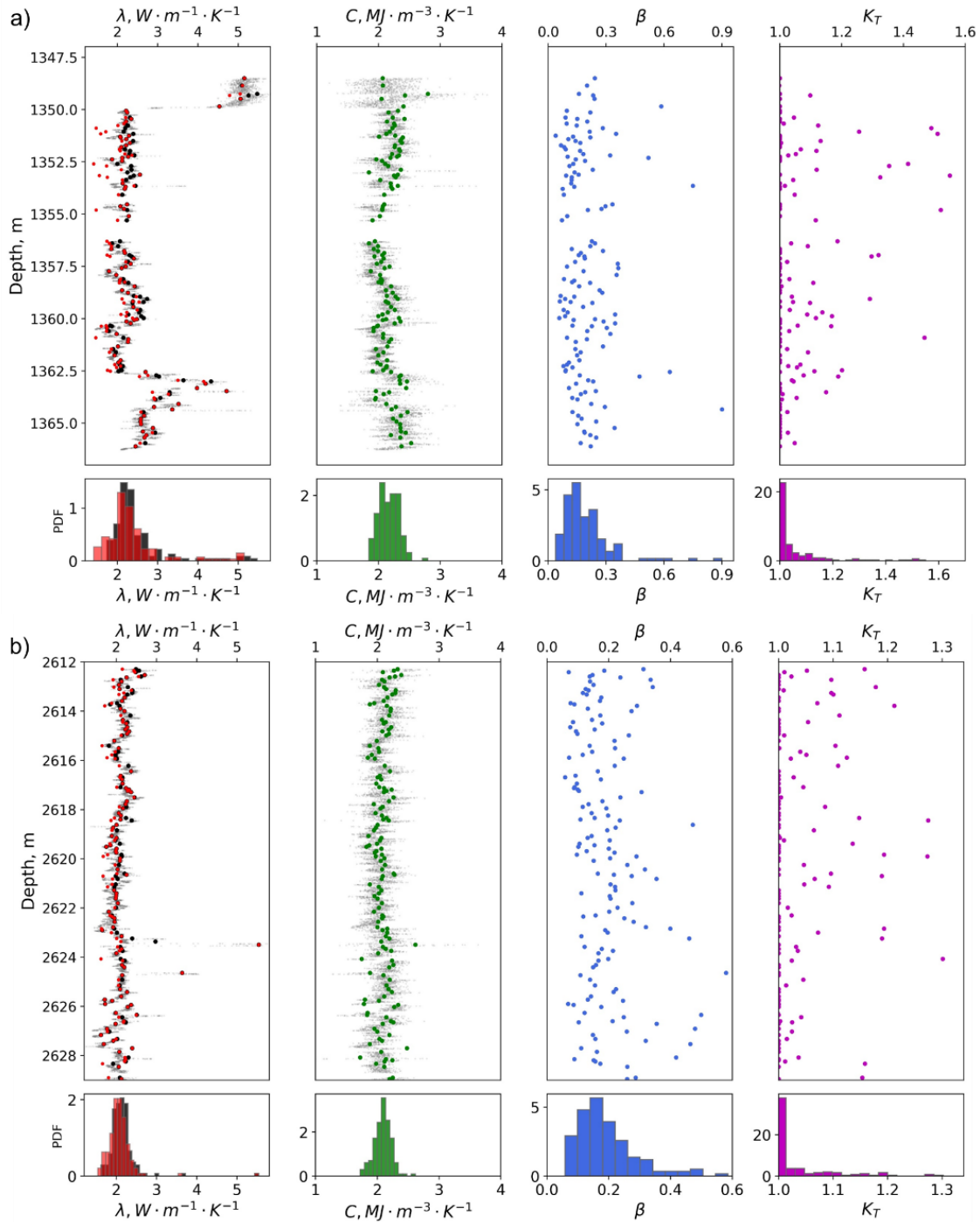
Figure 43. Results of continuous thermal core logging for depth intervals 1348.5-1366.1 m (upper panel) and 2612.29-2629.2 m (lower panel) (Popov et al., 2021b). Black coloured dots represents thermal conductivity parallel to the bedding plane, red colored dots represent thermal conductivity perpendicular to the bedding plane, green coloured dots represent volumetric heat capacity, blue coloured dots represent thermal heterogeneity factor, and purple coloured dots represent thermal anisotropy coefficient. Grey coloured dots represent high-resolution profiles (with 1-mm spatial resolution) of thermal conductivity and volumetric heat capacity.

Additional measurements of thermal properties that were conducted on 19 cylindrical core plugs having the size of 30x30 mm at different saturations ("as received", dry and water-saturated) included the following stages:

- measurements on core samples at atmospheric conditions immediately after drilling them out of the full-sized core samples;
- drying samples following the standard procedure in the drying box;
- measurements on the dried core samples at normal pressure and temperature;
- vacuum saturating of core samples with mineralized water following the standard procedure;
- measurements on the water-saturated samples at normal pressure and temperature;
- measurements of rock thermal conductivity, volumetric heat capacity, and thermal anisotropy coefficient on water-saturated samples at in situ temperature (the temperature of measurements corresponds to the in situ temperature of the corresponding core sample).

Figure 44 plots the estimates of the relative variations of thermal conductivity (1) after drying and (2) after the saturation with synthetic brine under vacuum. The results of the measurements (Figure 44) show that:

- The thermal conductivity change after both drying and water saturation depends on the core sample porosity.
- Drying the samples resulted in a very small thermal conductivity decrease. The thermal conductivity reduction depends on the porosity and does not exceed 13%.
- After water saturation of the dried core samples, a substantial thermal conductivity increase is observed (from 7 to 62%).

144

There was no dependence established of the anisotropy degree of core samples on thermal conductivity variations by changing the pore-filling fluid.
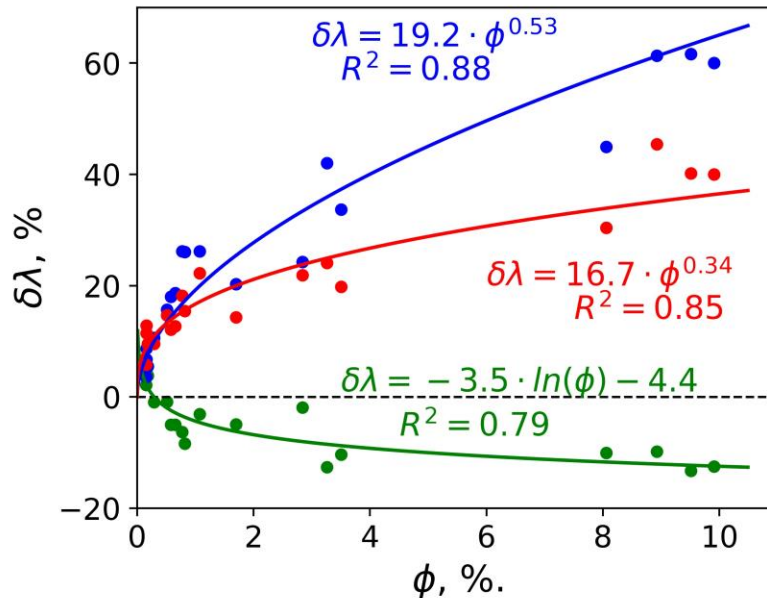
Figure 44. Thermal conductivity variations with porosity after drying core samples (green-coloured line) and after water saturation under vacuum (blue-coloured line) (Popov et al., 2021b). The red-coloured line characterizes the thermal conductivity change from «as received» state to «water-saturated».

Data in Figure 44 indicate that by the time of thermal core logging in the core storage, the samples were dried substantially and lost the majority of their pore fluid. Therefore, to correct the data on rock thermal conductivity for *in situ* saturation, it was necessary to adjust the results of thermal core logging depending on rock porosity via the regression trend that is presented by the red-colored curve in Figure 44.

Variations of the rock thermal conductivity perpendicular to the bedding plane, related to porosity and changes of the sample saturation degree are described by regression equations that are similar to those for the thermal conductivity parallel to the bedding plane and are the following:

- from "as received" state to dried: $\delta\lambda = -3.5 \cdot \ln(\phi) - 4.4$ with $R^2 = 0.79$,

145

- from dried to water-saturated state: $\delta\lambda = 19.2 \cdot \phi\, 0.53$ with $R^2 = 0.88$,
- from "as received" state to the water-saturated: $\delta\lambda = 16.7 \cdot \phi\, 0.34$ with $R^2 = 0.85$.

The corrections for data on rock thermal conductivity (inferred from the continuous thermal core logging) were determined using the data within coring intervals on rock porosity that was obtained via interpreting density log data and results of laboratory investigations of core plugs, for each depth interval and specific depth intervals that have significant porosity variations, using the regression equation (the red curve in Figure 44).

The thermal conductivity at the formation temperature was measured on 10 cylindrical 50x20 mm core samples that were saturated with synthetic brine under vacuum and selected based on results of continuous thermal core logging of full-sized cores. Thermal conductivity measurements on water-saturated samples were conducted at the temperature corresponding to the temperature of the corresponding depth interval. Pressure corrections for thermal conductivity were inferred from the literature data (Yakovlev, 1996; Kurbanov, 2007) for the rocks similar to those presented in the investigating geological profile.

5.2.3. Determining the equivalent thermal conductivity necessary for estimating the heat flow within non-coring intervals from standard well-logging data

Rock thermal conductivity was determined from well-logging data for the limestones in depth intervals of 1992.4–2090.1 m, 2629.16–2720.9 m, 2721.16–2916.36 m, and 2935.16–3249.36 m with WLBT. In addition to that, the rock thermal conductivity was determined for dolomites in the 2145.36–2359.56 m depth interval based on the results of regression analysis of well-logging data and data on thermal conductivity from an adjacent well that has a similar lithology.

Before regression analysis between well-logging data and rocks thermal conductivity data, the data preprocessing was conducted. The data preprocessing

146

included (1) matching depths of logging curves, (2) eliminating data from cavernous intervals, (3) averaging the continuous thermal conductivity profile in 0.5 m moving window (window size is equal to the average vertical resolution of well-logging tools), and (4) shifting core depth to match well-logging data using results of core gamma spectrometry. In addition to that, the Z-scaling (dividing the difference between a variable and its average value by its standard deviation) of neutron gamma logging and gamma-ray log data was performed to account for differences in technical conditions of well-logging (drilling agent properties, well diameter, etc.) and logging tools when predicting thermal conductivity of the dolomites in 2145.36–2359.56 m depth interval.

The well-logging suite used to predict rock thermal conductivity includes gamma-ray log, neutron gamma log, gamma-gamma density log, and sonic log. Rock thermal conductivity was determined within non-coring intervals based on multiple regression analysis of well-logging data and data on rock thermal conductivity. An outlier-resistant linear regression model (also known as Huber regression; Huber et al., 2009) was used during the regression analysis. The initial dataset of rocks thermal conductivity data and wells logging data was divided into the training dataset (67% of the entire data set) and the test dataset (33% of the data set) to estimate the generalization ability of the determined regression equations. Optimal hyperparameters of regression models were selected via the cross-validation method.

The results of training and testing regression models for determining rock thermal conductivity presented in Table 24.

Table 24. The results of training and testing regression models for determining rock thermal conductivity from well-logging.

Lithology (depth interval)	Regression equation*	Quality of prediction results on the test dataset				
		R^2	RMSE, $W \cdot m^{-1} \cdot K^{-1}$	P,%	A,%	N
Limestones (2611.76-2665.76)	$\lambda = -2.6 \cdot 10^{-4} \cdot \Delta t_P + 0.25 \cdot \rho + 0.26 \cdot \gamma + 0.34 \cdot NGR + 0.08$	0.70	0.10	9.48	-0.2	43
Limestones (2736.96-2812.16)	$\lambda = -3.7 \cdot 10^{-4} \cdot \Delta t_P + 0.12 \cdot \rho + 0.05 \cdot \gamma + 0.21 \cdot NGR + 2.15$	0.19	0.10	8.06	-0.4	67
Limestones (2916.56-2934.16)	$\lambda = -1.8 \cdot 10^{-4} \cdot \Delta t_P - 0.25 \cdot \gamma + 0.32 \cdot NGR + 2.44$	0.64	0.10	8.74	0.5	29
Dolomites (regression equation from the adjacent well)	$\lambda = -0.004 \cdot \gamma^{normilized} + 0.42 \cdot NGR^{normilized} + 4.34$	0.87	0.17	8.18	0.2	133

Figure 45 shows the predicted rock thermal conductivity in depth intervals without cores from well-logging data. Based on Table 24, it can be concluded that the established regression equations between well-logging data and data of thermal conductivity provide the predictions of rock thermal conductivity with total uncertainty of less than 10% for a 0.95 confidence level.
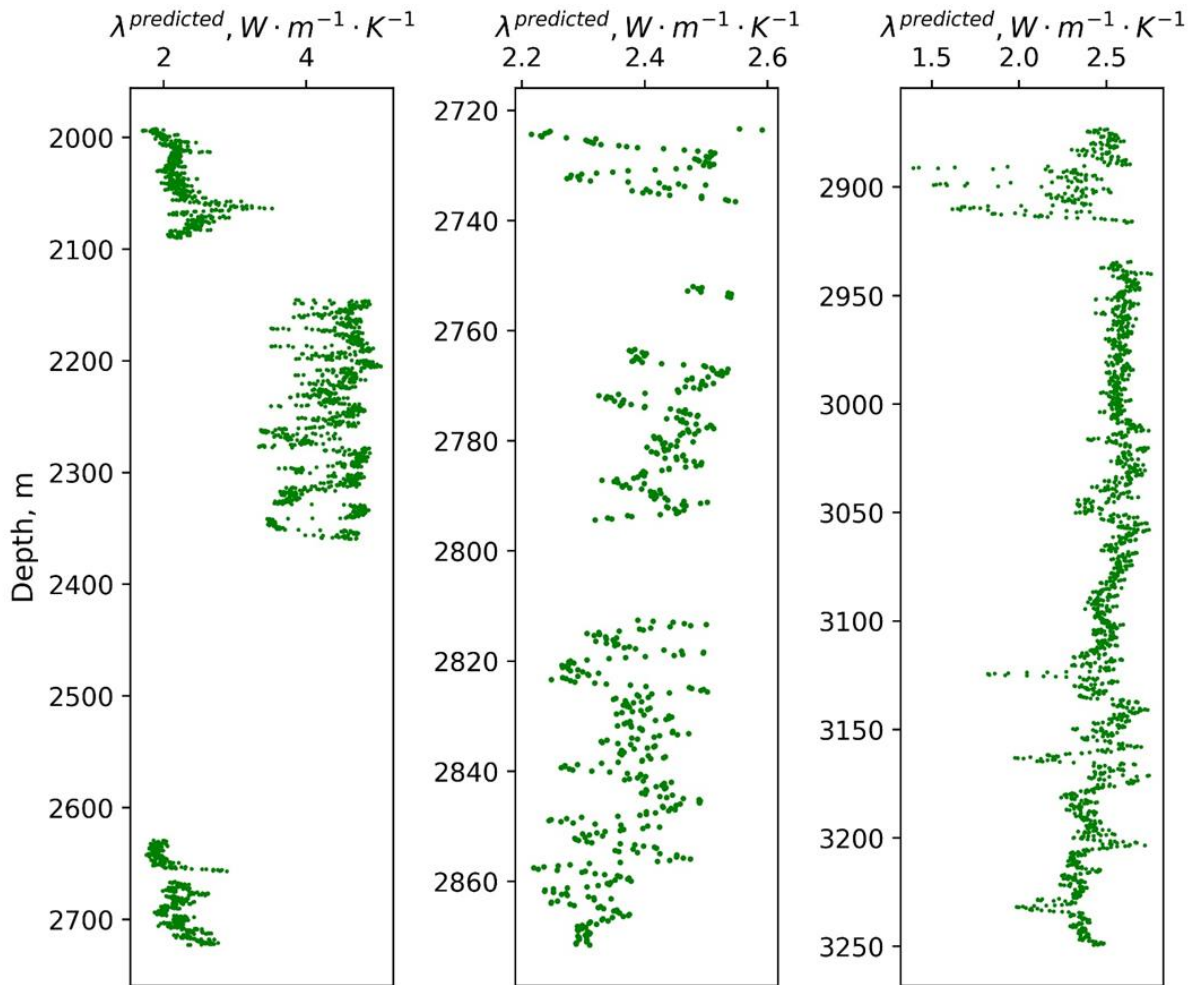
Figure 45. Thermal conductivity within not cored depth intervals predicted from well-logging data by means of the established regression equations.

The total length of the intervals with predictions of rock thermal conductivity from well-logging data is 860 m.

5.2.4. Determining vertical variations of heat flow density

To calculate the heat flow density for a vertical well using data on the temperature gradient and the thermal conductivity, the data on equivalent thermal conductivity for the vertical direction are required. Concurrently, it requires accounting for the textural anisotropy caused by the layered texture of rocks and the micro-anisotropy, which may be due to oriented cracks (technogenic or natural) or crystals or flakes of minerals that can be anisotropic themselves.

149

The results of experimental instigations of rock thermal conductivity have revealed that, with substantial k thermal conductivity variations along the well and significant anisotropy of core samples, two factors causing thermal anisotropy have to be considered:

- presence of thermal macro-anisotropy due to the ordered heterogeneity of rocks on core sample scale (Figure 46) - a layered texture at the whole profile scale conditioned by the alternation of subparallel layers with various thermal conductivity;
- presence of micro-anisotropy inherent even for homogeneous rocks and caused either by oriented anisotropic mineral grains or oriented microcracks.
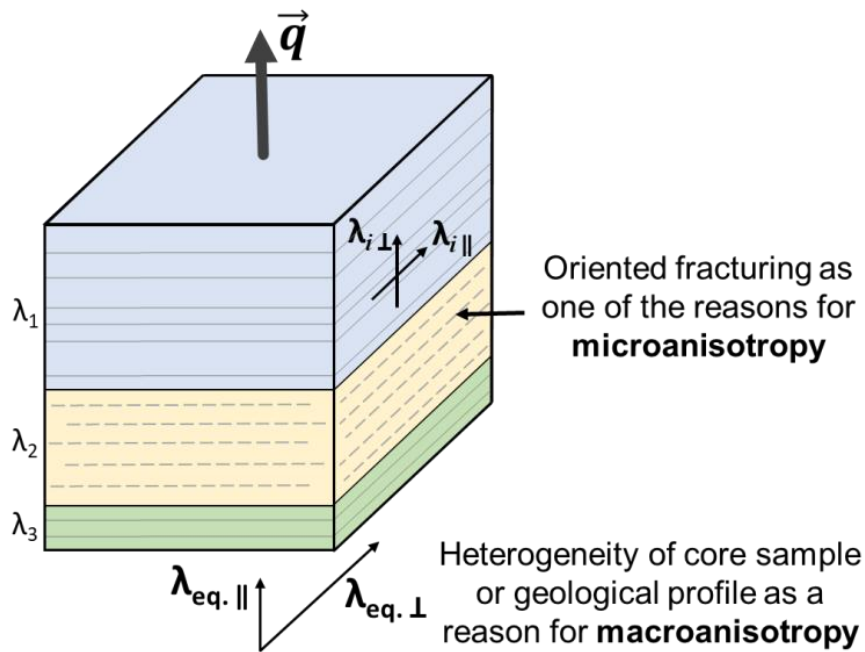
Figure 46. The reasons causing anisotropy of rocks that were accounted during determining equivalent thermal conductivity required for calculating heat flow density. λeq. – macroanisotropy, $\lambda_{i\perp}$ - microanisotropy (Popov et al., 2021b).

Analysis of the micro-anisotropy evaluation results for investigating rocks based on continuous thermal core logging data reveals the absence of significant anisotropy of limestones and dolomites from the investigated stratigraphic units.

Since the well understudy was drilled almost vertically, and stratigraphic borders may be considered horizontal, the principal axes of thermal conductivity are oriented parallel and perpendicular to the bedding plane, and temperature gradient is oriented along the well. It makes determining heat flow density less complicated. In this case, the equivalent thermal conductivity (λ_{equiv}) shall be determined as the vertical component of the rock's thermal conductivity tensor since vectors of the heat flow density and the temperature gradient are codirectional (vertical).

If the micro-anisotropy is due to natural factors (oriented anisotropic grains of minerals, or oriented natural microcracks) and has to be considered jointly with macro-anisotropy (textural or transversal anisotropy) of rocks, the following equation shall be used to determine the equivalent thermal conductivity (necessary for calculating the heat flow density):

$$\lambda_{equiv\perp2} = N\left(\sum_{i=1}^{N} \lambda_{i\perp}^{-1}\right)^{-1} \tag{27}$$

where N is the number of core samples in considering depth interval, $\lambda_{i\perp}$ is the thermal conductivity component perpendicular to the bedding plane for the i-th core sample accounting thermal micro-anisotropy coefficient that was registered during thermal core logging of full-sized cores.

In the presence of a technogenic induced micro-anisotropy (due to possible micro-cracks along the parallel direction to the bedding plane), and in the absence of a natural micro-anisotropy, the equivalent thermal conductivity should be determined excluding the effect of rocks' technogenic anisotropy and accounting only for macro-anisotropy (textural anisotropy). In this case, it is implied that the thermal conductivity parallel to the bedding plane ($\lambda_{||}$) for each core sample characterizes the thermal conductivity of undisturbed rocks. Therefore, the equivalent thermal conductivity for the heat flow calculation shall only account for rocks macro-anisotropy and be determined as follows:

$$\lambda_{equiv\perp1} = N\left(\sum_{i=1}^{N} \lambda_{i||}^{-1}\right)^{-1} \tag{28}$$

where $\lambda i_{\parallel}$ is the thermal conductivity component for parallel direction to the bedding plane for the i-th core sample.

Due to the lack of reliable information about the presence or absence of the induced technogenic anisotropy for the investigated core samples (which is a common cause of anisotropy), two cases were considered:

1. The equivalent thermal conductivity $\lambda_{equiv.max}$ was determined according to the formula (27), assuming that the micro-anisotropy was caused by technogenic fractures and has to be excluded from estimating the *in situ* thermal conductivity of rock mass and because of that thermal conductivity parallel to the bedding plane ($\lambda_{\parallel}$) is more objective and unbiased characteristic of the core sample compared to the thermal conductivity perpendicular to the bedding plane ($\lambda_{\perp}$). For that reason, an upper-bound estimate of rocks' thermal conductivity was made.

2. The equivalent thermal conductivity $\lambda_{equiv.min}$ was determined via the formula (26), assuming that the micro-anisotropy is typical for core samples at in situ conditions, i.e. is caused by natural factors and corresponds to undisturbed rocks. For that reason, a lower-bound estimate of thermal conductivity was made.

Equivalent thermal conductivity for the heat flow calculation was determined, accounting for multiscale rock heterogeneity (starting from each core sample), in situ saturation, the effect of core changes in core storage, textural anisotropy, micro-anisotropy, and in situ pressure and temperature. Table 25 provides the results of determining equivalent thermal conductivity at *in situ* conditions, temperature gradient, and the heat flow density for coring depth intervals and depth intervals with well-log based predictions.

Table 25. Results of determining equivalent thermal conductivity and heat flow density for coring depth intervals and intervals with well-log based predictions of rock thermal conductivity within non-coring intervals.

Depth interval, m	Estimation of equivalent thermal conductivity, $W \cdot m^{-1} \cdot K^{-1}$		Temperature gradient, $mK \cdot m^{-1}$	Heat flow estimate, $mW \cdot m^{-2}$		
	lower	upper		lower	upper	average
From results of continuous thermal core logging						
1348.50-1366.10	3.21	3.42	18.05	58.0	61.7	59.8
2612.29-2629.20	2.80	2.93	28.30	79.3	82.8	81.1
2657.00-2665.74	3.07	3.17	23.93	73.5	75.8	74.6
2737.30-2746.02	3.04	3.28	22.72	69.1	74.5	71.8
2754.90-2763.60	3.11	3.22	24.68	76.8	79.5	78.1
2794.90-2812.50	3.08	3.23	22.08	68.1	71.3	69.7
2916.90-2934.34	3.33	3.44	23.00	76.7	79.2	78.0
3506.40-3539.30	2.57	2.87	27.56	70.8	79.0	74.9
From results of well-log based predictions of rock thermal conductivity within non-coring intervals (average values of thermal conductivity and heat flow)						
1991 - 2091	3.23		22.96			74.1
2144 - 2361	5.54		13.51			74.8
2628 - 2658	2.74		24.63			67.4
2666 - 2737	3.02		22.76			68.7
2764 - 2794	3.13		23.62			73.9
2813 - 2915	2.99		22.98			68.6
2935 - 3100	3.08		22.75			70.1

The vertical variations of the heat flow density presented in Table 25 are plotted in Figure 47 together with the previously published data on average heat flow estimate that were inferred by Golovanova (2005), Hodyreva et al. (1985) and Gordienko et al. (1987).
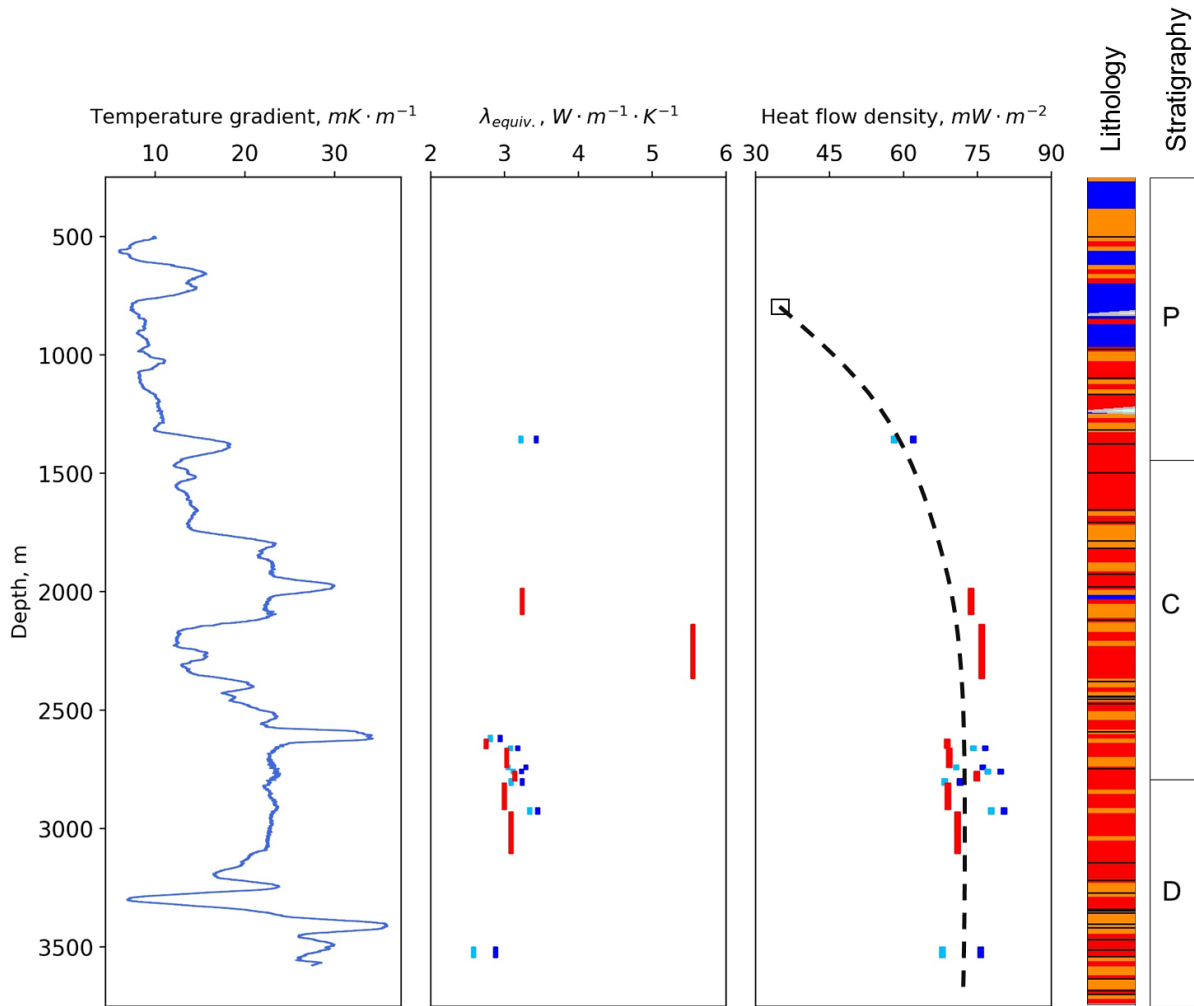
Figure 47. Heat flow density for the investigated depth intervals and previously published data on heat flow density for the well under study (Popov et al., 2021b). Blue line (left panel) presents the vertical variations of the temperature gradient (determined with 5 m moving window with a 10-cm step). Light-blue lines (central panel) present the lower estimate of the equivalent thermal conductivity within coring depth intervals. Blue lines (central panel) present the upper estimate of the equivalent thermal conductivity within coring depth intervals. Red lines present the average estimates of the equivalent thermal conductivity within the intervals with well-log based predictions of rock thermal conductivity. Light-blue and blue lines in the right panel of the figure represent the lower and upper estimate of heat flow density within coring depth intervals. Red lines in the right panel repre-sent the average estimate of the heat flow density within the intervals with well-log based predictions of rock thermal conductivity. The empty black box on the right panel represent the previously published data on heat flow density (34.0 mW·m^{-2}) for the are under study. Black vertical line on the right panel presents the regression trend of the increase of heat flow density (with average value of 72.6 mW·m^{-2} below 2000 m). Lithology legend was given in Figure 39.

Figure 47 demonstrates that all newly obtained data on heat flow density are significantly higher than the average value of previously published data. The heat flow density for the 1348.50–1366.10 m depth interval varies from 58.0 to 61.7 mW·m^{-2} with the average value of 59.8 mW·m^{-2}, which is essentially lower than the heat flow density for the deeper horizons (starting from 1991 m and below). This is coherent with the previously determined tendency suggesting that the heat flow density for depth shallower than 2000 m is in most cases smaller than the heat flow density for the larger depths due to the combined impact of paleoclimate and migration of fluids in rock masses (Clauser et al., 1997; Emmermann et al., 1997; Popov et al., 1999; Kukkonen et al., 2011; Popov et al., 2012; Popov et al., 2018; Kukkonen et al., 1997; Popov et al., 1988; Mottaghy et al., 2005).

The average heat flow density for 13 depth intervals that are between 2144 and 3539.30 m (Table 25) is 72.6 mW·m^{-2} with the standard deviation of 3.6 mW·m^{-2}. For 13 sampling elements and the corresponding Student's coefficient of 2.16 at the 0.95 confidence level, the absolute uncertainty of estimate of the average heat flow density is 2.2 mW·m^{-2}, whereas the relative uncertainty of estimate of the average heat flow density is 3.0%.

The published data contains geothermal information for seven wells in the drilling area: Orenburg, (Hodyreva et al., 1985), two unnamed wells (Gordienko et al., 1987), Goncharovskaya-16, Denisovskaya-1, Denisovskaya-3, and Yakshimbetovskaya-157 (Golovanova, 2005). These wells are 118, 87, 38, 118, 130, 103, and 113 km away from the studied well, respectively. The published heat flow estimates for these wells are 48, 38, 26 32, 33, 31, and 30 mW·m^{-2}, respectively, with the average heat flow density of 34.0 mW·m^{-2}. Thus, the obtained average heat flow value is greater than the previous heat flow average value for this territory by 114% (34.0 mW·m^{-2}).

5.3 Conclusion

The new techniques, including continuous thermal core logging, new laser optical scanning instrument in combination with rock thermal property measurements at elevated temperatures and on core samples saturated under vacuum with brine, provided investigations of more than 5200 rock samples and representative experimental data on rock thermal properties including thermal conductivity components along and perpendicular to the rock bedding plane, volumetric heat capacity and anisotropy coefficient for determining heat flow density in two wells. Application of WLBT for predicting rock thermal properties during geothermal investigations allowed registering detailed vertical variations of heat flow density within intervals where cores were not available.

The registered terrestrial heat flow density for the Bazhenovskaya 1 well is 87.1 mW·m^{-2} and for the Balyikinskaya 10 well is 72.6 mW·m^{-2}. The determined values of the heat flow density essentially exceed the previously published data for this area (by 45% and 114% for the Bazhenovskaya 1 Balyikinskaya 10 wells, respectively).

Similarly to the results of experimental geothermal investigations in deep and super-deep wells conducted between 1990 and 2010 (Popov et al., 2019b), the obtained data on heat flow and rock thermal properties demonstrated the necessity in a new special experimental estimations of the heat flow density and rock thermal properties when studying hydrocarbon fields at any stage that includes regional basin and petroleum system modelling to avoid serious errors in geothermal data (almost unavoidable otherwise).

Summary and Conclusions

1. An approach for predicting rock thermal properties from sonic log data accounting for thermal anisotropy, rock heterogeneity, *in situ* temperature, pressure, and saturation via the regression analysis was developed and tested for organic-rich shales of the Bazhenov Formation.

2. The developed approach was extended by applying advanced machine learning algorithms, involving additional well-log data and integrating the data on rock thermal properties inferred from continuous thermal core logging. The extended version of the approach was tested on representative experimental data from the heavy-oil field and yielded successful results.

3. From comparison of measured and predicted profiles of rock thermal properties it can be concluded that thermal conductivity for parallel and perpendicular direction to the bedding plane and volumetric heat capacity using the developed regression and theoretical model-based approaches can be predicted with uncertainties of less than 10%, 15%, 10% (for 0.95 confidential probability level), respectively. In most cases, the regression model-based approach yields more precise predictions of rock thermal properties than theoretical model-based.

4. The sensitivity study of the regression models for predicting rock thermal properties from gradient boosting revealed that the sonic, neutron and density logs are the most important pieces of information when predicting both thermal conductivity and volumetric heat capacity.

5. An approach for predicting rock thermal properties also considering thermal anisotropy, rock heterogeneity, *in situ* temperature, pressure, and saturation through advanced theoretical modelling was developed and also tested for organic-rich shales of the Bazhenov Formation.

6. An approach for assessing uncertainty in the correction factor of the Krischer-Esdorn model of thermal conductivity was suggested and tested. The approach relies on the application of the partial-derivative method. The developed approach is not limited only to the Krischer-Esdorn model. It can be applied for assessing uncertainty in correction factors of Lichtenecker-Rother and Lichtenecker-Asaad models.

7. The developed approaches (regression and theoretical modelling based) were unified and presented within the novel well-defined well-log based technique (WLBT) for determining rock thermal properties. The developed workflow is based on the application of advanced thermal core logging technique that provides continuous non-contact non-destructive profiling of thermal conductivity (principal components of thermal conductivity) and volumetric heat capacity on full-diameter cores, core plugs and broken cores. The comparison between WLBT and the commonly used Deming approach for predicting thermal conductivity accounting for thermal anisotropy revealed that WLBT provides more precise predictions for parallel and perpendicular directions to the bedding plane essentially.

8. WLBT was applied to geothermal investigations of two prospecting wells and allowed us registering detailed vertical variations of formation thermal properties and heat flow density within intervals where cores were unavailable. This yielded estimations of intervals and obtaining vast rock thermal properties and heat flow density data for regional basin and petroleum system modelling.

The research findings disclosed a qualitatively new framework for well-log based determination of rock thermal properties. The developed WLBT for determining rock thermal properties relies on the application of an advanced experimental basis. Testing on representative experimental data from various

158

hydrocarbon field, including organic-rich shales and heavy-oil field highlights the effectiveness of the WLBT for determining rock thermal properties. The implementation of WLBT for determining rock thermal properties within the geothermal investigations allowed us to obtain new data on vertical variations of heat flow density and formation thermal properties and opened new perspectives to subsequent studies on the hydrocarbon fields in the study areas.

Recommendations for future research

There are several highly important and principal research directions for the near future investigations to enhance the proposed well-log based technique for predicting rock thermal properties:

- Development of the database that includes both reliable data on rock thermal properties and well-logging data. The database should include information on thermal anisotropy, rock heterogeneity, lithology (including mineralogical composition of rocks), effects of additional saturation of rock thermal properties (along directions of principal axes of thermal conductivity tensor) and rock porosity. For unconventional reservoirs, data on organic matter content is also required. The database can be the basis for applying a well-log-based technique for predicting rock thermal properties in case of absence of data on rock thermal properties in the investigating area.

- Integration of similarity learning approaches within the suggested workflow. To apply effectively the previously mentioned database the assessment of similarities between the investigating geological objects or geological profiles should be performed during predictions of rock thermal properties. Various machine learning-based approaches (such as, e.g. siames neural networks or ensemble tree-based methods), were recently suggested to solve the task at hand. The effectiveness of the suggested similarity learning approaches was proven for solving various problems (see, e.g., Kang et al., 2017) and is a perspective way for enhancing the well-log based technique for predicting rock thermal properties.

- Enhancement of the theoretical model-based approach via integration of effective medium theory methods. Application of the effective medium

theory models was proven to be highly effective for predicting rock thermal properties (see, e.g., Bayuk et al., 2016). The benefit of applying effective medium theory approaches is the opportunity to predict thermal properties on the basis of data on elastic wave velocities and electrical resistivity without conducting regression analysis and necessity in experimental data on rock thermal properties.

- Comprehensive analysis of applicability of commonly used in geophysics approaches and models to characterize the stiffness and electrical resistivity tensors. Since the predictions of rock thermal conductivity in case of thermal anisotropy require knowledge on principal components of stiffness and electrical resistivity tensors, we need to enhance and verify the accepted models of anisotropic rocks and define their limitations.

- Adaptation and testing of the developed approaches on igneous and metamorphic rocks. For geothermal investigations and radioactive waste disposal, the data on rock thermal properties of igneous and metamorphic rocks are of a high interest. The enhancement of the suggested technique for predicting thermal properties of igneous and metamorphic rocks should account for peculiarities these rocks (such as low porosity, mineral composition, etc.).

- Investigating the effect of elevated pressure and temperature on rock thermal properties in case of thermal anisotropy. Literature review shows that there are only a few publications that are focused on experimental investigations of thermal properties of anisotropic rocks at elevated temperatures providing a comprehensive description of methodological and metrological basis. Thus, this research direction is highly relevant.

Bibliography

1. Abdulagatova, Z. Z., Abdulagatov, I. M., Emirov, S. N., 2009. Effect of temperature and pressure on the thermal conductivity of sandstone. International Journal of Rock Mechanics and Mining Sciences 46(6), 1055–1071, doi.org/10.1021/je050016a.

2. Anand, J., Somerton, W. H. & Gomaa, E., 1973. Predicting thermal conductivities of formations from other known properties. SPE J., 13(5), 267–272.

3. Asaad, Y.A. 1955. Study of the thermal conductivity of fluid bearing porous rocks. PhD thesis, University of California, CA, USA.

4. Balling, N., Kristiansen, J., Breiner, N., Poulsen, K.D., Rasmusen, R., Saxov, S., 1981. Geothermal measurements and subsurface temperature modelling in Denmark, Geologiske Skrifter, 16(1), 172.

5. Balushkina, N., Kalmykov, G., Khamidulin, R., Belokhin, V., Korobkova, N., Petrakova, N., Bakay, A., 2014. Complex lithophysical typization of Bazhenov formation rocks from core analysis and well logging. SPE Russian Oil and Gas Exploration & Production Technical Conference and Exhibition, 14-16 October, Moscow, Russia, doi.org/10.2118/171168-MS.

6. Bär, K., Reinsch, T., Bott, J., 2019. PetroPhysical Property Database. V. 1.0. GFZ Data Services. https://doi.org/10.5880/GFZ.4.8.2019.P3.

7. Bayuk, I., Goloshubin, G., Tcimbaluk, Y., Borkum, F. 2016. SEG Technical Program Expanded Abstracts. https://doi.org/10.1190/segam2016-13762472.1.

8. Bayuk, I., Popov, Y., Parshin,.A., 2011. New powerful tool for interpreting and predicting in reservoir geophysics: theoretical modelling as applied to laboratory measurements of thermal properties. Proceedings of the international symposium of the society of core analysts held in Austin (SCA), 18–21 September, SCA2011-39, 12 pp.

9. Bazhenova, T.K., 2017. Hydrocarbon resources estimation of bituminous formations of Russian oil and gas bearing basins. Oil and gas geology, 5, 37-50 (in Russian).

10. Beck, A., Anglin, E, and Sass, J., 1971. Analysis of heat-flow data-in situ thermal conductivity measurements. Canadian Journal of Earth Sciences 8, 1-20, doi.org/10.1139/e71-001.

11. Beziat, A., Dardaine, M. &Mouche, E., 1992. Measurements of the thermal conductivity of clay-sand and clay-graphite mixtures used as engineered

barriers for high-level radioactive waste disposal, Appl Clay Sci, 6(4), 245–263.

12. Birch F (1950) Flow of heat in the Front Range. Colorado. Bull Geol Soc Am 61:567–630

13. Blackwell, D., Steele, J. 1989. Thermal conductivity of sedimentary rocks: measurement and significance. Springer, doi.org/10.1007/978-1-4612-3492-0_2.

14. Breiman, L., 2001. Random forests, Mach. Learn., 45(1), 5–32.

15. Brigaud, F., Chapman, D.S. & Le Douaran, S., 1990. Estimating thermal conductivity in sedimentary basins using lithologic data and geophysical well logs, AAPG Bull., 74(9), 1459–1477.

16. Brigaud, F., Vasseur, G., 1989. Mineralogy, porosity and fluid control on thermal conductivity of sedimentary rocks. Int. J. Rock Mech. Min. Sci. 27(2), A77, doi.org/10.1111/j.1365-246X.1989.tb02287.x.

17. Bullard, E.C. & Day, A., 1961. The fow of heat through the floor of theAtlantic Ocean, Geophys. J. R. astr. Soc., 4(S1), 282–292.

18. Burkhardt, H., Honarmand, H., Pribnow, D., 1995. Test measurements with a newthermal conductivity borehole tool. Tectonophysics 224, 161–165.

19. Cermak, V., 1967. Coefficient of thermal conductivity of some sediments and its dependence on density and water content of rocks, Chem. Erde-Geochem., 26, 271–278.

20. Cermak, V., Rybach, L., 1982. Thermal conductivity and specific heat of minerals and rocks, in Geophysics-Physical Properties of Rocks, Vol. 1, Springer, pp. 305–343, doi.org/10.1007/10201894_62.

21. Chekhonin, E., Popov, E., Popov, Y., Gabova, A., Romushkevich, R., Spasennykh, M., Zagranovskaya, D., 2018. High-Resolution evaluation of elastic properties and anisotropy of unconventional reservoir rocks via thermal core logging. Rock Mech. Rock Eng. 51, 2747–2759. https://doi.org/10.1007/s00603-018-1496-z.

22. Chekhonin, E., Popov, Y., Peshkov, G., Spasennykh, M., Popov, E., Romushkevich, R., 2019. On the importance of rock thermal conductivity and heat flow density in basin and petroleum system modelling. Basin Research. 32 (4), doi.org/10.1111/bre.12427.

23. Chen, L., Goldgof, D., Hall, L., Eschrich, S., 2007. Noise-based feature perturbation as a selection method for microarray data. Bioinformatics Research and Applications. ISBRA 2007. Lecture Notes in Computer Science,

vol 4463, Springer, Berlin, Heidelberg, doi.org/10.1007/978-3-540-72031-7_22.

24. Chopra, N., Ray, L., Satyanarayanan, M., Elangovan, R., 2018. Evaluate best-mixing model for estimating thermal conductivity for granitoids from mineralogy: A case study for the granitoids of the Bundelkhand craton, central India, Geothermics, 75, 1–14, doi.org/10.1016/j.geothermics.2018.03.011.

25. Clauser, C. (2009). Heat transport processes in the earth's crust. Surveys in Geophysics, 30(3), 163–191, doi.org/10.1007/s10712-009-9058-2.

26. Clauser, C., 2006. Geothermal Energy, In: K. Heinloth (ed), Landolt-Börnstein, Group VIII: Advanced Materials and Technologies, Vol. 3: Energy Technologies, Subvol. C: Renewable Energies, Springer Verlag, Heidelberg-Berlin, pp. 493-604, doi.org/10.1007/b83039.

27. Clauser, C., 2006. Geothermal Energy, In: K. Heinloth (ed), Landolt-Börnstein, Group VIII: Advanced Materials and Technologies, Vol. 3: Energy Technologies, Subvol. C: Renewable Energies, Springer Verlag, Heidelberg-Berlin, pp. 493-604, doi.org/10.1007/b83039.

28. Clauser, C.; Giese, P.; Huenges, E.; Kohl, T. H.; Lehmann, H.; Rybach, L.; Zoth, G. The thermal regime of the crystalline continental crust: Implications from the KTB. Journal of Geophysical Research 1997, 102(B8), 18417–18441.

29. Corry, D., & Brown, C. (1998). Temperature and heat flow in the Celtic Sea basins. Petroleum Geoscience, 4, 317 - 326.

30. Dahnov, V., Djakonov, D., 1952. Thermal investigations of wells, Gostoptehisdat, Moscow, 252 p.

31. Deer, W., Howie, R., Zussman, J., 1992. Introduction to rock forming minerals, 2nd edition, John Wiley, New York, doi.org/10.1180/minmag.1992.056.385.20.

32. Deming, D., 1994. Estimation of the thermal conductivity anisotropy of rock with application to the determination of terrestrial heat flow. Journal of Geophysical Research 99, 22087– 22091, doi.org/10.1029/94JB02164.

33. Demongodin, L., Pinoteau, B., Vasseur, G. & Gable, R., 1991. Thermal conductivity and well logs: a case study in the Paris Basin, Geophys J. Int., 105(3), 675–691.

34. Dimopoulos Y, Bourret P, Lek S. Use of some sensitivity criteria for choosing networks with good generalization ability. Neural Processing Letters. 1995;2(6):1–4. DOI: 10.1007/ BF02309007

35. Dove, R.E. & Williams, C.F., 1989. Thermal conductivity estimated from elemental concentration logs, Nucl. Geophys., 3(2), 107–112.
36. Doveton, J.H., Förster, A. & Merriam, D.F., 1997. Predicting thermal conductivity from petrophysical logs: aMidcontinent Paleozoic case study, in Proceedings of the International Association for Mathematical Geology Annual Meeting, Barcelona, pp. 212–217.
37. Duchkov, A., Lisak, S., Balobaev, V., 1987. Thermal field of Siberia, Nauka, Novosibirsk, 196 p (in Russian).
38. Emmermann R., Lauterjung J. The German continental deep drilling program KTB: overview and major results // Journal of Geophysical Research: Solid Earth. Wiley Online Library, 1997. Vol. 102, № B8. P. 18179–18201.
39. Emmermann, R.; Lauterjung, J The German continental deep drilling program KTB: Overview and major results. Journal of Geophysical Research 1997, 102 (B8), 18179-18201, doi: 10.1029/96JB03945.
40. Evans, T.R., 1977. Thermal properties of North Sea rocks, Log Analyst, 18(2), 3–12.
41. Experimental heat transfer, fluid mechanics and thermodynamics. Proceedings of the 4th world congress on experimental heat transfer, fluid mechanics and thermodynamics, vol 1, Belgium, Brussels, pp 109–116
42. Fertl, W., Frost, E, 1980. Evaluation of shaly clastic reservoir rocks. Journal of Petroleum Technology 9(32), 1641 – 1646, doi.org/10.2118/8450-PA.
43. Flaum, C., Theys, P., 1991. Geometrical specifications of logging tools: the need for new standards, SPWLA 32nd Annual Logging Symposium, SPWLA-1991-YY, 23.
44. Freund, Y. & Schapire, R.E., 1997. A decision-theoretic generalization of on-line learning and an application to boosting, J. Comput. Syst. Sci., 55(1), 119–139.
45. Friedman, H., 1999. Stochastic gradient boosting, Comput. Stat. Data Anal., 38, 367–378.
46. Fuchs, S. & Förster, A., 2014. Well-log based prediction of thermal conductivity of sedimentary successions: a case study from the North German Basin, Geophys. J. Int., 196(1), 291–311.
47. Fuchs, S., Balling, N. & Förster, A., 2015. Calculation of thermal conductivity, thermal diffusivity and specific heat capacity of sedimentary rocks using petrophysical well logs, Geophys. J. Int., 203(3), 1977–2000.

48. Fuchs, S., F¨orster, H., Braune,K.&F¨orster, A., 2018. Calculation of thermal conductivity of low-porous, isotropic plutonic rocks of the crust at ambient conditions from modal mineralogy and porosity: a viable alternative for direct measurement?, J. geophys. Res., 123(10), 8602–8614.

49. Fuchs, S., Schütz, F., Förster, H.-J., Förster, A., 2013. Evaluation of common mixing models for calculating bulk thermal conductivity of sedimentary rocks: correction charts and new conversion equations. Geothermics 47, 40–52, doi.org/10.1016/j.geothermics.2017.01.005.

50. Gasior, I. & Przelaskowska, A., 2014. Estimating thermal conductivity from core and well log data, Acta Geophys., 62(4), 785–801.

51. Gegenhuber, N. & Sch¨on, J., 2012. New approaches for the relationship between compressional wave velocity and thermal conductivity, J. appl Geophys., 76, 50–55.

52. Golovanova, I.V. Thermal field of the Southern Urals; Nedra Publ.: Leningrad, Russia, 2005; p. 189.

53. Goodfellow, I., Bengio, Y., Courville, A., 2016. Deep Learning. MIT Press.

54. Gordienko, V.V.; Zavgorodskaya, O.V.; Moiseenko, U.I. Heat flow map of the territory of the USSR. Scale 1: 5,000,000. Explanatory note 1987 (in Russian).

55. Goss, R.D. & Combs, J., 1976. Thermal conductivity measurement and prediction from geophysical well log parameters with borehole application, Final Report, Institute for Geosciences, University of Texas at Dallas, NSF/RA–760364, 31 pp.

56. Goss, R.D., Combs, J.&Timur, A., 1975. Prediction of thermal conductivity in rocks from other physical parameters and from standard geophysical well logs, in Proceedings of the SPWLA 16th Annual Logging Symposium, 1975, 21 pp.

57. Goutorbe, B., Lucazeau, F. & Bonneville, A., 2006. Using neural networks to predict thermal conductivity from geophysical well logs, Geophys. J. Int., 166(1), 115–125.

58. Griffiths, C.M., Brereton, N.R., Beausillon, R.&Castillo, D., 1992. Thermal conductivity prediction from petrophysical data: a casestudy, Spec. Publ. Geol. Soc. Lond., 65(1), 299–315.

59. Hantschel, T.; Kauerauf, A. I. Fundamentals of basin and petroleum systems modeling, 1st ed.; Springer-Verlag: Berlin Heidelberg, Germany, 2009; p. 476.

60. Hartmann, A., Pechnig, R. & Clauser, C., 2008. Petrophysical analysis of regional-scale thermal properties for improved simulations of geothermal

installations and basin-scale heat and fluid flow, Int. J. Earth Sci., 97(2), 421–433.

61. Hicks Jr P.J. et al. Identifying and quantifying significant uncertainties in basin modeling. AAPG Special Volumes, 2012.

62. Hinton, G.E., 1989. Connectionist learning procedures, Artif. Intell., 40, 185–234.

63. Hodyreva, E.Y.; Shchulaev, V.F.; Netkach, A.Y.; Markov, A.I. Initial geothermal field of Orenburg gas-condensate field. Oil and gas geology 1985, 3, 43-48 (in Russian).

64. Horai, K., 1971. Thermal conductivity of rock-forming minerals. J. Geophys. Res. 76, 1278-1308.

65. Huber, P.J.; Ronchetti, E.M. Robust Statistics Concomitant scale estimates; John Wiley & Sons, Inc.: New Jersey, U.S.A., 2009; p. 172.

66. Huenges E, Burkhardt H, Erbas K (1990) Thermal conductivity profile of the KTB pilot corehole. Sci Drill 1:224–230

67. Kang, Z., Peng, C., Cheng, Q., 2017. Kernel-driven similarity learning. Neurocimputing, 267, 210-219. https://doi.org/10.1016/j.neucom.2017.06.005.

68. Khandelwal, M., 2010. Prediction of thermal conductivity of rocks by soft computing, Int. J. Earth Sci., 100(6), 1–7.

69. Khaustova, N., Tikhomirova, Y., Spasennykh, M., Popov, Y., Kozlova, E., Voropaev, A., 2019. U/Corg ratio within unconventional reservoirs: indicator of oil generation processes and criteria for productive intervals determination during the Bazhenov formation investigation. Conference Proceedings of EAGE/SPE Workshop on Shale Science 2019, 2019, p.1 – 5, doi.org/10.3997/2214-4609.201900476.

70. Kim, H., Cho, J., Song, I., Min, K., 2012. Anisotropy of elastic moduli, P-wave velocities, and thermal conductivities of Asan Gneiss, Boryeong Shale, and Yeoncheon Schist in Korea. Eng. Geol. 148, 68–77. https://doi.org/10.1016/j.enggeo.2012.07.015.

71. Krischer, O., Esdorn, H., 1956. Die Wermeubertragung in feuchten, porigen Stoffen verschiedener Struktur, Forsch. a. d. Gebiet d. Ingenieurwesens, 22, 1–8.

72. Kukkonen I.T. et al. Geothermal studies of the Outokumpu Deep Drill Hole, Finland: Vertical variation in heat flow and palaeoclimatic implications // Physics of the Earth and Planetary Interiors. Elsevier, 2011. Vol. 188, № 1–2. P. 9–25.

73. Kukkonen, I., Suppala, I., Korpisalo, A., Koshkinen, T., 2007. Drill Hole LoggingDevice TERO76 for Determination of Rock Thermal Properties. Posiva OY, pp.63.

74. Kukkonen, I.T. & Peltoniemi, S., 1998. Relationships between thermal and other petrophysical properties of rocks in Finland, Phys. Chem. Earth., 23(3), 341–349.

75. Kukkonen, I.T.; Golovanova, I.V.; Khachay, Yu.V.; Druzhinin, V.S.; Kosarev, A.M.; Schapov, V.A. Low geothermal heat flow of the Urals fold belt — implication of low heat production, fluid circulation or palaeoclimate? Tectonophysics 1997, 276, 63-85, doi: 10.1016/S0040-1951(97)00048-6.

76. Kukkonen, T.; Rath, V.; Kivekas, L.; Šafanda, J.; Čermak, V. Geothermal studies of the Outokumpu Deep Drill Hole, Finland: Vertical variation in heat flow and palaeoclimatic implications. Physics of the Earth and Planetary Interiors 2011, 188, 9–25, doi: 10.1016/j.pepi.2011.06.002.

77. Kurbanov, A.A. Regularities of behavior of thermophysical properties of fluid bearing reservoirs at in situ conditions and its applications. Ph.D. Thesis, Schmidt Institute of Physics of the Earth of the Russian Academy of Sciences, October 2007.

78. Kurchikov, A., Stavitskii, B., 1987. Geothermics of Western Siberia oil and gas regions, Nedra, Moscow, 134 p (in Russian).

79. L. Eppelbaum et al., Applied Geothermics, Lecture Notes in Earth System Sciences, 2014.

80. Larose, D.T., 2014. Discovering Knowledge in Data: An Introduction to Data Mining, Wiley.

81. Liang, X., Philippov, V., Galushin, G., 2015. Paleogeographic reconstruction and structural morphology of Domanic fromation in the Republic of Tatarstan. Proceedings of SPE Russian Petroleum Technology Conference, SPE-176610-RU, doi.org/10.2118/176610-MS.

82. Lichtenecker, K., 1924. Der elektrische Leitungswiderstand künstlicher und natürlicher Aggregate, Physikalische Zeitschrift 25, 169–181,193–204, 226–233.

83. Lichtenecker, K., Rother, K., 1931. Die Herleitung des logarithmischen Mischungsgesetzes aus allgemeinen Prinzipien der stationaren Stromung. Physikalische Zeitschrift, 32, 255–260.

84. Lovell, M.A., 1985. Thermal conductivity and permeability assessment by electrical resistivity measurements in marine sediments, Mar. Geotechnol., 6(2), 205–240.

85. Maosen, C., Nizar, A., Lixia, P., Drahomir, N., 2016. Advanced Methods in Neural Networks-Based Sensitivity Analysis with their Applications in Civil Engineering. https://doi.org/10.5772/64026.

86. Merkel, R.H., Maccary, L.M., Chico, R.S., 1976. Computer techniques applied to formation evaluation. Log Analyst 17(3), 3–10.

87. Midttømme, K., Roaldset, E. & Aagaard, P., 1997. Thermal conductivity of argillaceous sediments, in Modern Geophysics in Engineering Geology, Vol. 12, pp. 355–363, eds. McCann, D.M., Eddleston, M., Fenning, P.J. & Reeves, G.M., Geological Society Engineering Geology.

88. Molnar, P., Hodge, D., 1982. Correlation of thermal conductivity with physical properties obtained from geophysical well logs. In Proceedings of the AAPG Annual Convention with Divisions SEPM/EMD/DPA, Calgary, Canada, 608–609 pp.

89. Montano, J., Palmer, A., 2003. Numeric sensitivity analysis applied to feedforward neural networks. Neural Computing and Applications 12(2), 119–125. https://doi.org/10.1007/ s00521-003-0377-9.

90. Mottaghy, D., Schellschmidt, R., Popov, Y., Clauser, C., Romushkevich, R., Kukkonen, I.; Nover, G.; Milanovsky, S., 2005. New heat flow data from the immediate vicinity of the Kola super-deep borehole: Vertical variation in heat flow confirmed and attributed to advection. Tectonophysics 401 (1-2), 119-142. https://doi.org/10.1016/j.tecto.2005.03.005.

91. Ozkahraman, H.T., Selver, R., Isık, E., 2004. Determination of the thermal conductivity of rock from P-wave velocity, Int. J. Rock Mech. Min. Sci., 41(4), 703–708.

92. Pasquale, V., Gola, G., Chiozzi, P., Verdoya, M., 2011. Thermophysical properties of the Po Basin rocks. Geophysical Journal International 186, 69 – 81. doi.org /10.1111/j.1365-246X.2011.05040.x.

93. Peterson, J., Clarke, J., 1983. Petroleum geology and resources of the Volga-Ural Province, U.S.S.R. USGS Geological Survey circular. https://doi.org/ 10.3133/cir885.

94. Pierre, G., Damien, E., Lois,W., 2006. Extremely randomized trees, Artif. Intell., 63, 3–42.

95. Platt, J., 1999. Probabilistic Outputs for Support Vector Machines and Comparisons to Regularized Likelihood Methods. Advances in large margin classifiers, MIT Press.

96. Popov E., 2020a. Development of the experimental base of thermal petrophysics for the study of rocks from deposits of hard-to-recover and unconventional hydrocarbons reserves. Schmidt Institute of Phycics of the Earth of the Russian Academy of Sciences, Moscow, Russia (in Russian).

97. Popov Y., Chekhonin, E., Shakirov, A., 2019a. Approach for determining thermal properties of organic-rich shales. Russian Patent № № RU 2704002 C1.

98. Popov, E., Goncharov, A., Popov, Y., Spasennykh, M., Chekhonin, E., Shakirov, A., Gabova, A., 2019. Advanced experimental basis for determining reservoir thermal properties at atmospheric and formation conditions. IOP conference series. https://doi.org/10.1088/1755-1315/367/1/012017.

99. Popov, E., Popov, Y., Chekhonin, E., Safonov, S., Savelev, E., Gurbatova, I., Ursegov, S., Shakirov, A., 2020b. Thermal core profiling as a novel and accurate method for efficient characterization of oil reservoirs. Journal of Petroleum Science and Engineering 193, 107384. https://doi.org/10.1016/j.petrol.2020.107384.

100. Popov, E., Romushkevich, R., Popov, Y., 2017. Measurments of the rock thermal properties on the standard core plugs as a necessary stage of the thermalphysic investigations of the hydrocarbon fields. Geol. Explor., 2, 56–70.

101. Popov, E., Trofimov, A., Goncharov, A., Abaimov, S., Chekhonin, E., Popov, Y., Sevostianov, I., 2018. Technique of rock thermal conductivity evaluation on core cuttings and nonconsolidated rocks. International Journal of Rock Mechanics and Mining Sciences 108, 15–22, https://doi.org/10.1016/j.ijrmms.2018.05.005.

102. Popov, Y., 1983. Theoretical models of the method of determination of the thermal properties of rocks on the basis of movable sources. Geological Prospecting 9, 97–105 (in Russian).

103. Popov, Y., 1997. Optical scanning technology for non-destructive contactless measurements of thermal conductivity and diffusivity of solid matter. In: Giot M, Mayinger F, Celata GP (eds).

104. Popov, Y., Berezin, V., Semenov, V., Korostelev, V. 1985. Complex detailed investigations of the thermal properties of rocks on the basis of a moving point source. Izv Phys Solid Earth 21(1), 64–70.

105. Popov, Y., Berezin, V., Solovev, G., Romushkevich, R., Korostelev, V., Kosturin, A., Kulikov, I., 1987. Thermal conductivity of minerals. Izvestiya, Earth Physics. 23(3), 245-253.

106. Popov, Y., Chekhonin, E., Parshin, A., Law, D., Pissarenko, D., Miklashevskiy, D., Popov, E., Spasennykh, M., Safonov, S., Romushkevich, R., Bayuk, I., Danilenko, A., Gerasimov, I., Ursegov, S., Konoplev, Y., Taraskin, E. 2013. Experimental investigations of spatial and temporal variations in rock thermal properties as necessary stage in thermal EOR. Paper presented at the SPE Heavy Oil Conference-Canada, Calgary, Alberta, Canada, June 2013. doi: https://doi.org/10.2118/165474-MS.

107. Popov, Y., Huddlestone-Holmes, C., Gerner. E., 2012. Evolution in the reliability of experimental geothermal data. In Proceedings of the 2012 Australian Geothermal Energy Conference, Sydney, Australia.

108. Popov, Y., Mandel, A., 1998. Geothermal investigations of anisotropic rock mass. Physics of the Solid Earth 11, 30-43 (in Russian).

109. Popov, Y., Pevzner, S., Pimenov, V., Romushkevich, R., 1999. New geothermal data from the Kola superdeep well SG-3. Tectonophysics 306, pp. 345–366. https://doi.org/10.1016/S0040-1951(99)00065-7.

110. Popov, Y., Pevzner, S., Pimenov, V., Romushkevich, R., 1999. New geothermal data from the Kola superdeep well SG-3. Tectonophysics 306, 343-366. https://doi.org/10.1016/S0040-1951(99)00065-7.

111. Popov, Y., Pimenov, V., Pevzner, L., Romushkevich, R., Popov, E., 1998. Geothermal characteristics of the Vorotilovo deep borehole drilled into the Puchezh-Katunk impact structure. Tectonophysics 291, 205-223. https://doi.org/ 10.1016/S0040-1951(98)00041-9.

112. Popov, Y., Popov, E., Chekhonin, E., Gabova, A., Romushkevich, R., Spasennykh, M., Zagranovskaya, D., 2017. Investigation of Bazhenov formation using thermal core logging technique. Oil Industry 3, 23-27. https://doi.org/10.24887/0028-2448-2017-3-22-27.

113. Popov, Y., Popov, E., Chekhonin, E., Spasennykh, M., Goncharov, A., 2019b. Evolution in information on crustal geothermal parameters due to application of advanced experimental basis. In Proceedings of the IOP Conference Series:

Earth and Environmental Science 249, 012042. https://doi.org/10.1088/1755-1315/249/1/012042.

114. Popov, Y., Rabe, F., Bangura, A., 1993. Adequacy of theoretical and experimental models of the optical scanning method. Geological Prospecting 6, 65–72 (in Russian).

115. Popov, Y., Romushkevich, R., Gorobtsov D., Korobkov, D., Esipko, O., Karaseva, T., Sirotenko, L., 2008. Rock thermal properties and heat flow in the area of super-deep En-Yahinskaya well. Geology and Exploration 2, 59-65 (in Russian).

116. Popov, Y., Romushkevich, R., Korobkov, D., Mayr, S., Bayuk, I., Burkhardt, H., Wilhelm, H., 2011. Thermal properties of rocks of the borehole Yaxcopoil-1 (Impact Crater Chicxulub, Mexico), Geophys. J. Int. 184(2), 729–745.

117. Popov, Y., Romushkevich, R., Popov, E., Bashta, K., 1999. Results of drilling and investigating super-deep Ural well, Nedra, YAroslavl, pp. 77-88.

118. Popov, Y., Spasennykh, M., **Shakirov**, A., Chekhonin, E., Romushkevich, E., Savelev, E., Gabova, A., Zagranovskaya, D., Valiullin, R., Yuarullin, R., Golovanova, I., Sal'manova, R., (2021a). Investigations of geothermal parameters of oil field with unconventional reservoir in European part of Russia with advanced experimental basis. Submitted to Geosciences.

119. Popov, Y., Tertychnyi, V., Romushkevich, R., Korobkov, D., Pohl, J., 2003. Interrelations between thermal conductivity and other physical properties of rocks: experimental data. Pure appl. Geophys. 160(5–6), 1137–1161. https://doi.org/ 10.1007/PL00012565.

120. Popov, Y., 1984. Peculiarities of the method of detailed investigations of rock thermal properties. Geological Prospecting 4, 76–84 (in Russian).

121. Popov, Yu, Beardsmore, G., Clauser, C., Roy, S., 2016b. ISRM suggested methods for determining thermal properties of rocks from laboratory tests at atmospheric pressure. Rock Mech. Rock Eng. 49 (10), 4179–4207. https://doi.org/10.1007/ s00603-016-1070-5.

122. Popov, Yu., Spasennykh, M., Shakirov, A., Chekhonin, E., Romushkevich, R., Savelev, E., Zagranovskaya, D. 2021b. New Data on Heat flow for Modeling Areas of Hydrocarbon Systems of The Bazhenov and Domanik Formations. Conference Proceedings of EAGE/SPE Workshop on Shale Science 2021, p. 1-5. doi.org/10.3997/2214-4609.202151027.

123. Poulsen, K., Saxov, S., Balling, N., Kristiansen, J., 1981. Thermal conductivity measurements on Silurian limestones from the Island of Gotland, Sweden. Geologiska Foreningen i Stockholm Forhandlingar 103(3), 349–356.

124. Poulsen, S., Balling, N., 2012. Estimation of the equilibrium formation temperature in the presence of bore fluid invasion. Geophysical Journal International 190, 1551-1561. https://doi.org/10.1111/j.1365-246X.2012.05571.x.

125. Prats M., O'Brien, S., 1975. Thermal conductivity and diffusivity of Green River Oil Shale. J. Pet. Technol. 27, 97-106. https://doi.org/10.2118/4884-PA

126. Pribnow, D., Umsonst, T. 1993. Estimation of thermal conductivity from the mineral composition: Influence of fabric and anisotropy. Geophys. Res. Lett., 20, 2199–2202. https://doi.org/10.1029/93GL02135.

127. Rasmussen, C., Williams, C., 2006. Gaussian Processes for Machine Learning, the MIT Press, Massachusets, 248 p.

128. Roy, R., Beck, A., Touloukian, Y., 1981. Thermophysical properties of rocks. Physical properties of rocks and minerals 11, 409-502.

129. Sahlin, T., Middleton, M., 1997. Correlation of thermal conductivity with well log derived petrophysical parameters. In Proceedings of the Second Nordic Symposium on Petrophysics, Reykjavık, Orkustofnun, 263–281 pp.

130. Sanner, B., Hellström, G., Spitler, J., Gehlin, S., 2005. Thermal response test – currentstatus and world-wide application. Proceedings World Geothermal Congress.

131. Sauer, D., Wagner, S., Amro, M., Popov, Y., Rose, F., Schramm, A., Börner, E., Wünsch, T., Redondo-Robles, H., Hesse, G., Pfeiffer, J., 2017. Development of a new borehole probe for thermal conductivity scanning. Geothermics 67, 95-101. https://doi.org/10.1016/j.geothermics.2017.02.003.

132. Savest, N., Oja, V., 2013. Heat capacity of Kikersite oil shale: literature review. Oil Shale 30(2), 184–192. https://doi.org/10.3176/oil.2013.2.08.

133. Sayers, C. 2013. The effect of anisotropy on the Young's moduli and Poisson's ratios of shales. Geophys Prospect 61, 416–426. https://doi.org/10.1111/j.1365-2478.2012.01130 .x.

134. Schoen, J., 2015. Physical properties of rocks: Fundamentals and principles of petrophysics, Elsevier.

135. Schoenberg, M., Muir, F., Sayers, C., 1996. Introducing ANNIE: a simple three-parameter anisotropic velocity model for shales. J Seism Explor, 5, 35–49.

136. Serra, O., 1986. Fundamentals of Well-Log Interpretation - The Interpretation of Logging Data, Elsevier, 423 p.

137. Shakirov, A., Chekhonin, E., Popov, Y., Popov, E., Spasennykh, M., Zagranovskaya D., Serkin M., 2021. Rock thermal properties from well-logging data accounting for thermal anisotropy. Geothermics 92(6), 102059. https://doi.org/ 10.1016/j.geothermics.2021.102059.

138. Singh, R., Bhoopal, R.S., Kumar, S., 2011. Prediction of effective thermal conductivity of moist porous materials using artificial neural network approach. Build Environ. 46(12), 2603–2608.

139. Singh, T.N., Sinha, S., Singh, V.K., 2007. Prediction of thermal conductivity of rock through physico-mechanical properties, Build Environ. 42(1), 146–155.

140. Skauge, A., Fuller, N. Hepler, L., 1983. Specific heats of clay minerals: Sodium and calcium kaolinites, sodium and calcium montmorillonites, illite, and attapulgite, Thermochim. Acta 61, 139–145. https://doi.org/10.1016/0040-6031(83)80310-4.

141. Stolyarov, M., Popov, Y., Tertichnii, V., Korobkov, D., 2007. Peculiareties of method for determining rock thermal conductivity based on theoretical model of Lichtenecker-Asaad. Geology and Exploration 5, 69-73.

142. Stone, M., 1974. Cross-validation and multinomial prediction, Biometrika, 61(3), 509–515.

143. Storn, R., Price, K., 1997. Differential evolution – a simple and efficient heuristic for global optimization over continuous spaces. Journal of Global Optimization 11, 341–359. https://doi.org/10.1023/A:1008202821328.

144. Sundberg, J., Back, P.-E., Ericsson, L.O. & Wrafter, J., 2009. Estimation of thermal conductivity and its spatial variability in igneous rocks from in situ density logging, Int. J. Rock Mech. Min. Sci. 46(6), 1023–1028.

145. Tanikawa, W., Tadai, O., Morita, S., Lin, W., Yamada, Y., Sanada, Y., Moe, K., Kubo, Y., & Inagaki, F., 2016. Thermal properties and thermal structure in the deep-water coalbed basin off the Shimokita Peninsula, Japan. Marine and Petroleum Geology 73, 445-461.

146. Tikhotsky, S., Fokin, I., Bayuk, I., Beloborodov, D., Berezina, I., Gafurova, D., Dubinya, N., Krasnova, D., Makarova, A., Patonin, A., Ponomarev, A., Khamidulin, R., Tselmovich, V. 2018. Comprehensive Laboratory Core Analysis at CPGR IPE RAS. Seismic Instruments, 54, 586–597 (2018). https://doi.org/10.3103/S0747923918050146.

147. Tissot, B., Welte, D., 1984, Petroleum Formation and Occurrence, 2 ed., Springer-Verlag, 699 p. https://doi.org/10.1007/978-3-642-96446-6.

148. Ulmishek, G. 2003. Petroleum Geology and Resources of the West Siberian Basin, Russia. USGS Bulletin, 2201–G.

149. Vacquier, V., Mathieu, Y., Legendre, E. & Blondin, E., 1988. Experiment on estimating thermal conductivity of sedimentary rocks from oil well logging, Int. J. Rock Mech. Min. Sci. 26(2), 63–63.

150. Vashkevich, A., Strizhnev, K., Shashel, V., Zakharova, O., Kasyanenko, A., Zagranovskaya, D., Grebenkina N., 2018. Forecast of prospective areas for sediment type Domanic in the Volga-Ural oil and gas Province. Oil Industry 12, 14-17. https://doi.org/10.24887/0028-2448-2018-12-14-17 (in Russian).

151. Vasseur, G., Brigaud, F. & Demongodin, L., 1995. Thermal conductivity estimation in sedimentary basins, Tectonophysics 244, 167–174.

152. Wang, G., Yang, D., Kang, Z., Zhao, J., 2018. Anisotropy in thermal recovery of oil shale—Part 1: thermal conductivity, wave velocity and crack propagation. Energies 11. https://doi.org/10.3390/en11010077.

153. Wang, L., Tian, Y., Yu, X., Wang, C., Yao, B., Wang, S., Winterfeld, P., Wang, X., Yang, Z., Wang, Y., Wu, Y., 2017. Advances in improved/enhanced oil recovery technologies for tight and shale reservoirs. Fuel 210, 425–445. https://doi.org/10.1016/j.fuel.2017.08.095.

154. Waples, D.W., Waples, J.S., 2004. A review and evaluation of specific heat capacities of rocks, minerals, and subsurface fluids. Part 2: fluids and porous rocks. Nat. Resour. Res 13, 123–130, https://doi.org/ 10.1023/B:NARR.0000032648.15016.49.

155. Yakovlev, B., 1996. Prediction of hydrocarbon potential via geothermal data, Nedra, Moscow, 240 p.

156. Zamora, M., Dung, V.T., Bienfait, G. & Poirier, J.P., 1993. An empirical relationship between thermal conductivity and elastic wave velocities in sandstone, Geophys. Res. Lett. 20(16), 1679–1682.

157. Zeng, X., Yeung, D., 2003. A quantified sensitivity measure for multilayer perceptron to input perturbation. Neural Computation, 15(1), 183–212. https://doi.org/ 10.1162/089976603321043757.

158. Zierfuss, H., Vliet, G., 1956. Laboratory measurements of heat conductivity of sedimentary rocks, AAPG Bull. 40(10), 2475–2488.